ON STATIONARY AND NONSTATIONARY FATIGUE LOAD MODELING USING AUTOREGRESSIVE MOVING AVERAGE (ARMA) MODELS

by

Christoph Leser

Dissertation submitted to the Faculty of the

Virginia Polytechnic Institute and State University

in partial fulfillment of the requirements for the degree of

DOCTOR OF PHILOSOPHY

in

Engineering Mechanics

APPROVED:

S. Thangjitham, Chairman

N. E. Dowling

M. P. Singh

R. W. Landgraf

A. L. Wicks

November, 1993

Blacksburg, Virginia

ON STATIONARY AND NONSTATIONARY FATIGUE LOAD MODELING USING AUTOREGRESSIVE MOVING AVERAGE (ARMA) MODELS

by

Christoph Leser

Surot Thangjitham, Chairman

Engineering Mechanics

(ABSTRACT)

The concise description of one- and multidimensional stationary and nonstationary vehicle loading histories for fatigue analysis using stochastic process theory is presented in this study. The load history is considered to have stationary random and nonstationary mean and variance content. The stationary variations are represented by a class of time series referred to as Autoregressive Moving Average (ARMA) models, while a Fourier series is used to account for the variation of the mean and variance. Due to the use of random phase angles in the Fourier series, an ensemble of mean and variance variations is obtained. The methods of nonparametric statistics are used to determine the success of the modeling of nonstationarity. Justification of the method is obtained through comparison of rainflow cycle distributions and resulting fatigue lives of original and simulated loadings. Due to the relatively small number of Fourier coefficients needed together with the use of ARMA models, a concise description of complex loadings is achieved. The overall frequency content and sequential information of the load history is statistically preserved. An ensemble of load histories can be constructed on-line with minimal computer storage capacity as used in testing equipment. The method can be used in a diversity of fields where a concise representation of random loadings is desired.

ACKNOWLEDGMENTS

My deepest gratitude goes to my major advisor Dr. Surot Thangjitham for all his direction, support, and sharing of interest throughout the preparation of this dissertation. In many late nights we sorted out details with regard to Fourier series coefficients and world politics. Dr. Norman E. Dowling helped keep the project focused and was always able to point out what the actual problem was we had to solve, which is half the solution in itself. Furthermore, I want to thank Drs. Ronald W. Landgraf, Mahendra P. Singh, and Alfred L. Wicks for their encouragement, counsel, and different perspectives provided throughout the preparation of this dissertation.

I want to thank the sponsor MTS Systems Corporation of Minneapolis, MN for continued financial and technical support of this project. In particular, I want to thank the technical monitors, Phil E. Grote and (formerly) Dr. James W. Fash, for providing field data and valuable suggestions.

I want to thank Lokesh Juneja for his contributions to this work, particularly for the multiaxial fatigue life calculations and the experimental work performed by him. Of the many other students I met while studying at Virginia Tech I want to thank particularly Farhad Ameen, Fahad Khalil, Jeff Kline, and Michael Laurent for encouragement and friendship. Finally, I owe great thanks to Gerd Berning for joint study sessions in Braunschweig, Germany, and friendship ever since.

Most, of all the people I have to thank, is my wife Colleen, for her unconditional support in all I do.

DEDICATION

I want to dedicate this dissertation to my loving parents Rosemarie and Peter Leser who made it possible for me to pursue this education. They always trusted in me and my capabilities and encouraged me to make the most of myself.

TABLE OF CONTENTS

LIST OF ILLUSTRATIONS

LIST OF TABLES

CHAPTER 1. INTRODUCTION

Engineering's primary objective is to design structures to fulfill a function and guard this design against failure. A common failure mode is fatigue, i.e. cracking or disintegrating of parts of the structure caused by repeated loading. Fatigue analysis, therefore, is an important part of the design process for any structure or component subject to repetitive dynamic loading.

The analysis with respect to fatigue failure gains more importance as structures are designed, primarily for economic reasons, to have a finite life. Weight and size consideration in efficient design mandate for a structure to survive safely all anticipated operating loads, yet a structure must not be *over designed* to the degree that it becomes uneconomical to built or operate. Particularly in the area of vehicle design it has become the objective to design components to safely perform only over a prescribed service interval.

One of the crucial elements in fatigue analysis is detailed knowledge of the operation conditions and the associated loading to which the component in question is subjected. For some cases the loadings can be estimated in advance of the analysis in many cases of structural analysis, however, a preliminary design is necessary to obtain actual loadings, which is done by subjecting the preliminary design to the environment in which the final structure is supposed to operate.

Because the phenomenon of fatigue failure is still not fully understood, for complex structures, analytical studies alone cannot provide sufficient information for a fatigue safe design. Two methods for verification of a design are simulation studies and fatigue testing. Fatigue testing exposes a structure to dynamic loads as they would be anticipated under operating conditions and records the life to failure. For more effective and better controlled testing it has become customary to perform many fatigue tests in a laboratory rather than in the actual environment of operation. As testing equipment has become more advanced, these laboratory fatigue tests provide the means for reliable and efficient repetition of complex loadings. Simulation studies, such as Monte Carlo simulations, on the other hand, are computer based calculations of the fatigue life according to a model for the structure and the fatigue phenomenon, including uncertainties with respect to structural and or loading parameters. For both fatigue testing and simulation studies an efficient description of the loading environment is necessary.

In general, fatigue loadings are lengthy because fatigue failure occurs only after many repetitions of the applied load. In the case of complex loadings with a variety of different loading events, it is desired to reduce these lengthy records for further analysis. The two main methods of reduction are the building of mathematical models to describe the loads, or the actual loading data are condensed to fatigue relevant information only. From either the formed model or condensed description, fatigue load histories then can be reconstructed for simulation studies or for laboratory testing of test specimen or actual components. The accurate and concise modeling of lengthy fatigue loadings is the objective of this study.

Load modeling can be accomplished by two principal methods. Depending on the

problem, either a deterministic function or a stochastic process is used to reproduce essential features of the original history. The deterministic approach uses a well defined function to describe the original history. The stochastic approach attempts to describe the load data in terms of a random process which has statistical characteristics similar to that of the original history. If the load records are of random nature, as they are for many structural components exposed to environmental loads, the stochastic approach is most suitable.

Stochastic methods can further be divided into regression analysis and time series analysis, where the former method assumes that the observations are statistically independent and therefore disregards information with regard to the sequence of observations. The latter method, on the other hand, takes into account the relation of observations over time. Because for dynamic loadings observations will be related to each other, time series analysis methods are used in this study to model loadings. In particular, a class of stochastic processes referred to as Autoregressive Moving Average models, *ARMA*, are used to represent random variations in load records.

Another distinction among random processes can be made with respect to stationarity. A nonstationary record is recognized as one for which some characteristics, such as mean or variance, change over time. This nonstationary behavior can be modeled in variety of ways. In the current study a Fourier series description is chosen to account for nonstationarities.

Depending on the type of loading, a single channel or multichannel description may be necessary. For the case where only one variable is under observation, such as strain in one direction, a single channel description is appropriate. For the case, however, where a

multiaxial state of strain is to be investigated, a multichannel history will be observed and needs to be modeled as such to account for interdependencies among channels.

The model proposed herein gives the first complete description of nonstationary multichannel fatigue loadings using ARMA models. In comparison to other commonly used methods of history reconstruction such as the Rainflow method, the To-From matrix method and the power spectral density (PSD) method, the presented approach is superior on four accounts. First, the model requires fewer parameters to accurately describe the original loading. Second, the dynamic characteristics, also referred to as correlations, are preserved in the reconstruction as it is the case only for the PSD method. Third, multichannel situations are covered as a consistent extension of the single channel case. Finally, a truly stochastic description is achieved, such that regenerated records can be infinitely long with no periodicity.

Including this introduction, the dissertation consists of the following chapters. A literature review containing an overview of random fatigue load modeling and ARMA models in structural dynamics is presented in Chapter 2. The theory of ARMA models is presented in Chapter 3. Fatigue life calculations as they are used in this study are reviewed in Chapter 4. The proposed random fatigue load model is presented in Chapter 5. Case studies for uniaxial and multiaxial loadings are shown in Chapters 6 and 7, respectively The dissertation is concluded in Chapter 8 with summarizing remarks and recommendations for further work.

CHAPTER 2. LITERATURE REVIEW

A review of the literature pertinent to this dissertation is presented. First a review of common methods for random fatigue load representations is provided. Furthermore, the use of ARMA models in stochastic structural dynamics is reviewed.

2.1 Random Fatigue Load Modeling

Fatigue load histories are in general lengthy and of irregular nature. Three reasons (Beste et al., 1991) make it desirable to find a concise description. First, the amount of storage required can be reduced. Secondly, concentration on the fatigue relevant content allows reducing the length of the history. Finally, manipulation of histories becomes possible, including the superposition and extrapolation of histories.

In fatigue load reconstruction the strategy is to define some characteristic of the original loading such as power spectral density, rainflow cycle content, etc., as the *target* spectrum. A simulated history has to have similar characteristics to be a faithful reconstruction, i.e., it has to meet the target spectrum. Furthermore, the load description needs to allow for efficient regeneration of histories, preferably in real time (Buxbaum, 1979). Two basic approaches exist to random load modeling (Bílý and Bukoveczky, 1976). Either only extreme values are being recorded and subsequently reconstructed, or the whole history is taken into account.

2.1.1 Methods of Modeling Extreme Values

These methods are model free and they evaluate the time series via a count. Methods of reconstructing only the extreme values reduce the required storage by discarding all intermediate points. These methods work well for fatigue loading histories in the absence of creep, because only the extremes induce fatigue damage, while intermediate points are irrelevant.

In the *Rainflow Matrix* method (Dowling, 1972; Perret, 1987; ten Have, 1989) the fatigue relevant information is summarized in the form of a rainflow range mean matrix containing the distribution of closed stress-strain hysteresis loops formed by the original history. As a result, the rainflow cycles of the reconstructed histories are identical to those of the original history, while the reconstruction yields histories with a different sequence of loadings. The loading sequence, however, has been shown to affect the fatigue life (Gassner, 1941; Buxbaum et al., 1991) and should therefore be preserved. Finney and Denton (1986) quantified this effect on life for different reconstructions. The sequence of events in a history reconstructed from a rainflow matrix is governed by principals of the rainflow counting method, yet many possible sequences can be reconstructed. Khosrovaneh (1989) and Khosrovaneh and Dowling (1990) show a method to obtain reconstructed records which do not exhibit any distinct pattern, i.e., they appear to be of random nature as the original loading. A more formalized approach, not yet accepted in the international community though, to obtaining sequences with random characteristics is presented by Krüger (1985) and more recently Krüger et al. (1992).

The *To-From Matrix* method (Haibach et al., 1976; Dowling and Thangjitham, 1987; Fash et al., 1989) requires information concerning the transition behavior between adja-

cent peaks and valleys. Similar to the rainflow matrix method of reconstruction, the load history is discretized into a convenient number of levels. The time series for peaks and valleys is regenerated using the To-From Matrix without considering the intermediate points. This method provides an identical number of peaks and valleys as of the original history but results in different rainflow cycles and sequence of the original loading.

2.1.2 Methods of Modeling Complete Histories

These methods are concerned with the descriptions of random loadings based on correlation theory. For these techniques, a model is formed which becomes a substitute for the data, this leads to a concise description with few parameters. A model may be defined either in the time or frequency domain.

A commonly used method proposed by Yang (1972) represents the random data by its power spectral density, i.e., the distribution of the power of the process over frequency. Wirsching and Shehata (1977) used this type of simulation, also known as the PSD method, and verified experimentally its suitability. Therefore, it is generally accepted that if the power spectral density of the model matches the data, a successful reconstruction can be obtained.

Approaches in the time domain include the Markov method, which is based on a random process that has a single step memory, i.e. the current value of the process depends only on the previous value. Transition probabilities for any two adjacent points are de-

duced from the original history. This method is particularly successful for processes which contain only correlation between two adjacent points. An extension to this method is shown by Sørensen and Brincker (1989) who derive a reconstruction method yielding only extreme values.

A more general class of time series models called Autoregressive Moving Average (ARMA) models also have been used in fatigue load modeling. These models in essence match the spectral content of data to any desired degree. Moreover, they lead to concise descriptions and operate in the time domain, allowing for efficient load reconstruction. Figure 1 (Dowling et al., 1992) shows a typical stationary random load history and reconstructions using the Power Spectral Density method, an ARMA model, the To-From method, and the Rainflow Matrix method.

2.1.3 Fatigue Damage Estimation without Simulation

The most accurate procedure for fatigue analysis is to simulate a time history, identify rainflow cycles, and then using a damage accumulation model, calculate fatigue life. However, because this procedure is lengthy and requires many simulations to obtain an accurate estimate, considerable effort has been made to estimate fatigue damage without simulating time series.

Commonly used models for the description of the loading are the power spectral density function (Wirsching and Haugen, 1973; Wirsching and Light, 1980; Wu and Huang, 1993) and the Markov process (Krüger and Petersen, 1985; Frendahl and Rychlik, 1993). The distribution functions of rainflow cycles can also be estimated without simulating time series. For the case of a Markov process, contributions are due to Rychlik (1989)

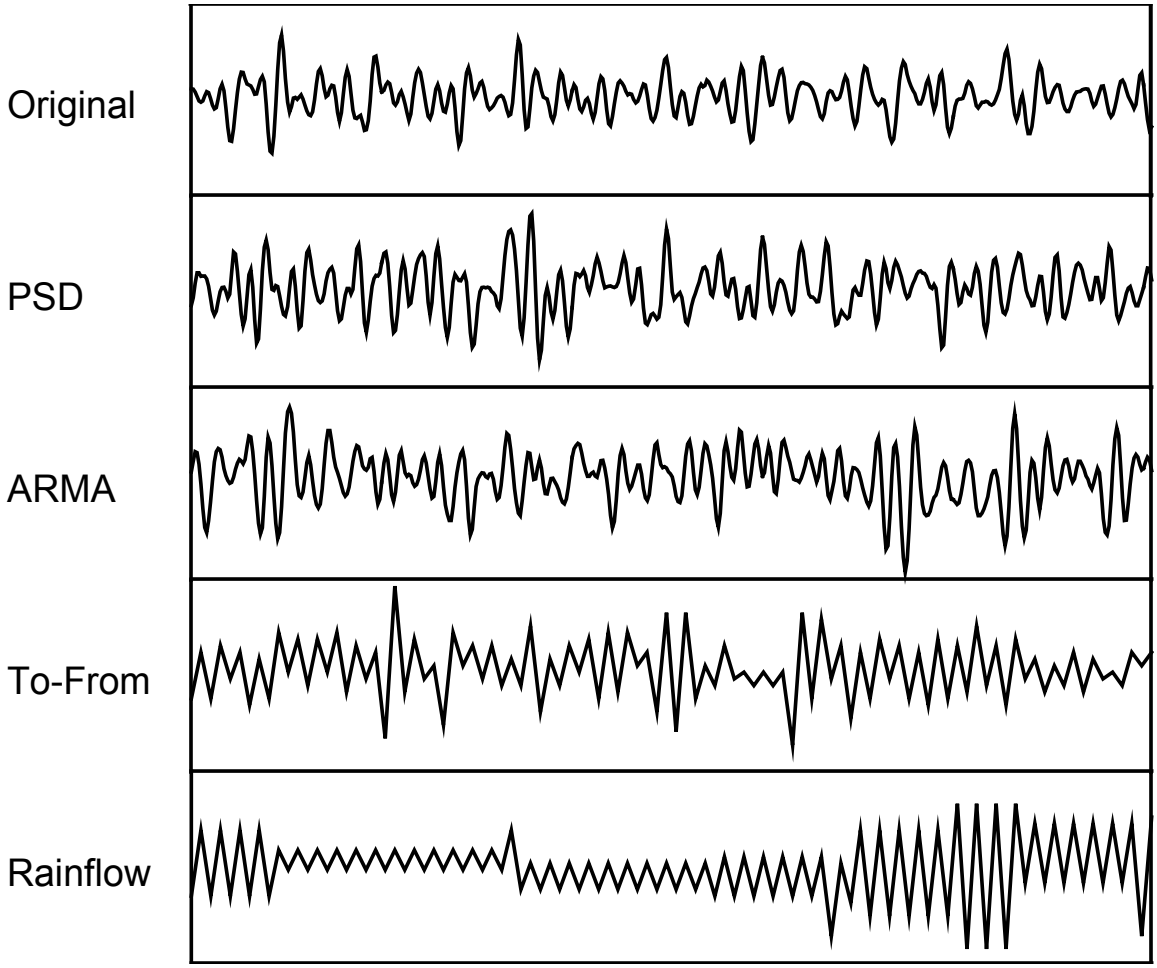

Figure 2.1. Portion of an original fatigue loading history and typical reconstructions by PSD, ARMA, To-From, and Rainflow method, respectively.

and Bishop and Sherratt (1990) and for general Gaussian loads due to Rychlik (1992).

2.2 ARMA Models in Structural Dynamics

Autoregressive models were introduced by Yule (1927) in the context of modeling sun-spot activity. Slutzky (1927) was the first to use moving average models to detect cyclical trends in economic time series. Bartlett (1946) noted the important relationship between ARMA models and systems characterized by linear differential equations. A linear system sampled at discrete points in time will lead to a time series that is identical to one obtained from an appropriate ARMA model. The book *Time Series Analysis Forecasting and Control* by Box and Jenkins (1970 and 1976) unified different approaches to ARMA model building and has become the standard reference. Applications to engineering problems using ARMA models have appeared in an increasing number since the early 1970's.

Efficiency with respect to storage requirement and regeneration effort and the equivalence of an ARMA model and the response of a linear elastic system to random loads led to the use of ARMA models in the field of stochastic structural mechanics. In particular, the estimation of the response of randomly excited linear systems and the simulation of load records have received attention. Random load modeling using ARMA models has traditionally been concentrated in the fields of earthquake-, wind-, and ocean-engineering.

Gersch et al. (1973) obtained estimates of the period and damping values of a linear multi-degree-of-freedom structure from random load histories via an ARMA model. Pi and Mickelborough (1988) identified modal parameters of a structure from load records using ARMA models. Li and Kareem (1990) obtained the response of a linear system

excited by a forcing function formulated as an ARMA model. An emerging technique in random vibration analysis called Monte Carlo simulation requires a large number of records of random loads to obtain reliable response estimates. Spanos and Mignolet (1989) review at length the literature on ARMA models for Monte Carlo studies.

Methods for efficient simulation of random processes have been presented by Samaras et al. (1985), Mignolet and Spanos (1987), and Spanos and Mignolet (1987) for the univariate case. Methods for modeling multivariate time series are due to Gersch and Yonemoto (1977) and Tiao and Box (1981). Random fields were introduced to ARMA models by Naganuma et al. (1987), with the most recent extensions by Spanos and Mignolet (1992) and Mignolet and Spanos (1992).

The modeling of a stationary fatigue loading is demonstrated by the matching of a frequency domain target spectrum using an autoregressive model by Lin and Hartt (1984). An experimental study showing the applicability of autoregressive processes to fatigue load modeling is due to Sarkani (1990). Dowling et al. (1992) and Thangjitham et al. (1993) showed the good agreement of rainflow matrices and fatigue life (both simulated and experimentally obtained) for a typical stationary random ground vehicle loading. Leser et al. (1993) show good agreement of the same measures for a nonstationary record.

For the case of earthquake ground motion modeling, both random variation and nonstationarity are present. The so called Kanai Tajimi spectrum has been developed as representative for the stationary random component of earthquakes. Spanos and Mignolet (1987) developed ARMA models which approximated this target spectrum well. Polhemus and Cakmak (1981), Cakmak and Sherif (1984), and Turkstra et al. (1988) use a stationary ARMA model modulated by a deterministic function to account for the

typical build up and decay of variance in earthquake acceleration time series. The assumption of the earthquake records being piece-wise stationary led Chang et al. (1982) to the method of modeling segments of the record individually by low order ARMA models. Finally, time varying ARMA parameters can be employed to account for the nonstationary nature of the observed series (Nau et al., 1982; Gersch and Kitagawa, 1985; Toki et al. 1985; Deodatis and Shinozuka, 1988). Hoshiya et al. (1988) use an AR model to describe a temporally and spatially propagating earthquake. A review of the literature describing the use of ARMA models in earthquake engineering is due to Kozin (1988).

Wind velocities are simulated using ARMA models in the context of structural design of buildings. The von Karman spectrum is deemed an authentic target spectrum for wind loads. Good approximation to this target spectrum using ARMA models have been obtained by Spanos and Schultz (1985, 1986). A tri-directional wind loading is modeled by Spanos and Mignolet (1987), and wind velocity and air pressure on a cooling tower were represented with an ARMA model by Reed and Scanlan (1983). The extreme values of a wind loading were investigated by Tavares (1977), while Li and Kareem (1990) represented both input and output of the model of a wind loaded structure by ARMA models.

The simulation of wave kinematics is important in ocean engineering. The so called Pierson Moskowitz (P-M) spectrum is often used as a realistic target to verify simulations. Spanos (1983) shows pure autoregressive, moving average, and ARMA models which agree with the P-M spectrum. Spanos and Mignolet (1987) and Mignolet and Spanos (1988) demonstrate an ARMA model obtained via pure AR or MA models respectively, which almost perfectly matches this spectrum. Other contributions to the modeling of wave elevation are due to Holm and Hovem (1979), Houmb and Overvik (1981) and Fines et al. (1981).

Textbooks covering model order and parameter estimation techniques and practical applications of ARMA models have appeared since the work by Box and Jenkins (1970, revised 1976) by Chatfield (1980), Pandit and Wu (1983), Brockwell and Davis (1987), Marple (1987), Kay (1988), Wei (1990), and Pandit (1991).

CHAPTER 3. AUTOREGRESSIVE MOVING AVERAGE MODELS

Characteristics regarding estimation and model building for Autoregressive Moving Average, ARMA, models are discussed here. ARMA models are employed in this study to represent the stationary content of random fatigue loading histories as they provide a versatile method for accurate and concise modeling.

3.1 Model Description

According to Box and Jenkins (1976), the dynamic relationship between two sequences y_t and x_t observed at discrete time intervals, $t = 1,\ 2,\ \ldots$, which are related to each other, can be represented by the linear, time invariant, and causal system

$$y_t = \nu_0 x_t + \nu_1 x_{t-1} + \nu_2 x_{t-2} + \ldots = \left(\nu_0 + \nu_1 B + \nu_2 B^2 + \ldots\right) x_t = \nu(B) x_t \tag{3.1}$$

where B is the so called back-shift operator such that $B^i x_t = x_{t-i}$. For brevity, $\nu(B)$, which in general is of infinite order can, often with sufficient accuracy, be efficiently represented by two polynomials, each of lower order than $\nu(B)$, such that $\nu(B) = \Theta(B)/\Phi(B)$. Therefore, Eq. (3.1) can be rewritten as:

$$\Phi(B)y_t = \Theta(B)x_t \tag{3.2}$$

where $\Phi(B) = \left(1 - \phi_1 B - \phi_2 B^2 - \ldots - \phi_p B^p\right)$ and $\Theta(B) = \left(1 - \theta_1 B - \theta_2 B^2 - \ldots - \theta_q B^q\right)$.

When both y_t and x_t are observed time series, for example they present the input and output of a system, the modeling of $\nu(B)$ is referred to as transfer function modeling and $\nu(B)$ is called the linear transfer function. If, however, only y_t is observed due to lack of information or desired simplification of the analysis, one can postulate an input $x_t = e_t$ and determine a transfer function $\nu(B)$ such that:

$$y_t = \nu_0 e_t + \nu_1 e_{t-1} + \ldots = \nu(B)e_t \tag{3.3}$$

where e_t is a Gaussian white noise sequence, i.e. a sequence of independent normally distributed random variables with zero mean and constant variance, σ_e^2, having a power spectral density that is flat over a wide range of frequencies (Bendat and Piersol, 1986). Then, y_t is called the general linear process.

The desire for a parsimonious description of y_t leads to the substitution of $\nu(B)$ with $\left(\Theta(B)/\Phi(B)\right)$ and the observed series, y_t, then can be rewritten as

$$y_t = \frac{\Theta(B)}{\Phi(B)} e_t = \nu(B)e_t \tag{3.4}$$

This leads to the equivalent notations of an ARMA model in backshift operator form

$$\Phi(B)y_t = \Theta(B)e_t \tag{3.5}$$

and in summation notation

$$\sum_{i=0}^{p} \phi_i y_{t-i} = \sum_{i=0}^{q} \theta_i e_{t-i} \qquad \phi_0 = -1, \;\; \theta_0 = -1 \tag{3.6}$$

Therefore, the technique of fitting an ARMA model to an observed sequence of data can be seen as an attempt to transform the observed sequence, y_t, to white noise, e_t, via the inverse transfer function $\nu^{-1}(B) = \Phi(B)/\Theta(B)$.

The two components of an ARMA(p,q) model are the autoregressive part AR(p) defined by $\Phi(B)$ and the moving average part MA(q) given by $\Theta(B)$. The autoregressive and moving average components form individually meaningful models, $\Phi(B)y_t = e_t$ and $y_t = \Theta(B)e_t$ respectively, but it is usually the full ARMA model that leads to the most concise form equivalent to the general linear process of Eq. (3.3). Another characteristic of ARMA models that can be useful in parameter estimation is that an ARMA model of finite order can be represented by an equivalent AR or MA model of infinite order.

There are two important restrictions on the values the ARMA parameters can assume (Box and Jenkins, 1976). The first restriction is with regard to the AR parameters. In order to yield a stable model, i.e. a model leading to a time series that does not become unbounded, the following must hold. The roots of $\Phi(B) = 0$ must lie outside the unit circle of the complex plane. Similarly, a restriction on the MA parameters can be made. In order for the inverted ARMA model, $e_t = (\Phi(B)/\Theta(B))y_t$, to yield bounded output, e_t, the following must hold. The roots of $\Theta(B) = 0$ must lie outside the unit circle of the complex plane. However, one can always transform the MA parameters, such that an invertible model is obtained. While stability is necessary for a model to be used in simulating

stationary series, invertibility is mainly useful in the step of model building and does not have to be satisfied for simulating a time series.

The ARMA model can also be conveniently represented in the frequency domain (Priestley, 1981). The one sided power spectral density, $S(f)$, corresponding to an ARMA(p,q) model is given in a closed form description as a function of the ARMA parameters

$$S(f) = 2\sigma_e^2 \frac{\left|1 - \theta_1 e^{-2i\pi f} - \theta_2 e^{-4i\pi f} - \ldots - \theta_q e^{-2qi\pi f}\right|^2}{\left|1 - \phi_1 e^{-2i\pi f} - \phi_2 e^{-4i\pi f} - \ldots - \phi_p e^{-2pi\pi f}\right|^2} \qquad 0 \le f \le \frac{1}{2} \tag{3.7}$$

where f is the linear frequency and $i = \sqrt{-1}$.

3.2 Vector ARMA Models

For the case where more than one time series needs to be considered a vector ARMA model is introduced. The reason to model time series jointly is to incorporate dependencies among them.

The n-dimensional time series $\mathrm{y}_t = \left[y_t^{(1)} \quad y_t^{(2)} \quad \ldots \quad y_t^{(n)}\right]^T$ is expressed as

$$\sum_{i=0}^{p} \boldsymbol{\phi}_i \mathbf{y}_{t-i} = \sum_{i=0}^{q} \boldsymbol{\theta}_i \mathbf{e}_{t-i} \tag{3.8}$$

in which $\boldsymbol{\phi}_i$ and $\boldsymbol{\theta}_i$ are matrices of order $n \times n$, such as $\left[\phi_{kl}\right]_i$ and $\left[\theta_{kl}\right]_i$ and superscript T indicates the transpose of a vector or matrix. While $\boldsymbol{\phi}_0 = -\mathbf{I}_n$ and $\boldsymbol{\theta}_0 = -\mathbf{I}_n$ are without

loss of generality assumed to be negative identity matrices of order $n \times n$, $\mathbf{e}_t$ is an n-dimensional Gaussian white noise series with zero mean and crosscorrelation according to

$$E\left[\mathbf{e}_r \mathbf{e}_s^T\right] = \mathbf{V}\delta_{rs} \tag{3.9}$$

where $\mathbf{V}$ is a symmetric, positive definite, $n \times n$ covariance matrix of the noise and δ_{rs} is the Kronecker delta. Contemporaneous cross-correlations (correlations between channels) are expressed through off diagonal terms in $\boldsymbol{\phi}_i$ and $\boldsymbol{\theta}_i$, while auto-correlations (correlations within a series) are governed by diagonal terms in $\boldsymbol{\phi}_i$ and $\boldsymbol{\theta}_i$.

Equivalently to the one-dimensional closed form representation of the power spectrum, the spectrum, $\mathrm{S}(f)$, of the n-dimensional process is (Kay, 1988)

$$\mathrm{S}(f) = 2\left[\sum_{j=0}^{p} \boldsymbol{\phi}_j e^{-2i\pi f}\right]^{*^{-1}} \left[\sum_{j=0}^{q} \boldsymbol{\theta}_j e^{-2i\pi f}\right]^{*} \mathrm{V} \left[\sum_{j=0}^{q} \boldsymbol{\theta}_j e^{-2i\pi f}\right]^{T} \left[\boldsymbol{\phi} \sum_{j=0}^{p} \mathrm{f}_j e^{-2i\pi f}\right]^{T^{-1}} \tag{3.10}$$

with $0 \le f \le 1/2$ and where * indicates the complex conjugate of a matrix.

3.3 Parameter Estimation

Statistical inference of ARMA parameters from observed data may be performed either through maximum likelihood estimators or through moment estimators. Both techniques yield efficient, unbiased and consistent estimates. However, the maximum likelihood estimation leads to nonlinear equations with possibly more than one relative maximum (Kay, 1988). The nonlinearities are so severe that the commonly used Newton-Raphson

(Akaike, 1973) approach will not always converge to a solution. Therefore, approximate procedures in linear form based on the method of moments estimators are often used. Two principal methods coexist using an intermediate approximate model either of pure autoregressive or pure moving average type. These methods, while approximate in nature, will converge to the statistically optimal maximum likelihood estimates for estimations based on long time series (Kay, 1988).

Using the autocorrelation function of the given data, a large order AR model can be built, which is assumed to be a reliable approximation of the target spectrum. The autoregressive parameters can be estimated via a system of linear equations. The parameters of the desired ARMA model are arrived at by minimizing the difference between the transfer functions of the pure AR model and of the ARMA model. The two stage least square procedure, as introduced by Theil (1958) and applied to ARMA modeling by Durbin (1960), provides the means for the minimization. Algorithms are described for one dimensional ARMA models by Gersch and Liu (1976) and Gersch and Yonemoto (1977), for multidimensional cases by Samaras et al. (1985) and for modeling random fields by Mignolet and Spanos (1992).

For the case of multidimensional time series, a similar two stage parameter estimation technique, going from a pure MA model to an ARMA model, has been proposed by Spanos and Mignolet (1990) and has been extended to the random field case by Spanos and Mignolet (1992).

The procedure by Samaras et al. (1985) for multi-dimensional ARMA models is chosen in this study for its numerical efficiency. An analogous procedure for single channel

estimation is presented by Gersch and Liu (1976). However, the algorithms shown are for the special case where autoregressive and moving average part are of the same order. Therefore, to allow for more flexible modeling, the method was extended to the general case where both parts may be of different order. This generalized algorithm is reviewed in the following.

To estimate the ARMA parameters for the vector time series, $\mathbf{y}_t$, shown in Eq. (3.8) the target crosscorrelation matrices $\mathrm{C}_{yy}(k)$ will be used, where

$$\mathrm{C}_{yy}(r-s) = E\left[\mathrm{y}_r \mathrm{y}_s^T\right] \tag{3.11}$$

However, knowledge of $\mathrm{C}_{ye}(-k)$ for $(k = 0, 1, \ldots, q)$ will also be required and is therefore derived first, the so called first stage, via a large order AR model. An AR model of infinite order is defined as,

$$\sum_{i=0}^{\infty} \widetilde{\boldsymbol{\phi}}_i \mathbf{y}_{t-i} = -\mathbf{I}_m \mathbf{e}_t \tag{3.12}$$

where $\widetilde{\boldsymbol{\phi}}_o = -\mathbf{I}_m$ and $\widetilde{\boldsymbol{\phi}}_i$ are the autoregressive parameters to be inferred from $\mathbf{y}_t$. This description via an AR model is equivalent to the ARMA model of Eq. (3.8) and will also possess the same cross-covariance matrix, $\mathrm{C}_{ye}(k)$. Therefore, by post-multiplying both sides of Eq. (3.12) by $\mathbf{y}_{t-k}^T$, taking the expectation, and making use of

$$E\left[\mathrm{e}_t \mathrm{y}_{t-k}^T\right] = \mathrm{C}_{ey}(-k) = 0 \quad \text{for} \quad k > 0 \tag{3.13}$$

the following is obtained

$$\sum_{i=0}^{\infty} \widetilde{\phi}_i \mathrm{C}_{yy}(i-k) = 0 \quad \text{for} \quad k > 0 \tag{3.14}$$

Rewriting Eq. (3.14) in matrix from leads to the so called *Yule-Walker* equations

$$\begin{bmatrix} \widetilde{\phi}_1 & \widetilde{\phi}_2 & \dots \end{bmatrix} \begin{bmatrix} \mathrm{C}_{yy}(0) & \mathrm{C}_{yy}^T(1) & \mathrm{C}_{yy}^T(2) & \dots \\ \mathrm{C}_{yy}(1) & \mathrm{C}_{yy}(0) & \mathrm{C}_{yy}^T(1) & \dots \\ \mathrm{C}_{yy}(2) & \mathrm{C}_{yy}(1) & \mathrm{C}_{yy}(0) & \dots \\ \dots & \dots & \dots & \dots \end{bmatrix} = \begin{bmatrix} \mathrm{C}_{yy}^T(1) & \mathrm{C}_{yy}^T(2) & \dots \end{bmatrix} \tag{3.15}$$

In practice, it is necessary to truncate the infinitely long expression of Eq. (3.15) to an approximate relationship such as

$$\begin{bmatrix} \widetilde{\phi}_1 & \widetilde{\phi}_2 & \dots & \widetilde{\phi}_P \end{bmatrix} = \begin{bmatrix} \mathrm{C}_{yy}^T(1) & \mathrm{C}_{yy}^T(2) & \dots & \mathrm{C}_{yy}^T(P) \end{bmatrix} \begin{bmatrix} \mathrm{C}_{yy}(0) & \mathrm{C}_{yy}^T(1) & \dots & \mathrm{C}_{yy}^T(P-1) \\ \mathrm{C}_{yy}(1) & \mathrm{C}_{yy}(0) & \dots & \mathrm{C}_{yy}^T(P-2) \\ \vdots & \vdots & \ddots & \vdots \\ \mathrm{C}_{yy}(P-1) & \mathrm{C}_{yy}(P-2) & \dots & \mathrm{C}_{yy}(0) \end{bmatrix}^{-1} \tag{3.16}$$

If a sufficiently large value for P is chosen, the AR model will provide a good approximation to the ARMA model of Eq. (3.8). In order to obtain values for $\mathrm{C}_{ye}(-k)$, Eq. (3.12) is post-multiplied by $\mathbf{e}_t^T$, $\mathbf{e}_{t-1}^T$, … , $\mathbf{e}_{t-p}^T$ respectively, and after taking expected values one obtains

$$\mathrm{C}_{ye}(0) = \mathrm{V} \tag{3.17}$$

and

$$-\mathrm{C}_{ye}(-k)+\sum_{i=1}^{k}\widetilde{\phi}_i\mathrm{C}_{ye}(i-k)=0 \quad \text{for} \quad k=1,2,\ldots,q \tag{3.18}$$

where use has been made of the relation

$$\mathrm{C}_{ye}(k)=0 \quad \text{for} \quad k>0 \tag{3.19}$$

which states that the model is causal, i.e. current observations are independent of future noise input.

In order to obtain the matrix $\mathbf{V}$, both sides of Eq. (3.12) are post-multiplied by $\mathbf{y}_t^T$ and the expectation is taken, leading to

$$\sum_{i=0}^{P}\widetilde{\phi}_i\mathrm{C}_{yy}(i)=-\mathrm{C}_{ey}(0) \tag{3.20}$$

If Eq. (3.17) is substituted into Eq. (3.20), it yields

$$\mathrm{V}^T=-\sum_{i=0}^{P}\widetilde{\phi}_i\mathrm{C}_{yy}(i) \tag{3.21}$$

Using Eqs. (3.17) and (3.18) the crosscorrelation matrices $\mathrm{C}_{ye}(0)$, $\mathrm{C}_{ye}(-1)$, ... , $\mathrm{C}_{ye}(-q)$ can be obtained recursively.

Now the parameters $\boldsymbol{\phi}_i$ and $\boldsymbol{\theta}_i$ in the ARMA model may be determined in the second stage of the estimation. Rewriting Eq. (3.8) as

$$\mathbf{y}_t = \left[\boldsymbol{\theta}_1 \quad \dots \quad \boldsymbol{\theta}_q \quad \boldsymbol{\phi}_1 \quad \dots \quad \boldsymbol{\phi}_p\right]\left[-\mathbf{e}_{t-1} \quad \dots \quad -\mathbf{e}_{t-q} \quad \mathbf{y}_{t-1} \quad \dots \quad \mathbf{y}_{t-p}\right]^T + \mathbf{e}_t \tag{3.22}$$

and post-multiplying both sides of equation (3.22) by the matrix $\left[-\mathbf{e}_{t-1}^T \quad \dots \quad -\mathbf{e}_{t-q}^T \quad \mathbf{y}_{t-1}^T \quad \dots \quad \mathbf{y}_{t-p}^T\right]$ and taking the expectation, the following relation is obtained

$$\begin{aligned}\left[-\mathrm{C}_{ye}(-1) \quad \dots \quad -\mathrm{C}_{ye}(-q) \quad \mathrm{C}_{yy}^T(1) \quad \dots \quad \mathrm{C}_{yy}^T(p)\right] \\ = \left[\theta_1 \quad \dots \quad \theta_q \quad \phi_1 \quad \dots \quad \phi_p\right]\mathrm{D}\end{aligned} \tag{3.23}$$

where **D** is defined as

$$\mathrm{D} = \left[\begin{array}{ccc:ccc} \mathrm{V} & \dots & 0 & -\mathrm{C}_{ye}^T(0) & \dots & 0 \\ \vdots & \ddots & \vdots & \vdots & \ddots & \vdots \\ 0 & \dots & \mathrm{V} & -\mathrm{C}_{ye}^T(1-q) & \dots & -\mathrm{C}_{ye}^T(p-q) \\ \hdashline -\mathrm{C}_{ye}(0) & \dots & -\mathrm{C}_{ye}(1-q) & \mathrm{C}_{yy}(0) & \dots & \mathrm{C}_{yy}(p-1) \\ \vdots & \ddots & \vdots & \vdots & \ddots & \vdots \\ 0 & \dots & -\mathrm{C}_{ye}(p-q) & \mathrm{C}_{yy}(p-1) & \dots & \mathrm{C}_{yy}(0) \end{array}\right] \tag{3.24}$$

which can be solved for the ARMA parameters

$$\begin{aligned}\left[\theta_1 \quad \dots \quad \theta_q \quad \phi_1 \quad \dots \quad \phi_p\right] \\ = \left[-\mathrm{C}_{ye}(-1) \quad \dots \quad -\mathrm{C}_{ye}(-q) \quad \mathrm{C}_{yy}^T(1) \quad \dots \quad \mathrm{C}_{yy}^T(p)\right]\mathrm{D}^{-1}\end{aligned} \tag{3.25}$$

This concludes the derivation of the estimation algorithm. It is seen that two sets of linear equations need to be solved in order to estimate ARMA parameters for the observed vector time series, $\mathbf{y}_t$.

3.4 Model Building

The interpretation of an ARMA model as the transfer function that transforms an observed series to white noise is underlying all criteria for model order determination found in the literature. ARMA models for various values of (p,q) are fitted to the data and the appropriate model is sought through criteria based on the residuals, e_t, obtained from $e_t = \Phi(B)/\Theta(B)\, y_t = \nu^{-1}(B) y_t$. In essence, these criteria state that the proper model has been found when the series of residuals, e_t, is *close* to white noise. Where *closeness* is measured by some statistical criterion.

Some commonly used criteria are *Akaike's Information Criterion*, *AIC*, (Akaike, 1974) which investigates the relation of a weighted sum of the variance of the residuals and the model order. Pandit (1973) uses a test based on the *F*-distribution to compare the variance of residuals for competing models. Finally, Box and Jenkins (1976) introduced a measure called the *Q-statistic* that indicates proper model order through measuring the autocorrelation of the residuals.

Most time series literature is concerned with series that contain 50 to 500 observations. For such short records a statistical test will lead to an ARMA model with orders p and q well below hundred, in fact, often below ten. For the case where the observed series is much longer, say of order 10^4 to 10^5, however, any statistical test will be restrictive and demand ARMA models of very large order.

Therefore, a new criterion for model order determination is presented that is based on the comparison of the observed time series and the time series obtained from a proposed

model. The advantage of this scheme is that a more concise model will be obtained than would be if any of the above mentioned methods was chosen. This is particularly true for the case where one needs to find an ARMA model for a large data set.

After the parameters for a number of ARMA models are estimated, a preliminary selection is made based on the closeness of the power spectrum of an ARMA model to the spectrum of the original loading. A generally applicable measure of association between two variables is provided through the correlation coefficient. For two random variables, x and y, the correlation coefficient is defined via the covariance, $\mathrm{cov}(x,y)$, and standard deviations, σ_x and σ_y, as (Miller and Freund, 1977)

$$r_{xy} = \frac{\mathrm{cov}(x,y)}{\sigma_x \sigma_y} \tag{3.26}$$

while an estimator is obtained as

$$\rho_{xy} = \frac{\sum_{i=1}^{N}(x_i - \bar{x})(y_i - \bar{y})}{\sqrt{\sum_{i=1}^{N}(x_i - \bar{x})^2 \sum_{i=1}^{N}(y_i - \bar{y})^2}} \tag{3.27}$$

where x_i and y_i are sample points and $\bar{x}$ and $\bar{y}$ are estimators for the mean of the respective variables and N is the number of sample points. This definition implies that $-1 \le \rho_{xy} \le 1$ and for $\rho_{xy} = 0$ observations of x and y are uncorrelated, while for $\rho_{xy} = 1$ they are identical. In general, the nearer the value of ρ_{xy} to unity, the closer the resemblance between the two.

The closeness of the power spectrum, $S(f)$, of the original loading to the one obtained from an ARMA model is therefore measured by their respective correlation coefficient, $\rho_S^{(p,q)}$. The model with the smallest number of parameters at a given correlation level, e.g. $\rho_S^{(p,q)} = 0.8$, $\rho_S^{(p,q)} = 0.9$, etc., is chosen for further study. This allows ruling out a large number of models due to their lack of matching the dynamic characteristics of the original record. The final model selection is based on a comparison of fatigue lives obtained for the original loading and a loading reconstructed using the ARMA model corresponding to a particular correlation level. A criterion for this comparison is introduced in Chapter 4. Unlike the rest of the time series literature, this study ties the step of model building directly to the application of the simulated time series.

3.5 Nonstationarity and ARMA Models

In many cases of structural dynamics the loadings are of nonstationary nature. The two most common parameters to change with time are the mean value and the variance. Nonstationarity with respect to the mean value is handled through subtraction of the presumed mean variation. This subtraction is commonly referred to as *detrending* (Box and Jenkins, 1976) and is usually the first step in any time series analysis. ARMA models are inherently stationary descriptions of random processes. However, attempts have been made to apply them to cases which involve nonstationarities, particularly for the case where the variance changes over time. This is due to the fact that ARMA models were originally applied to earthquake loadings, which are inherently nonstationary with respect to their variance.

One method used for handling such nonstationarity is to divide the observed loading into segments which can be considered stationary (Chang et al., 1982). An ARMA model

then is fitted to each segment. This approach works well if it is clear how to decide on the length of the segment. Applications concerned with modeling earthquake loadings have used this method successfully because the variance changes in a characteristic manner, similar for all earthquakes. However, this approach is problematic in the case of rapidly changing values of variance since the segment to be considered stationary needs to be short, but it is difficult to obtain a reliable estimate of the ARMA parameters if the series is short.

Another approach is to estimate ARMA parameters that vary in time. This includes the parameters describing the autoregressive part, the moving average part and the variance of the input white noise sequence (Gersch and Kitagawa, 1985, Nau et al., 1982). It is often difficult, however, to obtain reliable estimates for such parameters, particularly when only a limited amount of data is available.

A third approach, chosen in this study, is to estimate a scaling function, s_t, which will model the nonstationarity with respect to variance. The function s_t is inferred from the observed record, x_t, such that the quotient, x_t/s_t, is stationary with respect to variance (Hsu and Hunter, 1976; Polhemus and Cakmak, 1981; Nau et al., 1982).

3.6 Justification for the Use of ARMA Models

There are four desirable characteristics of ARMA models that make them suitable for application to random fatigue loadings of dynamically loaded structures:

First, the ARMA model framework allows for systematic direct analysis of discretized

load records sampled at equidistant time intervals. The complete cycle of model building and parameter estimation can be performed without additional knowledge of the underlying dynamics of the system. Therefore, a load model can be obtained on an empirical basis from observed data and regeneration performed by evaluating a system of difference equations. This is in contrast to building a dynamic model of the structure via a system of differential equations, the *equations of motion*, and obtaining response data through numerical integration of this system.

Secondly, there is a theoretical basis for using ARMA models to simulate the sampling of a continuous time random process. Bartlett (1946) stated the physically meaningful interpretation of an ARMA model as the solution of a linear differential equation. Given a linear dynamic system of order *n*, subjected to a white noise forcing function and sampled at equal time intervals, the samples will be identical to those obtained from an ARMA$(n, n-1)$ model given the right parameters ϕ_i and θ_i. This important result provides a link between dynamic systems in discrete time and continuous time. Moreover, the simplicity in forming a time series via an ARMA model is not achieved at the cost of accuracy. The ARMA model correctly accounts for the irregular behavior of the equivalent continuous time process and it is in fact more efficient to simulate a time series via an ARMA model than numerically integrating a differential equation (Nau et al., 1982).

Thirdly, ARMA models lead to the most concise description of a random loading of all proposed methods. The level of reduction is due to the fact that the actual data are replaced by a model instead of being summarized through some counting method. No arbitrary level of discretization needs to be imposed as necessary for the counting methods. It

is rather the observed data and its inherent correlation structure that will dictate the necessary number of parameters for an accurate description. An observed record of theoretically infinite length can be characterized by a number of parameters that is usually much less than one-hundred and often in the range of five to twenty-five (all references in the literature review fall into this range). This is in contrast to the counting methods for which the storage requirement depends on the desired resolution. Typically, rainflow matrices are of size 32x32 or even 64x64, which translates into storage requirements of 1024 or 4096 parameters, respectively.

Finally, the reconstruction of random load records is extremely efficient. Regeneration merely involves the backward calculation of a difference equation of low order. This is in contrast to the power spectral density method, for which, for each point in the time series to be generated, all frequency components need to be used via a discrete inverse Fourier transform. While this process has become more efficient since the introduction of the *Fast Fourier Transform* (Cooley and Tukey, 1965), it still requires more calculations than an ARMA reconstruction. Moreover, truly randomly distributed records are obtained, whereas for the case of Rainflow reconstruction no clear method has evolved to achieve this. This is particularly true for the case where more than one variable needs to be considered, since it is physically not clear what constitutes a cycle for the case of multiaxial loading.

On the other hand, ARMA models are problematic in their application to fatigue loadings for the following reasons:

The procedure of model building and parameter estimation is not straightforward but rather iterative.

Moreover, practical estimation procedures are necessarily approximate. Model order determination and handling of nonstationarity are areas of current research and have not been resolved entirely, particularly for the multidimensional case.

For the case of fatigue load modeling it is necessary only to obtain time series that consist of extreme values only. ARMA models, however, generate time series that contain extremes and intermediate points necessitating removal of the intermediate points prior to some application.

CHAPTER 4. FATIGUE LIFE CALCULATION

Fatigue calculations as used in this study are presented here. The first in depth study on fatigue is due to Wöhler (1858) who investigated failures in railroad axles. Research in the area is still active till today, because the actual phenomenon of fatigue is still not quite understood.

Failure due to fatigue occurs in two stages. The first stage is the so called initiation stage, i.e., the time it takes for the loaded component to show a detectable, *engineering size*, crack. The second stage is the crack growth stage, i.e. the time it takes for the initial crack to grow until final failure of the component occurs. This study will consider only the life of the component until an initial crack occurs, the so called initiation life.

Today two approaches dominate the analysis of predicting fatigue life until the initiation of cracks. The so called stress based approach as introduced by Wöhler (1858) analyzes stresses in the component under study. It is still the most popular method in fatigue analysis due to its simplicity and overall reliability. The so called local strain approach, was developed in the late 1950's through early 1960's (e.g. Coffin and Tavernelli, 1959; Manson, 1965), an overview is being provided by Dowling et al. (1977). The strain based approach concerns itself with the plastic strains occurring at the point in the material under investigation. Both the local strain and stress based approaches relate the fatigue life of a component to the applied loads through a strain or stress versus life curve. This

curve relates the number of cycles to failure for a given stress or strain range, where the term cycle refers to a complete reversal of stress or strain, and the range is twice the amplitude of this reversal. Most materials will deform plastically under cyclic loading, and this plastic deformation will induce hysteresis loops, causing fatigue damage.

Cycle counting refers to the analysis of spectrum loadings to identify damaging hysteresis loops. A variety of methods, such as peak counting, range counting, and level crossing counting have been proposed to count cycles, but the *rainflow counting method* introduced by Endo et al. (1974) is now the most widely accepted; see also ASTM (1987).

The term *cumulative damage* was introduced to account for fatigue due to loadings where not all cycles have the same range. This type of general irregular loading is often referred to as a *spectrum loading*. The damage caused by a single cycle is the inverse of the number of cycles to failure. To calculate the total damage for an irregular loading a variety of damage accumulation rules exist, e.g. Manson et al., 1967; Miller and Zachariah, 1977; Hashin and Rotem, 1978. The Palmgren (1924, 1945) - Miner (1945) rule, which asserts that fatigue failure occurs when the summation of damage of all cycles reaches unity, is the best available method, Schütz (1976) concluded. This simple rule works satisfactorily according to Dowling (1972) if care is taken with respect to cycle counting, mean stress effect of the loading, and overstrain effects.

4.1 Uniaxial Case

Loading situations where the applied load causes proportional stressing are the most widely studied. It is for this situation, such as bending, or tension, or torsion, that the lo-

cal strain approach was developed. The local strain approach assumes that fatigue damage is controlled by the surface strain at a critical location such as a notch. After performing a rainflow cycle count on the loading histories, there are two possible approaches. They are the so called *full* analysis, which takes actual mean stresses into account, and the so called *bounded* life calculation, which does not consider actual mean stresses, but places physically meaningful bounds on the expected life.

Usually, the first step in the local strain approach is to convert the given nominal stress to a local notch stress-strain response. This is achieved through elastic plastic analysis incorporating the geometry of the specimen and is well established in the literature, e.g. Bannantine et al. (1990), Dowling (1993), Fuchs and Stephens (1980), and Socie (1977). In this study, however, the issue of obtaining the local stains is avoided by assuming that the recorded loading histories are the surface strain at some critical location. Local stresses, therefore, can be obtained directly from local strains using the cyclic stress-strain curve.

If the loading history is assumed to repeat itself, the resulting stress-strain hysteresis loops will consist of one major cycle due to the extreme peak and valley in the history and all remaining minor cycles will lie inside the major cycle. A typical stress strain response for the major and a minor cycle is shown in Fig. 4.1.

To perform the fatigue life calculation, it is necessary to have the stable (half-life) cyclic stress-strain curve (Landgraf et al., 1969) and the strain-life curve for the material, i.e.,

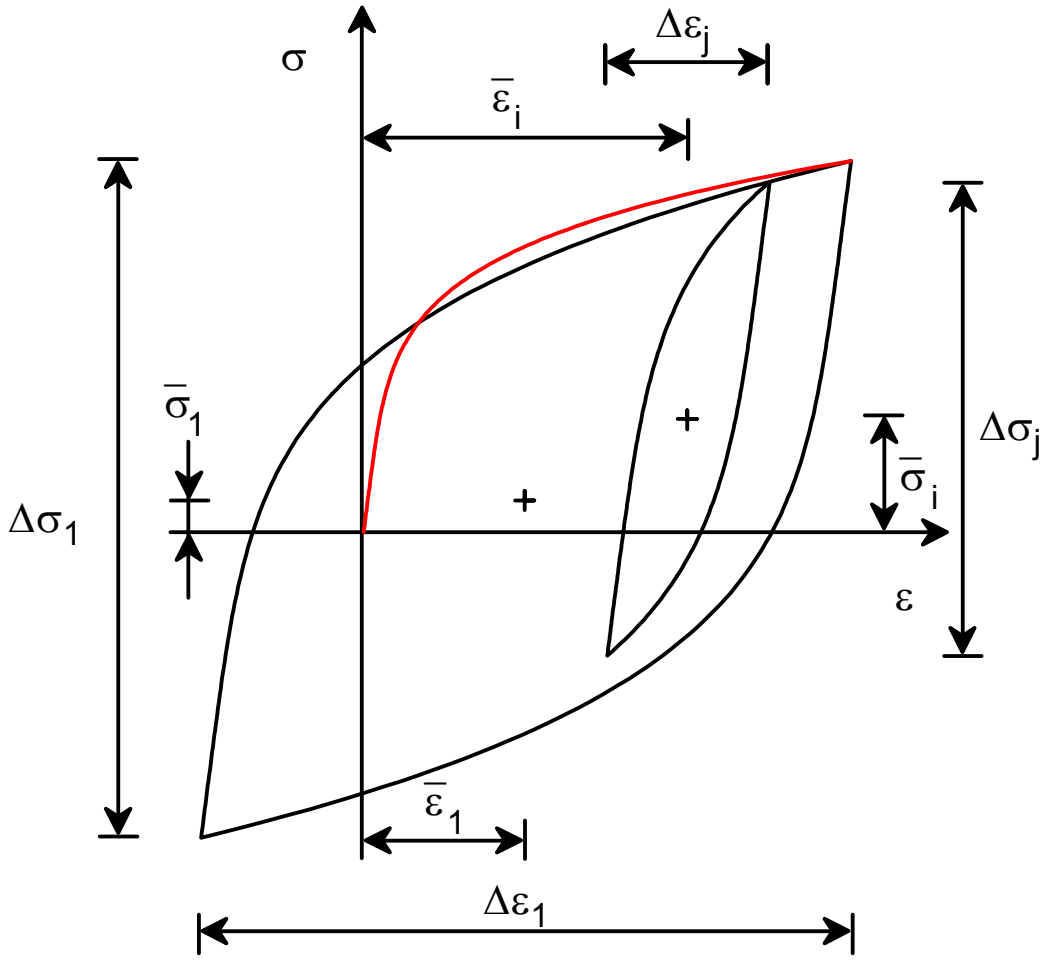

Figure 4.1. Outermost, L_{11}, and a typical inner, L_{ij}, stress-strain hysteresis loop.

$$\varepsilon_a = \frac{\sigma_a}{E} + \left(\frac{\sigma_a}{H'}\right)^{\frac{1}{n'}} \tag{4.1}$$

$$\varepsilon_a = \frac{\sigma'_f}{E}(2N_0)^b + \varepsilon'_f(2N_0)^c \tag{4.2}$$

where ε_a and σ_a are the strain and stress amplitudes, respectively, E is the elastic modulus, N_0 is the life in cycles for the case of zero mean stress, and the remaining quantities, ε'_f, σ'_f, H', n', b, and c are material constants obtained from curve fitting experimentally obtained fatigue stress-strain-life data.

The effect of mean stress $\overline{\sigma}$ on life may be estimated, for example according to Morrow (1968) using the following relation

$$N = N_0\left(1 - \frac{\overline{\sigma}}{\sigma'_f}\right)^{-\frac{1}{b}} \tag{4.3}$$

where N is the life in cycles for the case of nonzero mean stress.

A particular rainflow cycle, C_{ij}, which forms a closed local stress-strain hysteresis loop, L_{ij}, such as the one shown in Fig. 4.1, with means, $\overline{\sigma}_i$ and $\overline{\varepsilon}_i$, and ranges, $\Delta\sigma_j$ and $\Delta\varepsilon_j$, causes damage, D_{ij}. According to the Palmgren-Miner rule, the damage, D_{ij}, is defined as

$$D_{ij} = \frac{n_{ij}}{N_{ij}} \tag{4.4}$$

where n_{ij} and N_{ij}; i, j = 1, 2, ... , M , are the numbers of cycles counted and the number of cycles to failure (life) for the given cycle, C_{ij}, respectively, and M is the number of equal class intervals the loading range was divided into. The component life, N_B, is then calculated from the induced damage due to $\sum_{i=1}^{M}\sum_{j=1}^{M} n_{ij}$ rainflow cycles as

$$N_B = \left(\sum_{i=1}^{M}\sum_{j=1}^{M} D_{ij} \right)^{-1} \tag{4.5}$$

where N_B is given in terms of the number of blocks (repetitions) of the load history.

4.1.1 *Full* Analysis

For the case where the complete loading history is available and assumed to repeat itself continuously, the history may be reordered to start with the highest absolute value of strain. This reordering simplifies the subsequent calculation of stress and strain for each cycle significantly. Using Eqs. (4.1)-(4.3), the fatigue life for each cycle formed can be calculated, where it is possible to detect mean stress and strain for each cycle and account for their influence on fatigue life accurately. This leads to the most accurate analytical life prediction currently available (MTS Systems, 1991).

4.1.2 *Bounded* Life Calculation

When the load history is reduced to a rainflow matrix, information regarding the sequence of loading is lost despite the fact that this sequence may affect fatigue life. Socie et al. (1979), therefore, motivated the idea to put bounds on the expected life of a

component subjected to loadings reconstructed from rain-flow matrices. Conle and Landgraf (1983) submitted a complete solution to this problem, Dowling and Khosrovaneh (1989) and Khosrovaneh (1989) provided more detail.

Cycles that are identified by their range and mean value in strain then permit one to place bounds on the possible local mean stress for the sub-cycle, as shown in Fig. 4.1 for the lower bound, and in Fig. 4.2 for the upper bound. Similar bounds may be placed on the local mean stresses for all rainflow subcycles. These can then be used in two separate life calculations based on Eqs. (4.1)-(4.3). These bounds represent the extremes in life from all possible sequence that could be reconstructed from a rainflow matrix. A life prediction according to the full analysis, will, therefore, always fall within these bounds. It should be noted that these bounds are usually reasonably close and give life predictions that are well within the scatter of experimentally obtained results. Moreover, for low strain levels, i.e. at long lives, the damage induced by small cycles becomes insignificant. It is the major cycle which determines almost entirely the resulting fatigue life. The mean stress of the major cycle is properly accounted for and, therefore, the bounds will converge to each other as the strain level is lowered.

4.1.3 Criterion to Compare Uniaxial Fatigue Lives

In Chapter 3 it was shown that a criterion to compare the closeness of two records with respect to their fatigue lives is needed. The *bounded* life calculation places physically meaningful bounds on the life of a component. If this calculation is applied to an original loading, a possible criterion is to demand that any reconstructed loading has a life, calculated according to the full analysis, which is (nearly) inside these bounds.

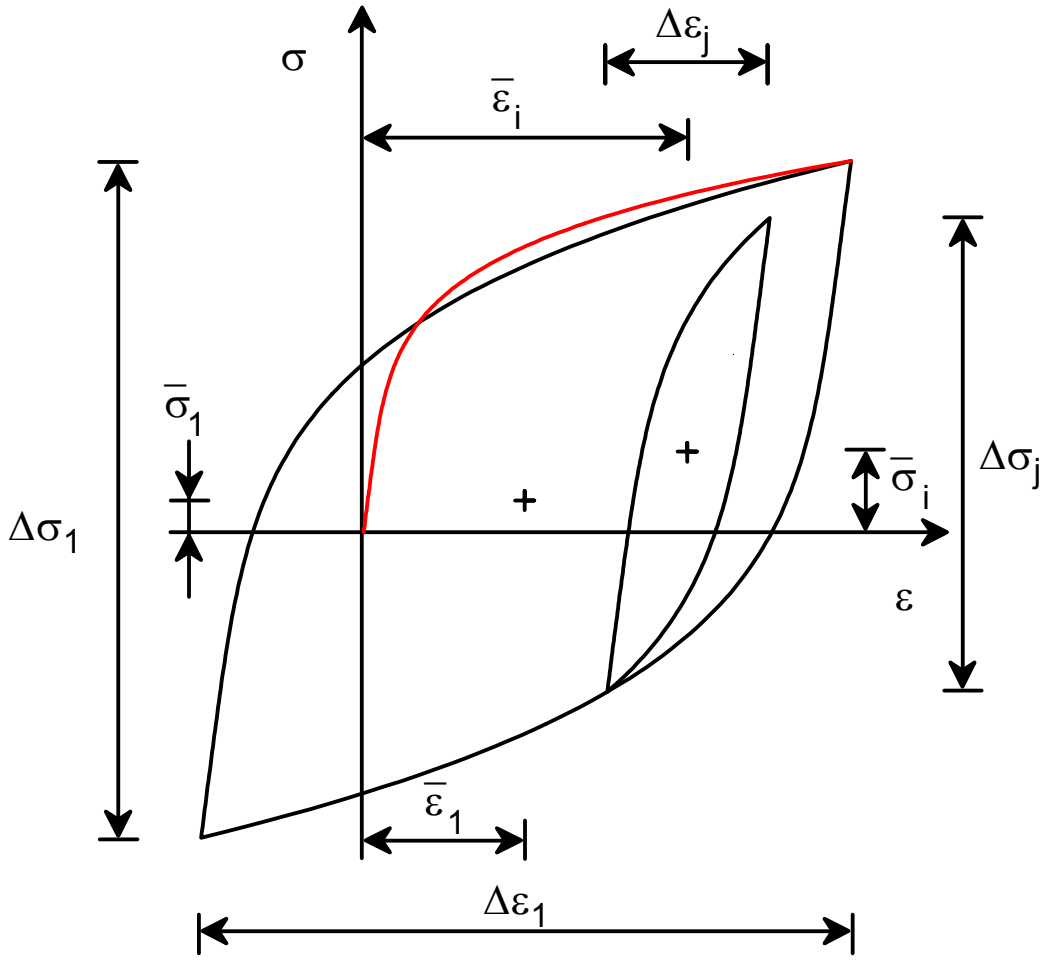

Figure 4.2. Outermost, L_{11}, and the inner, L_{ij}, stress-strain hysteresis loop corresponding to upper bound of loop in Fig. 4.1.

4.2 Multiaxial Case

Multiaxial stress or strain states occur when the loading on the structure is in more than one direction, or when the geometry of the component is complex. Fatigue life calculations for a multidimensional stress or strain state are an area of current research. No single method has emerged as a reliable analysis tool to predict fatigue life and correlate test results. Rather three different approaches are pursued and reviewed by Leese (1988).

The first method uses an energy based criterion to identify the amount of plastic work required to cause fatigue failure (Garud, 1981). While this method gives predictions which agree with experimental results, it is difficult to integrate this method into design and testing of components. Furthermore, for long life, only little plastic work is involved and the effect is difficult to quantify. Finally, fatigue damage is induced along preferred directions, but an energy approach is a scalar concept thereby ignoring the physical process.

Another approach is based on the effective stress or strain concept as derived from classical theory of yield criteria. This procedure reduces the three dimensional state of stress to an equivalent or effective uniaxial stress. This effective stress then can be used in combination with the uniaxial local strain approach to estimate fatigue life. Brown and Miller (1982) reviewed the different methods in this approach. An advantage of this method is its simplicity, which makes it useful for basic engineering applications. Also, this method gives good predictions in high cycle fatigue, i.e. long life. On the other hand this method performs poorly in the case of nonproportional loading, i.e. where the princi-

pal axes of stress or strain rotate during loading. Moreover, no physical interpretation between the effective stress or strain and the fatigue phenomenon exists.

The third and most recently developed method to model fatigue life is the critical plane approach (Brown and Miller, 1973). This model considers the plane in the material on which the combined shear stress amplitude and mean normal stress, responsible for initiating fatigue, are most severe. Brown and Miller (1985) point out the need for two critical planes to distinguish between crack initiation and crack growth. The critical plane approach yields good agreement between experiment and prediction, even for nonproportional loading. Even though a commonly agreed on criterion for defining the critical plane has not been found, the critical plane approach seems to be the most suitable approach. This is because of its correct physical interpretation of how damage is induced and cracks will actually grow.

4.2.1 Simplified Critical Plane Approach

Juneja (1992) developed a multiaxial fatigue damage model for approximately proportional loading. This model is used in the current study to confirm the agreement in life for multiaxial load reconstructions, and it is therefore briefly reviewed. The analysis, based on the physical interpretation of the fatigue damage process, is conducted by first obtaining the critical fatigue damage orientation. The critical plane is found via a histogram technique, introduced by Bonnen et al. (1991). First, the principal strain vectors, i.e., the principal strain values and their corresponding orientations, with respect to a reference orientation, are obtained for each point in the history. A histogram of the principal strain values and their corresponding orientations is then formed for the entire

history. Since the counts in the histogram represent the number of data points in the history for which a particular combination of principal strain value and respective orientation occurred, the distribution of these counts for a particular principal strain angle indicates the cycling of the strain events for that orientation. The orientation for which the largest spread of principal strain values is covered with the most nonzero values in different bins is chosen to be the critical direction. The fatigue cracks initiate and grow on this critical plane and lead to failure of the component. After selecting the critical plane, the strain history is transformed along and perpendicular to this plane, and these are taken to be the new principal directions.

Two fatigue failure modes are considered. First, an analysis investigating failure due to normal strain on the critical plane is performed. The uniaxial cyclic stress-strain relation of Eq. (4.1) is modified to a similar form

$$\hat{\varepsilon}_a = \frac{\hat{\sigma}_a}{E_n} + \left(\frac{\hat{\sigma}_a}{H'_n} \right)^{\frac{1}{n'_n}} \tag{4.6}$$

where $\hat{\varepsilon}_a$ is the effective strain and $\hat{\sigma}_a$ the effective stress amplitude, respectively. Moreover, the material constants, E, H', and n' of Eq. (4.1) are adjusted to reflect the biaxial state stress state on the critical plane and become E_n, H'_n, and n'_n, respectively.

The modified strain life equation then becomes

$$\hat{\varepsilon}_a = \frac{\sigma'_f}{E} \frac{1-\nu\lambda}{\sqrt{1-\lambda+\lambda^2}} (2N_0)^b + \varepsilon'_f \frac{1-0.5\lambda}{\sqrt{1-\lambda+\lambda^2}} (2N_0)^c \tag{4.7}$$

where ν is Poisson's ratio and λ is the principal stress amplitude ratio.

Juneja (1992) proposes to account for mean stresses by modifying Morrow's model such as

$$N = N_0\left(1-\frac{\hat{\bar{\sigma}}}{\hat{\sigma}'_f}\right)^{-\frac{1}{b}} \tag{4.8}$$

where $\hat{\bar{\sigma}}$ is the effective mean stress and $\hat{\sigma}'_f$ the effective fatigue strength coefficient.

The strain life equation incorporating mean stresses according to the Smith-Watson-Topper (Socie, 1987) model is

$$\sigma_{max}\frac{\varepsilon_a}{2} = \sigma'_f\varepsilon'_f(2N)^{b+c} + \frac{\sigma'^2_f}{E}(2N)^{2b} \tag{4.9}$$

where ε_a is the principal strain amplitude and σ_{max} is the maximum stress on the principal strain plane during a cycle.

The other failure criterion considers the case where shear strains dominate the damage on the critical plane. The shear strain model proposed by Socie (1987) considers the maximum shear strain amplitude, coupled with the tensile stress perpendicular to the plane of maximum shear strain, to be the damage parameter in the strain life equation. Including mean stress effect the strain life equation is

$$\gamma_{max}\left(1+\frac{\sigma_n}{\sigma_y}\right)=\gamma'_f(2N)^c+\frac{\tau'_f}{G}(2N)^b \tag{4.10}$$

where γ'_f is the shear fatigue ductility coefficient, τ'_f is the shear fatigue strength coefficient, G is the shear modulus, γ_{max} is the maximum shear strain amplitude, σ_n is the maximum tensile stress perpendicular to the maximum shear strain plane, and σ_y is the yield strength. According to Socie (1987), the shorter of the two lives of Eqs. (4.9) and (4.10) should be taken as the most appropriate estimate of life.

Using the Palmgren-Miner rule, the fatigue life can be calculated for irregular loadings. All three life calculations are performed in this study according to Eqs. (4.7), (4.9), and (4.10) and the shortest life, i.e. the most conservative estimate, will be reported.

CHAPTER 5. RANDOM FATIGUE LOAD MODEL

The model developed to describe fatigue random load histories is introduced here. It is applicable to both stationary and nonstationary cases, and nonstationarities can be modeled as being either deterministic or stochastic. Moreover, the single channel case is included as the limiting case of the presented multichannel model.

5.1 Assumptions

The time history is a superposition of a zero-mean stationary random process and events which affect the variation of both the mean and variance. Mean and stationary random components contribute distinctly to the power spectral density (PSD) of the combined process. The mean variation is of slowly varying nature and contributes only to the low frequency range of the PSD, while the stationary random variation, however, may affect the PSD at any frequency. The variation in variance, even though also assumed to be of slowly varying nature, however, cannot be detected in a PSD plot of the whole history. It could only be seen if the *evolutionary power spectral density* (Priestley, 1965), i.e., the PSD as a function of time, was known.

Mean and variance variation of each channel are assumed to be independent of the variations of other channels, while stationary random variations are assumed to be corre-

lated among channels. Moreover, the nonstationary variance and stationary random components are independent of each other.

For the cases studied, the random loadings represent actual data of the strain response at a given point of a vehicle traveling over a rough road. The irregular road profile induces strain, which has a stationary random nature, while maneuvers, such as steering or change in velocity, induce nonstationary variations in strain with respect to mean and variance. The assumption of maneuvers being of slow varying nature is justified through the analysis of actual driving behavior (McLean and Hoffmann, 1971).

5.2 Time Series Model

To represent the multichannel random fatigue loading history with nonstationary mean and variance variation, the following model then is employed:

$$\mathbf{x}_t = \mathbf{m}_t + \mathbf{s}_t \cdot \mathbf{n}_t \tag{5.1}$$

where $\mathrm{x}_t = \left[x_t^{(1)} \quad \ldots \quad x_t^{(n)}\right]^T$ represents the underlying history, consisting of n channels, $\mathrm{m}_t = \left[m_t^{(1)} \quad \ldots \quad m_t^{(n)}\right]^T$ is the nonstationary variation in the mean value, $\mathbf{s}_t$ is a $(n \times n)$ diagonal matrix with elements $s_t^{(i)}$ as the scaling functions accounting for the variation in variance, and $\mathrm{n}_t = \left[n_t^{(1)} \quad \ldots \quad n_t^{(n)}\right]^T$ a zero-mean stationary random process. The following sections will show how each of the components of Eq. (5.1) are modeled. For simplicity, the derivation will be shown only for the scalar components, $m_t^{(i)}$, $s_t^{(i)}$, $n_t^{(i)}$, where the vector and matrix expressions are obtained by combining all n components. Also for convenience, the superscript i will be dropped where it is clear that a component of the

vector or matrix is implied. Also, it is understood that the parameter *t* refers to discrete points in time, as this study is concerned with modeling sampled time series.

5.2.1 Mean Description

To minimize the number of parameters necessary to characterize the mean variation in a deterministic manner a truncated Fourier series is used such that

$$m_t = \frac{1}{2}a_0 + \sum_{k=1}^{M_m}\left[a_k \cos\left(\omega_0 kt\Delta t\right) + b_k \sin\left(\omega_0 kt\Delta t\right)\right] \tag{5.2}$$

where Δt is the length of the sample interval, $\omega_0 = 2\pi/\left(N\Delta t\right)$ is the fundamental frequency, M_m and N are the number of terms in the truncated Fourier series and the total number of sample points of the history, respectively, and a_k and b_k are the discrete Fourier coefficients. For the case of $M_m \ll \left(N/2-1\right)$, m_t will be approximating the low frequency content of x_t, i.e., its mean variation. The value of M_m is found such that the difference between the original history and truncated Fourier series yields a process, d_t, which is stationary with respect to it's mean,

$$d_t = s_t \cdot n_t = x_t - m_t \tag{5.3}$$

To find the parameter M_m one method is given by Buxbaum and Zaschel (1977), who analyze the dynamic system to decide which part of the response spectrum is due to stationary random loadings and nonstationary loadings. Filtering in the frequency domain allows one to separate the two components. This, however, is often difficult as information regarding the dynamic system characteristics and the actual input spectrum are

seldom available. Therefore, to determine whether the series d_t is indeed stationary with respect to its mean value, the methods of nonparametric statistics are used.

5.2.2 Variance Description

The remaining zero mean component, $s_t \cdot n_t$, then needs to be separated into its respective components. To model the scaling function, s_t, in a deterministic manner, a method similar to the one for the mean description is used. The scaling function, s_t, is defined as the function that renders the quotient d_t / s_t stationary with respect to variance. This is equivalent to saying that s_t is defined as an estimator of the standard deviation of d_t. In order to estimate the standard deviation of d_t a procedure as shown by Nau et al. (1982) is employed.

For the zero mean time series, d_t, sampled at discrete equally spaced intervals, a simple estimate, $\tilde{\sigma}_t^2$, for the true variance, σ_t^2 , is obtained via a moving window such as

$$\tilde{\sigma}_t^2 = \sum_{j=0}^{n} w_{j-\frac{n}{2}} d_{t+j-\frac{n}{2}}^2 \tag{5.4}$$

where n is the width of the window and the window weights, w_j, are such that

$$\sum_{j=0}^{n} w_{j-\frac{n}{2}} = 1 \qquad w_j \geq 0 \tag{5.5}$$

To determine an appropriate size, *n*, of the window, inference methods from classical statistics can be used. Via a Chi Square test a confidence interval can be constructed (Miller and Freund, 1977) such as

$$\left(\frac{\chi^2_{n-1,1-\alpha}}{n-1}\right) \le \frac{\widetilde{\sigma}_t^2}{\sigma_t^2} \le \left(\frac{\chi^2_{n-1,\alpha}}{n-1}\right) \tag{5.6}$$

where σ_t^2 is the value of the true variance, $\widetilde{\sigma}_t^2$ is the estimated variance, and $\chi^2_{n-1,\alpha}$ indicates the Chi Square distribution with $(n-1)$ degrees of freedom at confidence level α. For an acceptable relative maximum error of 25% the following must hold $0.75 \le \widetilde{\sigma}_t^2 / \sigma_t^2 \le 1.25$. These bounds, with a chosen value of $\alpha = 0.9$, require a minimum number of $n = 96$, therefore, a value of $n = 100$ is chosen to accurately estimate the true variance, σ_t^2. For other confidence levels and relative maximum errors see Table 5.1.

The simplest weighting function is the rectangular one, i.e. $w_j = 1/(n+1)$. However, it is usually preferable to use a more gradually varying window, such that neighboring points have a stronger influence on the estimate of the variance than points that are further away from the current observation. Nau et al. (1982) use a cosine bell shaped window, while in this study, for simplicity, a triangular window is introduced such that

$$w_j = \begin{cases} \dfrac{4}{n^2} j & \text{for} \quad 0 \le j \le \dfrac{n}{2} \\ -\dfrac{4}{n^2} j + \dfrac{4}{n} & \text{for} \quad \dfrac{n}{2} \le j \le n \end{cases} \tag{5.7}$$

Nau et al. (1982) show that the estimate of the variance via Eq. (5.4) tends to be biased in a systematic way. Peak values in variance will be underestimated, while

Table 5.1. Chi-Square distribution confidence intervals.

	n - sample size		
error	$\alpha = 0.98$	$\alpha = 0.95$	$\alpha = 0.90$
10%	1024	731	519
20%	274	193	134
25%	196	138	**96**
30%	132	93	64
40%	79	56	38
50%	54	38	26

Table 5.2. Student's *t*-distribution confidence intervals.

	n - sample size		
error	$\alpha = 0.98$	$\alpha = 0.95$	$\alpha = 0.90$
10%	451	320	226
20%	126	90	64
25%	90	63	**45**
30%	60	43	31
40%	36	26	19
50%	25	18	13

rate estimate a correction could be introduced to account for this known deviation. However, as a concise, and therefore only approximate, description of the variance is desired, no further refinement is performed.

$\tilde{\sigma}_t$ then gives an estimation of the standard deviation of d_t and can, therefore, be used to derive an estimate for the scaling function, s_t.

The next step is to concisely represent the standard deviation, $\tilde{\sigma}_t$. The fact that $\tilde{\sigma}_t$ is not evenly distributed makes it difficult to postulate models that would describe it. Therefore, a transformation due to Box and Cox (1964) is commonly used to enhance symmetry

$$\tilde{\sigma}_t^{BC} = \begin{cases} \tilde{\sigma}_t^{\lambda} & \text{for} \quad \lambda \neq 0 \\ \log \tilde{\sigma}_t & \text{for} \quad \lambda = 0 \end{cases} \tag{5.8}$$

where $\tilde{\sigma}_t^{BC}$ indicates the Box Cox transform of $\tilde{\sigma}_t$. The parameter λ of this power transformation leads to a logarithmic transformation for $\lambda = 0$ and to no transformation for $\lambda = 1$. The parameter λ is chosen such that the transformed series has zero skewness, i.e. it becomes symmetrically distributed about it's mean, in order to facilitate modeling by a harmonic function. If more than one value of λ fulfills this criterion, the transformed time series corresponding to these values of λ are obtained and their respective mean and variance are calculated. The distribution of the transformed series are compared to normal distributions with the given values of mean and variance for each λ. A normalized error, ε, between the frequency histogram of the transformed series and the *probability density function* (pdf) of the corresponding normal distribution is obtained according to Ang and Tang (1975) as

$$\varepsilon = \sum_{i=1}^{I} \frac{(h_i - f_i)^2}{f_i} \tag{5.9}$$

where, I denotes the number of intervals the total range of $\tilde{\sigma}_t^{BC}$ was divided into, h_i indicates the relative frequency of a certain value of $\tilde{\sigma}_t^{BC}$, and f_i indicates the magnitude of the pdf evaluated at the same value of $\tilde{\sigma}_t^{BC}$. The value of λ that leads to the minimum error, ε, is chosen as the optimal parameter.

In this study, the scaling function, s_t, is a truncated Fourier series

$$s_t^{BC} = \frac{1}{2}c_0 + \sum_{k=1}^{M_s}\left[c_k \cos(\omega_0 kt\Delta t) + d_k \sin(\omega_0 kt\Delta t)\right] \tag{5.10}$$

where as before Δt is the length of the sample interval, $\omega_0 = 2\pi/(N\Delta t)$ is the fundamental frequency, M_s and N are the number of terms in the truncated Fourier series and the total number of sample points of the history, respectively, and c_k and d_k are the discrete Fourier coefficients. For the limiting case where $M_s = (N/2-1)$, $s_t^{BC} = \overline{\sigma}_t^{BC}$, while for $M_s < (N/2-1)$, s_t^{BC} is an approximation of $\overline{\sigma}_t^{BC}$ leading to s_t as a suitable scaling function. The value of M_s is found such that s_t^{BC} and $\overline{\sigma}_t^{BC}$ have a prescribed correlation coefficient of $\rho_s^{M_s} = 0.95$. M_s is much smaller than $(N/2-1)$, since the variation in variance has been calculated via an average and is therefore of slowly varying nature.

5.2.3 Random Component Description

The remaining stationary random component, n_t, can be represented by an ARMA model of appropriate order. A vector ARMA model is employed to account for correlations among components, $n_t^{(i)}$, of $\mathbf{n}_t$. No commonly agreed on approach of model selection for

vector ARMA models has been found. In this study, therefore, the criterion of model order selection will be identical for both single- and multi-channel case. The selection of the proper ARMA model is made such that a *parsimonious* model is chosen according to Section 3.4.

5.3 Nonparametric Statistics

In order to determine whether a sequence of observations is of random nature, statistical tests can be performed. Observations can be either individual events, or a common measure of a collection of events, such as the interval mean, μ_i, for a given *i*-th interval of a history. If no information about the distribution function of the sequence is available, a nonparametric test is desired because no assumptions regarding distributions are necessary. In nonparametric inference, the methods are based only on the relative occurrence of an underlying event. Therefore, information or assumptions regarding the underlying population are not necessary to assess whether a sequence is of random nature or contains deterministic trends (Gibbons, 1971).

Three nonparametric tests are presented here to determine the stationarity of d_t with respect to the mean value. In general, given a time series of length *N*, one divides this series into N_I intervals each containing N_P points, such that $N = N_I \times N_P$. The means are calculated for each interval, μ_i, where $i = (1, 2, \ldots, N_I)$, and are considered as the sequence of observations to be tested for randomness.

These intervals need to be sufficiently long to give reliable estimates for the mean, yet short enough to be able to detect variations in the mean of the whole record. Furthermore, for proper statistical analysis, it is desirable to treat the estimates of the interval

means as if they were uncorrelated to each other. No common rule has been established in the literature as to what this interval length should be. An argument to support the choice of interval size, however, can be made using inference methods from classical statistics. To establish the necessary number of data points to estimate the interval mean, μ_i, a Student's t-test can be used (Miller and Freund, 1977)

$$\left(\bar{x}_i - t_{\alpha,N_P-1}\frac{S_i}{\sqrt{N_P}}\right) \le \mu_i \le \left(\bar{x}_i + t_{\alpha,N_P-1}\frac{S_i}{\sqrt{N_P}}\right) \tag{5.11}$$

where $\bar{x}_i$ is the estimated interval mean, S_i is the square root of the unknown interval variance, and t_{α,N_P-1} indicate Student's t-distribution with α level of confidence and $N_P - 1$ degrees of freedom. An expression indicating the relative maximum error in estimating μ_i can be derived as

$$\text{relative maximum error} = \left|\frac{\bar{x}_i - \mu_i}{S_i}\right| \le \frac{t_{\alpha,N_P-1}}{\sqrt{N_P}} \tag{5.12}$$

For a chosen value of $\alpha = 0.9$ and an acceptable relative maximum error of 25% in estimating μ_i, the required minimum number of sample points is $N_P = 45$ leading to the actual choice of $N_P = 50$ for other confidence levels and relative maximum errors see Table 5.2.

The first test is based on the variable R_T, the total number of runs. A single run is defined as successive observations of the interval mean or interval standard deviation below or above the median and is completed when two succeeding observations are separated by the median. This is the best known and most general run test. The test is focused on a single quantity, the median, and gives a general measure of randomness or lack thereof

without identifying trends or cyclical pattern. Hald (1952) derives the mean and variance for the expected number of runs for a true random sequence. For the case where the total number of runs, R_T, is larger than twenty, the distribution of R_T is approximately normal. For a sequence of length N_I, the expected value and variance for R_T then are defined as, (Hald, 1952)

$$\mathrm{E}[R_T] = \mu_{R_T} = \frac{N_I + 2}{2} \tag{5.13}$$

$$\mathrm{E}\left[\left(R_T - \mu_{R_T}\right)^2\right] = \mathrm{var}[R_T] = \sigma^2_{R_T} = \frac{N_I}{4}\left(1 - \frac{1}{N_I - 1}\right) \tag{5.14}$$

Confidence limits for the expected number of runs can be established. A hypothesis test is based on the comparison of the observed number of runs, r_T, and the theoretically expected number of runs, μ_{R_T}. Confidence limits at level α are defined as (Hald, 1952)

$$\left(r_T - z_{\alpha/2}\sigma_{R_T}\right) \le \mu_{R_T} \le \left(r_T + z_{\alpha/2}\sigma_{R_T}\right) \tag{5.15}$$

where $z_{\alpha/2}$ is defined such that

$$1 - \alpha/2 = \int_{z_{\alpha/2}}^{\infty} e^{-\frac{1}{2}x^2}\, dx \tag{5.16}$$

If the observed number of runs, r_T, falls inside the confidence limits, Eq. (5.15), for a chosen confidence level, usually $\alpha = 0.95$, the hypothesis of the sequence being random is accepted, while for the case where r_T falls outside these limits the observed sequence must be considered deterministic.

The second run test is based on the variable for the length of the longest run, *K*. In a random sequence of length N_I, the longest of the runs described above follows the relation (Hald, 1952)

$$N_I \cong K - \frac{1}{K+1} - \frac{K+2}{2} K! \log_e \left(P\left(-z_{\alpha/2} < Z < z_{\alpha/2} \right) \right) \tag{5.17}$$

where

$$P\left(-z_{\alpha/2} < Z < z_{\alpha/2} \right) = \int_{-z_{\alpha/2}}^{z_{\alpha/2}} e^{-\frac{1}{2}x^2} dx \tag{5.18}$$

Since Eq. (5.17) cannot be solved directly for *K*, the test is indirect. The hypothesis test at confidence level α for the observed longest run requires checking whether the series is sufficiently long to admit a run of observed length, *k*, in a random sequence of length N_I. This test is best suited for identifying trends in a sequence.

Finally, tests based on the number of runs up and down, R_{UD}, provide another measure of randomness of a sequence of interval means. The magnitude of each observation is compared with that of the immediately preceding observation. If the next element is larger, a run up is started, and if smaller, a run down. A decision concerning randomness then is based on the number of these runs, while the length is not considered. This test traces the whole sequence of observations relative to each other, in contrast to the test based on the total number of runs. Therefore, a periodic fluctuation (cyclic content) of the observed sequence can be detected through the number or runs up and down. A hypothesis test can be derived for measuring whether the observed number of runs, r_{UD}, significantly deviates from the expected value, $\mu_{R_{UD}}$, for a random sequence.

The expected value and variance of the number of runs up and down for a random sequence of length N_I are (Hald, 1952)

$$\mathrm{E}[R_{UD}] = \mu_{R_{UD}} = \tfrac{1}{3}(2N_I - 1) \tag{5.19}$$

$$\mathrm{E}\left[\left(R_{UD} - \mu_{R_{UD}}\right)^2\right] = \mathrm{var}[R_{UD}] = \sigma^2_{R_{UD}} = \tfrac{1}{90}(16N_I - 29) \tag{5.20}$$

Confidence limits at level α are defined as

$$\left(r_{UD} - z_{\alpha/2}\sigma_{R_{UD}}\right) < \mu_{R_{UD}} < \left(r_{UD} + z_{\alpha/2}\sigma_{R_{UD}}\right) \tag{5.21}$$

Each run test detects a certain form of deviation from the case of a random sequence. Too few runs, runs of excessive length, or too many runs can be used as statistical criteria for the rejection of the hypothesis of randomness of the sequence μ_i. Therefore, all tests should be considered, and need to be passed successfully, for the sequence d_t to be considered stationary with respect to its mean.

5.4 Ensemble Generation

Successful load modeling for the purpose of realistic fatigue testing asks for an ensemble of load histories where each realization (history) is representative of the actual loading. In practice, it is often difficult to obtain sufficient information about the ensemble. It is common to have only a limited number of representative records for a particular loading situation. Therefore it is desired, given a single loading, to obtain a large number of realizations which are not identical, but contain variations which have statistical characteristics identical to the original history.

The proposed model of Eq. (5.1) allows for an extension from a single observed record to an ensemble in all its components. The ARMA models employed to account for the stationary variations of the loads are of stochastic nature. It is not a single time series that is embodied in a particular set of ARMA parameters, but a random process, which for each generation yields a different realization with identical stochastic characteristics, but a different sequence and values of relative extrema.

The ensemble of mean and variance variations can be obtained using a method introduced by Rice (1944). It is shown that a time series, y_t, of a random signal can be described by its discrete Fourier transform

$$y_t = \frac{1}{2} g_0 + \sum_{k=1}^{N-1/2} \left[g_k \cos(\omega_0 k t \Delta t - \eta_k) + h_k \sin(\omega_0 k t \Delta t - \tau_k) \right] \tag{5.22}$$

where g_k and h_k are Fourier coefficients, ω_0, Δt, and N were defined above, and η_k and τ_k are two random phase angles distributed uniformly over the interval $(0, 2\pi)$.

This presentation yields an ergodic random process, i.e., a process that is stationary, such that an average taken over time is identical to an average taken across the ensemble of histories. Histories with a different variation for each simulation of Eq. (5.22) are obtained, yet the overall characteristics, such as the frequency content and variance, are preserved. A stochastic description of the process y_t is obtained.

This formulation of a random process can be used to derive an ensemble of mean and variance variations by modifying the mean description in Eq. (5.2) and the scaling function in Eq. (5.9) in two ways. First, similarly to Eq. (5.22), random phase angles are added to each term of Eqs. (5.2) and (5.9). This leads to presentations which preserve the

spectral content, but the sequence of events, i.e. the occurrence of a relative or absolute maximum, will be different for each simulation. While these records are statistically identical, it might be desirable to obtain mean and variance variations which will have a prescribed similarity (correlation) to the deterministic descriptions. This would yield more realistic load simulations as the sequence of major events, such as relative extrema, can be preserved to any desired degree.

This objective leads to a second modification of Eqs. (5.2) and (5.9). The prescribed correlation between deterministic description and the ensemble is obtained through limiting the number of terms which carry a random phase angle in Eq. (5.22). Instead of η_k and τ_k being random phase angles for all *k*, η_k and τ_k will be restricted such that

$$\eta_k, \tau_k = \begin{cases} U & \text{for} \quad k \in (N_Z + 1, M) \\ 0 & \text{for} \quad k \in (0, N_Z) \end{cases} \tag{5.23}$$

and the ensemble description becomes

$$y_t^{N_Z} = \frac{1}{2} g_0 + \sum_{k=1}^{M} [g_k \cos(\omega_0 k t \Delta t - \eta_k) + h_k \sin(\omega_0 k t \Delta t - \tau_k)] \tag{5.24}$$

where N_Z indicates the number of terms with zero phase angles and *U* indicates the uniform distribution defined on the interval $(0, 2\pi)$.

From a strict theoretical standpoint, the random process of Eq. (5.24) with the definition of η_k and τ_k of Eq. (5.23) yields a non-ergodic process. This is due to the fact that the process contains deterministic components, i.e., terms with zero phase angles. However, the proposed method of using a limited number of random phase angles conserves the frequency content of the deterministic variation.

5.4.1 Ensemble Mean

Given the deterministic mean description of Eq. (5.2) and the derivation of an ensemble of Section 5.4, the ensemble of mean variations becomes

$$m_t^{N_Z^m} = \frac{1}{2}a_0 + \sum_{k=1}^{M_m}\left[a_k \cos(\omega_0 kt\Delta t - \alpha_k) + b_k \sin(\omega_0 kt\Delta t - \beta_k)\right] \tag{5.25}$$

with the random phase angles such that

$$\alpha_k, \beta_k = \begin{cases} U & \text{for} \quad k \in \left(N_Z^m + 1, M_m\right) \\ 0 & \text{for} \quad k \in \left(0, N_Z^m\right) \end{cases} \tag{5.26}$$

In order to measure the closeness between the deterministic description, m_t and a simulated mean $m_t^{N_Z^m}$, the correlation coefficient, $\rho_m^{N_Z^m}$, is obtained.

5.4.2 Ensemble Variance

An ensemble of variance variations can be derived in an analogous manner as the one for the mean description. The Fourier series to describe the scaling function, s_t, will be augmented by random phase angles, which in turn will be restricted according to the desired correlations between deterministic and stochastic scaling functions.

Given the Box-Cox transformation of the deterministic scaling function of Eq. (5.9) and the derivation of an ensemble of Section 5.4, the ensemble of Box-Cox transformed scaling functions becomes

$$s_t^{N_Z^s} = \frac{1}{2}c_0 + \sum_{k=1}^{M_s}\left[c_k \cos(\omega_0 kt\Delta t - \gamma_k) + d_k \sin(\omega_0 kt\Delta t - \delta_k)\right] \tag{5.27}$$

with the random phase angles such that

$$\gamma_k, \delta_k = \begin{cases} U & \text{for} \quad k \in \left(N_Z^s + 1, M_s\right) \\ 0 & \text{for} \quad k \in \left(0, N_Z^s\right) \end{cases} \tag{5.28}$$

As for the mean ensemble the closeness between the deterministic description, s_t and a simulated scaling function, $s_t^{N_Z^s}$, is measured by their respective correlation coefficient, $\rho_s^{N_Z^s}$.

CHAPTER 6. STUDIES OF UNIAXIAL LOADINGS

Three fatigue loading histories which represent data collected in field experiments were provided by the sponsor and are investigated. These histories are strain gauge measurements taken on a front suspension component. A fourth history was obtained by removing the variation in variance of one of these histories, yielding a history stationary with respect to variance, but nonstationary with respect to its mean. According to earlier stated assumptions, these records are considered to represent local strain data, collected at a critical location such as a notch, and, moreover, they are assumed to have been sampled at one point per second. Moreover, all records have been normalized without loss of generality such that their overall mean value is zero and their dimensionless root mean square (RMS) value is equal to unity. Basic statistics of original and reconstructed records are shown in Table 6.1. Some of these loadings exhibit a beginning that does not contain much variation. This can be explained by the fact that the vehicle started from rest and loads are consequently small. All fatigue life calculations are based on the material properties of SAE 1045 steel, stated in Table 6.2.

6.1 Stationary Mean and Variance

For the purpose of life analysis, a typical block of stationary zero-mean, constant variance strain-gauge data (22,592 observations) is chosen to represent the random fatigue load

Table 6.1. Statistics of original loadings and respective reconstructions.

	Stationary Mean and Variance		Nonstationary Mean		Nonstationary Variance		Nonstat. Mean and Variance	
	Original	Reconstruction	Original	Reconstruction	Original	Reconstruction	Original	Reconstruction
Mean	0.0	9.653E–5	0.0	– 2.647E–3	0.0	– 0.017	0.0	– 0.013
Variance	1.0	1.014	1.0	0.985	1.0	1.028	1.0	0.985
Skewness	– 0.131	– 7.583E–3	– 0.307	– 0.198	– 0.141	– 0.003	– 0.361	– 0.232
Minimum	– 4.784	– 4.132	– 3.785	– 3.884	– 6.076	– 7.096	– 3.931	– 3.253
Maximum	3.956	4.187	2.866	3.052	6.064	7.927	2.754	3.292

Table 6.2. Material properties for SAE 1045 steel, Kurath et al. (1989).

Modulus of Elasticity, E	202000	MPa	29297	ksi
Yield Strength, σ_Y	380	MPa	55.1	ksi
Ultimate Strength, σ_U	621	MPa	90.3	ksi
Fatigue Strength Coefficient, σ_f'	948	MPa	138	ksi
Cyclic Strength Coefficient, H′	1258	MPa	182	ksi
Cyclic Strain Hardening Exponent, n′		0.208		
Fatigue Strength Exponent, b		– 0.092		
Fatigue Ductility Coefficient, ε_f'		0.260		
Fatigue Ductility Exponent, c		– 0.445		

history in this study. A portion of this load history is shown in Fig. 6.1, and its corresponding power spectral density is plotted in Fig. 6.2.

Various orders of ARMA models are employed for the reconstruction of an equivalent history and are compared for the best model. Table 6.3 gives the autoregressive and moving average parameters, ϕ_i; i=1, 2, ..., p, and θ_i; i=1, 2, ..., q, for each ARMA model together with the variance of the white noise, σ_e^2. It is observed that the variance of the white noise decreases rapidly with increasing model order, indicating a better fit of the model to the data. The values of ARMA parameters for different models, however, do not exhibit any distinct pattern. Moreover, Table 6.4 shows the correlation coefficient between the power spectral density for the original record and power spectral densities obtained from the closed form presentation of Eq. (3.7) for various ARMA models. It can be seen, that, with increasing model order, the variance of the white noise, σ_e^2, and the correlation coefficient between the spectra does not monotonically decrease. This is due to the fact that increasing the model order can lead to *overfitting*, i.e. estimating of higher order models that in fact give a poorer fit than a lower order model.

Power spectral densities for ARMA(1,0), ARMA(2,1) and ARMA(3,1) models are shown in Fig. 6.2. It is noted that ARMA(0,0) is a stationary random process with a normally and independently distributed variable, i.e. white noise, having a constant power spectral density with a unit area. It is obvious that the lower order ARMA models, ARMA(0,0), ARMA(1,0), and ARMA(2,1), are inadequate in describing the stochastic characteristics of the original loading. This is due to the fact that these models do not include a sufficient number of parameters to reflect the correlation structure of the original record. The power spectral density for the ARMA(1,0) model is a monotonically decreas-

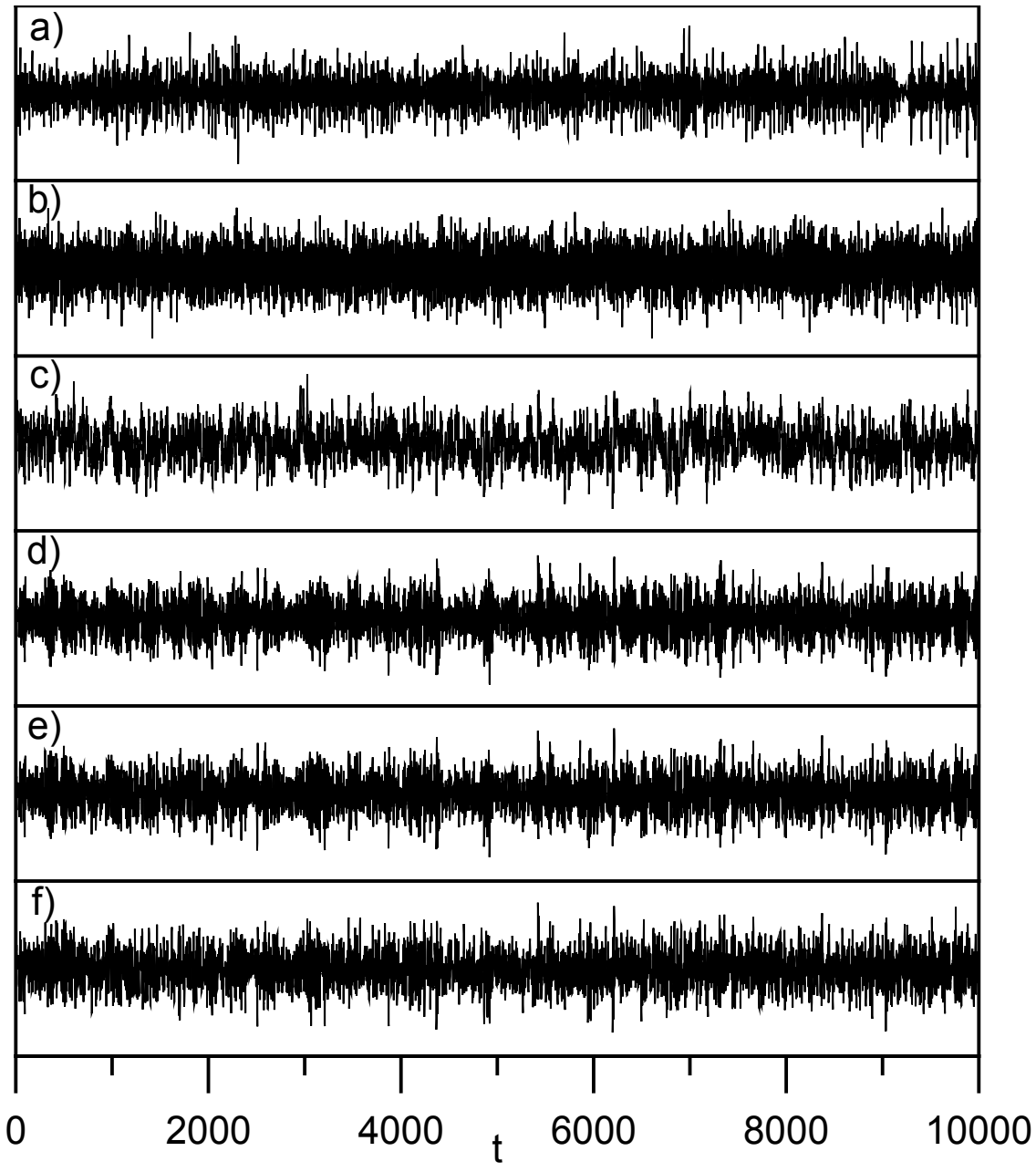

Figure 6.1. Time series plots for portion of (a) original history, (b) ARMA(0,0), (c) ARMA(1,0), (d) ARMA(2,0), (e) ARMA(2,1), and (f) ARMA(3,1) reconstructions - stationary case.

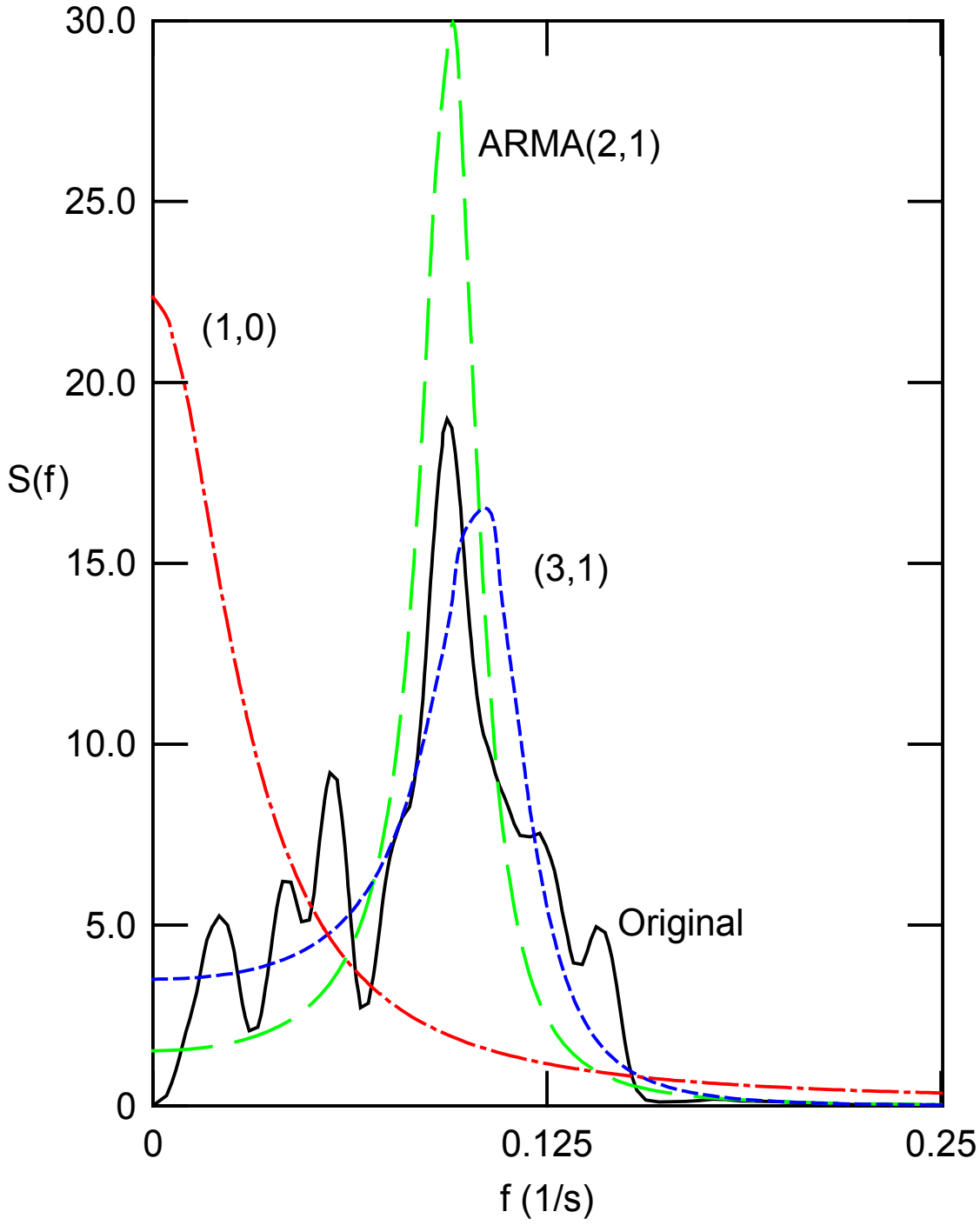

Figure 6.2. Power spectral densities for original and selected ARMA reconstructed histories - stationary case.

Table 6.3. ARMA parameters and variance of white noise input for selected ARMA models - stationary case.

ARMA(p,q)	(0,0)	(1,0)	(2,0)	(2,1)	(3,0)	(3,1)	(4,0)	(5,0)	(5,4)	(6,0)	(8,0)	(10,0)
ϕ_i; i = 1		0.836	1.596	1.548	2.226	1.927	2.495	2.548	3.327	2.625	2.639	2.703
2			0.909	0.875	– 2.014	– 1.540	– 2.799	– 3.031	– 4.885	– 3.349	– 3.405	– 3.630
3					– 0.692	0.422	1.559	2.006	3.997	2.706	2.854	3.283
4							– 0.390	– 0.806	– 1.796	– 1.776	– 2.096	– 2.684
5								0.172	0.351	0.950	1.462	2.147
6										– 0.297	– 0.809	– 1.550
7											0.283	1.025
8											– 0.059	– 0.652
9												0.308
10												– 0.072
θ_i ; i = 1				– 0.873		– 0.774			0.721			
2									0.190			
3									– 0.577			
4									0.200			
σ_e^2	1.000	0.3010	0.0519	0.0232	0.0271	0.0198	0.0230	0.0228	0.0274	0.0202	0.0206	0.0192

Table 6.4. Correlation coefficient of power spectra, $\rho_S^{(p,q)}$, for selected ARMA(p,q) models, where the bold number indicates the minimum order model for a given correlation value - stationary case.

p \ q	0	1	2	3	4	5	6
1	0.22						
2	**0.84**	**0.87**					
3	0.74	**0.92**	0.77				
4	0.94	0.94	0.90	0.83			
5	0.91	0.91	0.90	0.86	**0.95**		
6	0.87	0.84	0.84	0.8	0.90	0.95	
7	0.93	0.93	0.91	0.88	0.94	0.95	0.95

ing function that overestimates and underestimates the distribution of the power in the low and high frequency ranges, respectively. For the higher order ARMA models, the resulting spectral densities are similar to that of the original loading history, which is characterized by having most of its power concentrated around the critical frequency of $f \approx 0.09\,\text{Hz}$.

To compare models with respect to fatigue relevant characteristics, the distributions of rainflow cycles and the predicted component fatigue lives are investigated. In order to eliminate any bias toward any particular load history, the rainflow cycles and the component fatigue lives corresponding to each ARMA model are taken as the ensemble average of one hundred independently reconstructed histories.

For the purpose of rainflow cycle counting, the maximum range for the normalized original and ARMA reconstructed histories is set equal to 10, extending from –5 to 5. Such a range is chosen to be large enough so that the probability of it being exceeded by the reconstructed data is almost zero. This range is then divided into 32 equal class intervals of width 0.3125. Figure 6.3 shows the range-mean histograms of rainflow cycles for the original history and for the reconstructed histories by ARMA(0,0), ARMA(1,0), ARMA(2,1), and ARMA(3,1) models. The distributions of rainflow range mean histograms for the lower order models such as ARMA(0,0) and ARMA(1,0) are shown to be substantially different from that of the original history. Because the correlation among the consecutive data points is relatively low, these two lower order models describe sequences of peaks and valleys that are interrupted by only a small number of intermediate points. As a result, a much larger number of rainflow cycles with a smaller range is formed. Furthermore, it is also observed that the number of rainflow cycles with larger ranges is over-

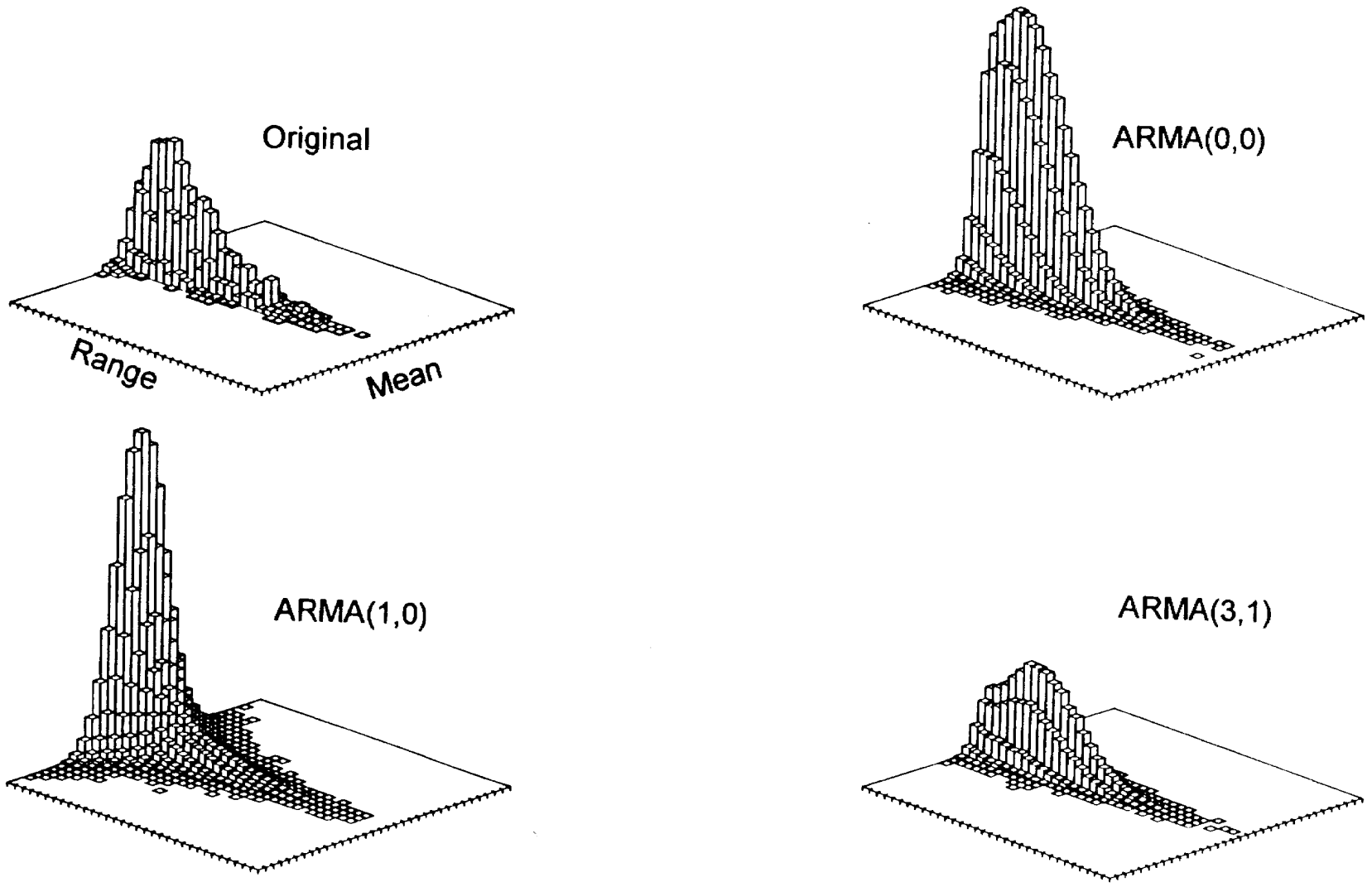

Figure 6.3. Rainflow histograms for original record and selected ARMA reconstructed histories - stationary case.

estimated by the ARMA(0,0) model while it is underestimated by the ARMA(1,0) model. The distributions of rainflow cycles for reconstructions corresponding to the higher order ARMA models are found to be similar to that of the original history. However, the distribution for the original history is irregular, whereas those for the ARMA reconstructions are relatively smooth due to averaging the one hundred sample histories.

In the following analysis, the variations of fatigue life as a function of RMS strain level, ε_{RMS}, are considered, the so called *strain life curve*. Consequently, the strain histories corresponding to various RMS levels are required. Because the original loading is of unit RMS value, this can be accomplished by simply multiplying the normalized history with the desired RMS value. Strain life curves for original loading and average values of one hundred ARMA reconstructions are shown in Fig. 6.4.

For low cycle fatigue, the component life for ARMA(3,1) reconstructed history is shown to be in good agreement with that for the original history. The fatigue life due to ARMA(0,0) reconstructed histories is the shortest. This is because the ARMA(0,0) model does not only overestimate the rainflow cycles with a smaller range but also those with an intermediate and larger ranges. In spite of the result shown earlier which indicates that the largest number of rainflow cycles is formed by the ARM(1,0) reconstructed histories, the longest fatigue life is predicted. This can be explained by the fact that the distribution of the resulting cycles is biased toward those with a smaller range for which the resulting damage is insignificant. Higher order models, however, approximate the fatigue life better. It is noted that strain life curves for ARMA(2,0) and ARMA(5,4) overlap with the ones for ARMA(2,1) and ARMA(3,1), respectively.

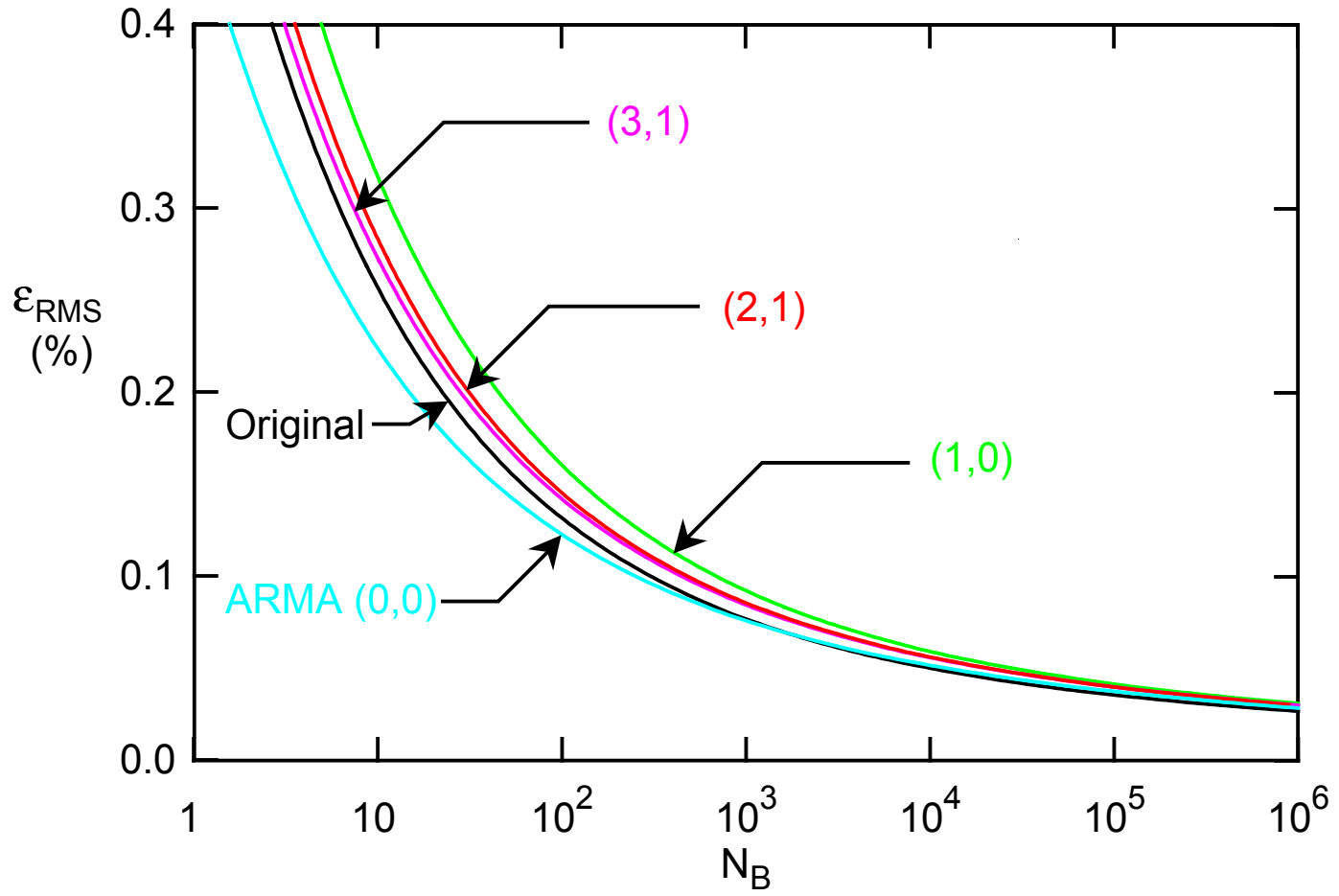

Figure 6.4. RMS strain level, ε_{RMS}, versus blocks to failure, N_B, for original and selected ARMA reconstructed histories - stationary case.

For high cycle fatigue, the calculations indicate that the predicted fatigue lives for the original and for ARMA reconstructed records are in good agreement. When the component life becomes relatively large, i.e. $N_B > 10^3$ blocks, all the reconstructed histories result in longer predicted life than that for the original loading. For these particular RMS stain levels, the damage is mainly the result of those hysteresis loops with the largest ranges. It is observed that all the proposed ARMA models slightly underestimate the number of rainflow cycles with such ranges.

The damage histograms for the original and for ARMA(0,0), ARMA(1,0), and ARMA(3,1) reconstructed histories are shown in Fig. 6.5 for the RMS strain level $\varepsilon_{RMS} = 0.1\%$. At this RMS strain level, the rainflow cycles with a small range contribute an insignificant percentage of damage. As a result, the shortest and longest fatigue lives are predicted when the expected load history is described by ARMA(0,0) and ARMA(1,0) models, respectively.

According to the selection criterion outlined in Section 3.4, ARMA models of minimum order whose power spectra have a specific correlation value, $\rho_S^{(p,q)}$, to the spectrum of the original are considered for further analysis with respect to fatigue life. Models with correlations of $\rho_S^{(p,q)}$ greater or equal than 0.8, 0.85, 0.9, and 0.95 are sought. The respective minimum order models can be read from Table 6.4 and are ARMA(2,0) with $\rho_S^{(2,0)} = 0.84$, ARMA(2,1) with $\rho_S^{(2,1)} = 0.87$, ARMA(3,1) with $\rho_S^{(3,1)} = 0.92$, and ARMA(5,4) with $\rho_S^{(5,4)} = 0.95$, respectively. It can also be seen from Table 6.4 that increasing the model order beyond ARMA(5,4) does not lead to better fitting models.

The model of lowest order for which the strain life curve falls within the bounds of life

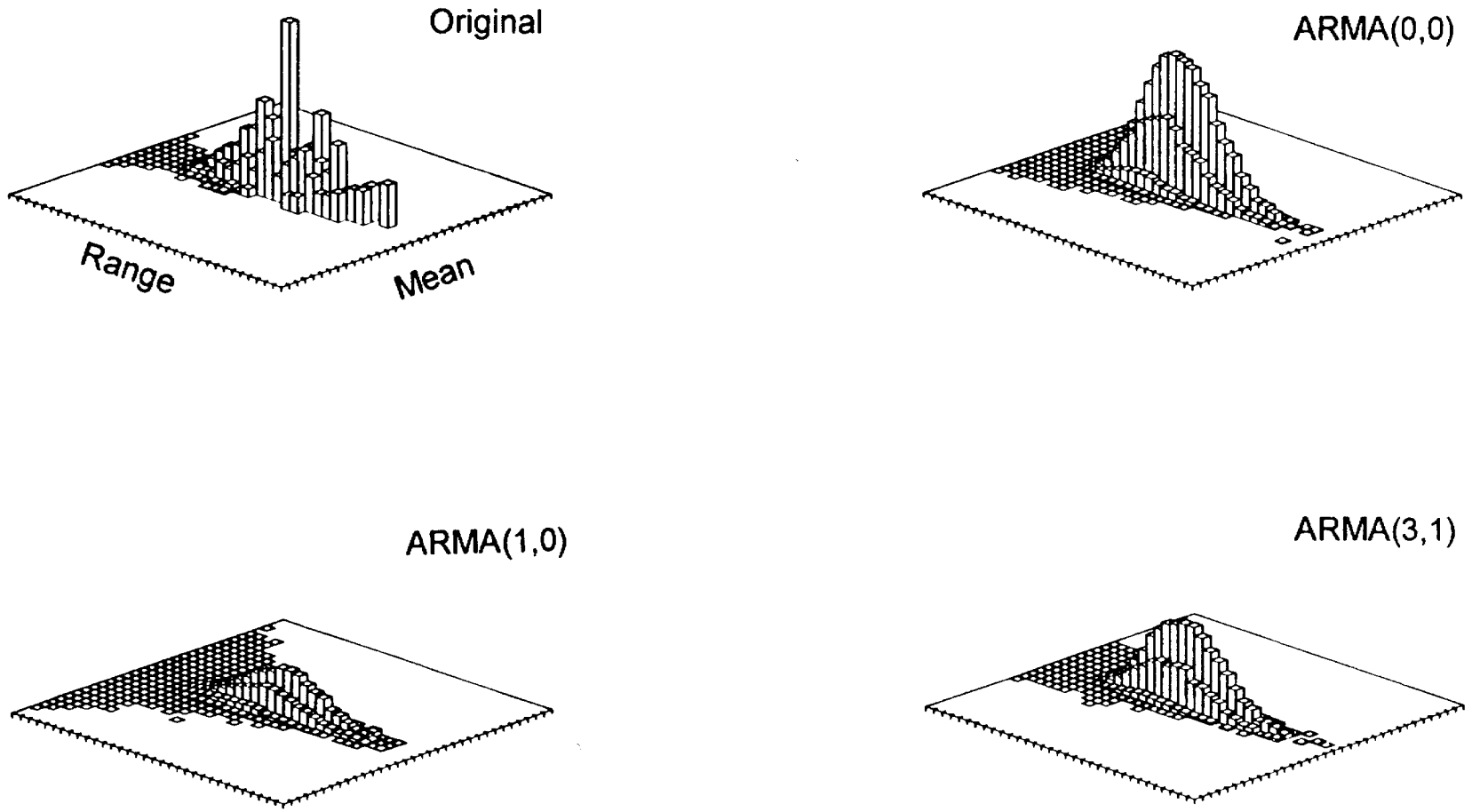

Figure 6.5. Damage histograms for original and selected ARMA reconstructed histories, ε_{RMS} = 0.1% - stationary case.

of the original is the ARMA(3,1) model, shown in Fig. 6.6. Therefore, according to the criterion of closeness with respect to fatigue life, the ARMA(3,1) model is chosen to be the most concise model that matches the fatigue life of the original loading with appropriate accuracy.

The application of random load history modeling for numerical analysis, such as Monte Carlo studies, and laboratory fatigue testing, generally requires a large number of load reconstructions. As a result, it is desirable that the proposed model has a high degree of consistency in terms of reproducing load histories which have identical statistical properties to the original. In other words, the variations of fatigue life of the same component subjected to various reconstructed load histories should be minimal. Statistical variations of the component fatigue life based on an ensemble of one hundred independently reconstructed ARMA(3,1) histories are plotted in Fig. 6.7 as a function of the RMS strain level, ε_{RMS}. Shown are the mean average life, $\overline{N}_B$, the mean lower bound life, $\overline{N}_B^L$, and the mean upper bound life, $\overline{N}_B^U$. Furthermore, a band formed by the lines $\overline{N}_B^L - 3\sigma_{N_B^L}$ and $\overline{N}_B^U + 3\sigma_{N_B^U}$, where $\sigma_{N_B^L}$ and $\sigma_{N_B^U}$ are the standard deviations of the lower bound and upper bound lives, respectively, is also given for measuring the degree of dispersion of the data. It is noted that the total probability that a given point to be within plus and minus three standard deviations from the mean value is approximately 99.7%. Because the resulting band is relatively narrow, only slight variation in the predicted fatigue life is to be expected. The variation reflects the fact that the loading history is of stochastic nature. In the subsequent studies, rainflow and damage histograms will be obtained for only one reconstruction, as the variability between reconstructions is small for histories of reasonable length.

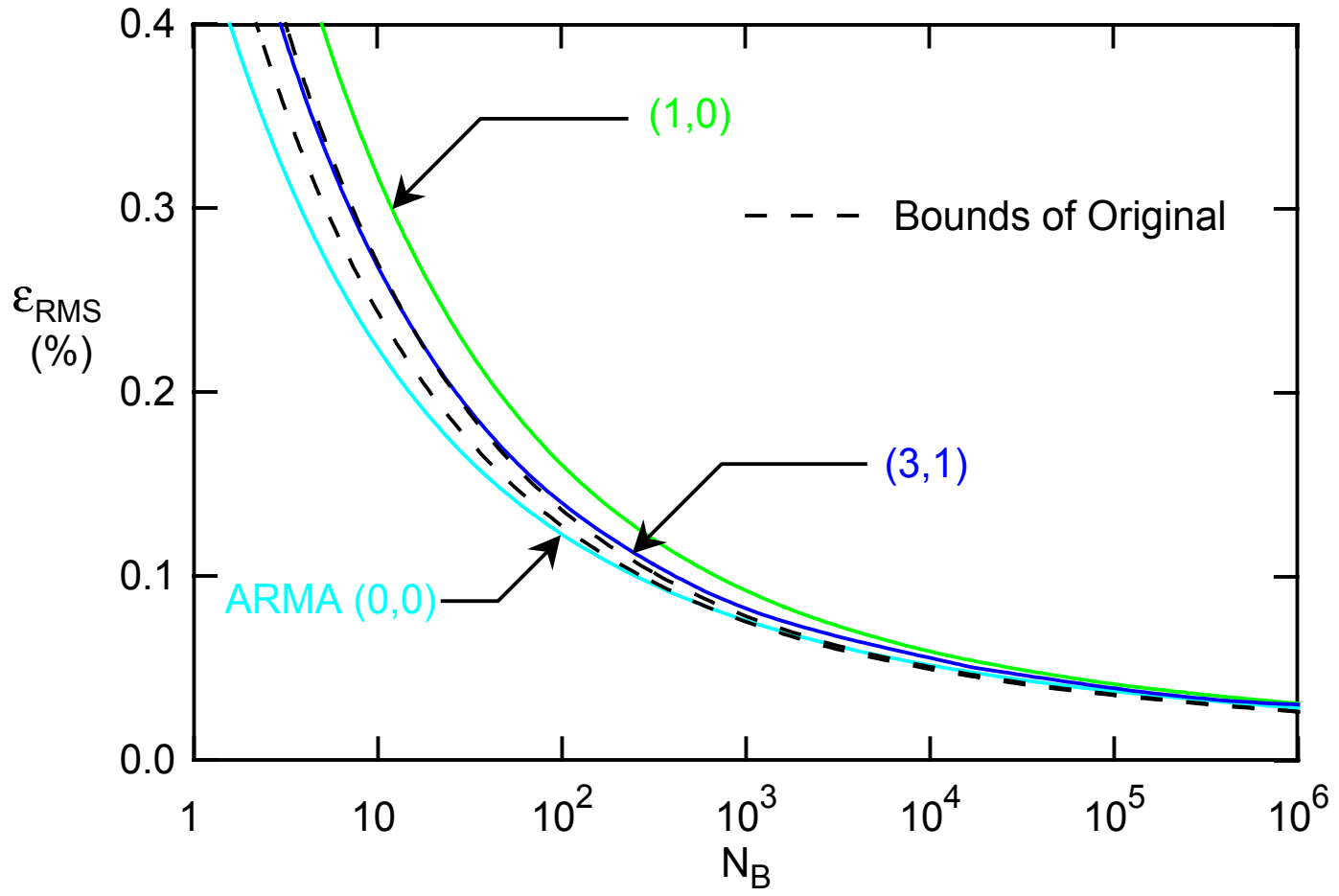

Figure 6.6. RMS strain level, ε_{RMS}, versus blocks to failure, N_B, for original and selected ARMA reconstructed histories - stationary case.

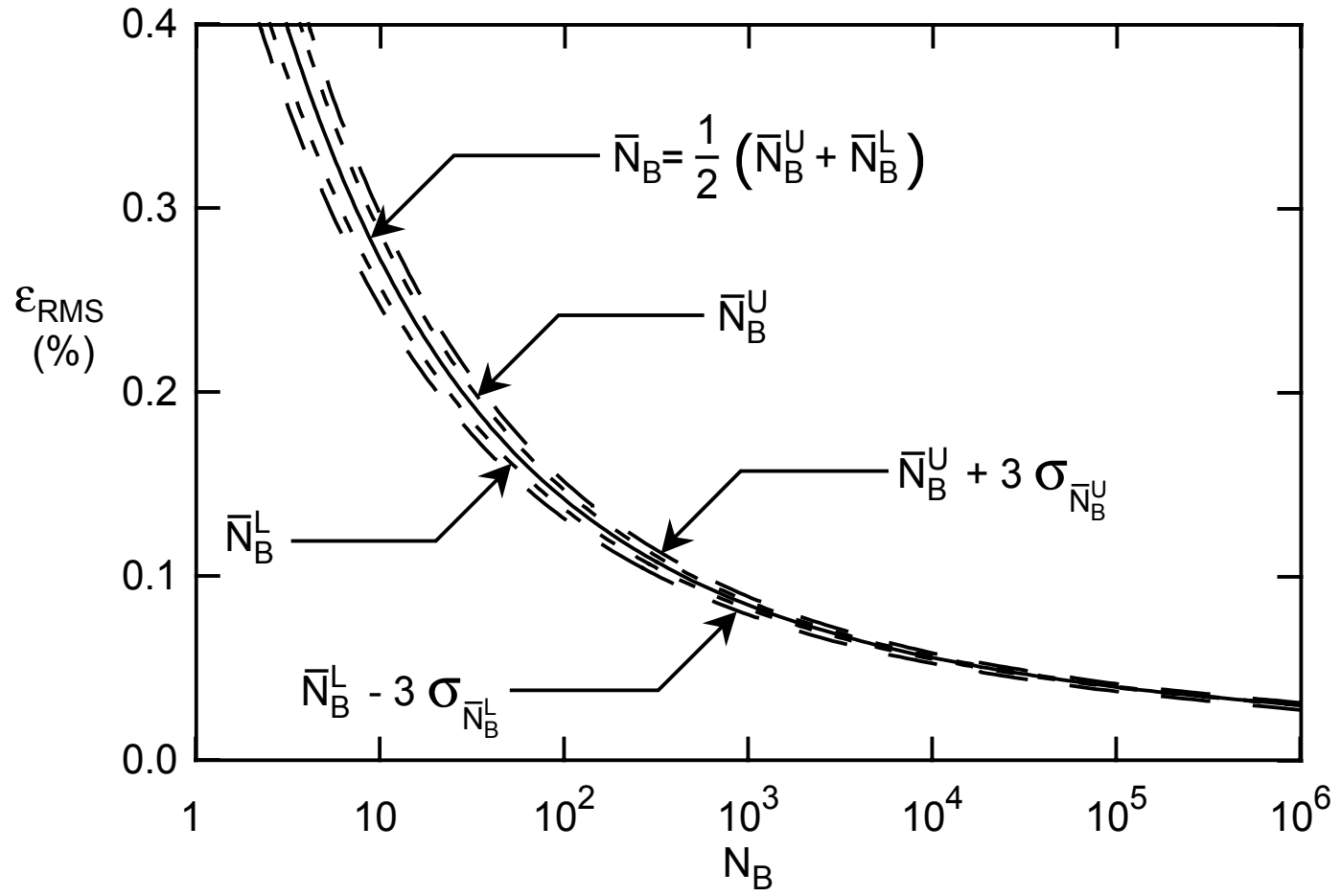

Figure 6.7. Statistical variations of fatigue life resulting from an ensemble of 100 independently reconstructed ARMA(3,1) histories - stationary case.

6.1.1 Experimental Verification

Juneja (1992) reported the results of an experimental verification of the proposed load modeling method. Unnotched axial test specimens were made of SAE 1045 steel from the same lot of material, where the material constants, Table 6.1, were the same as used in the life calculations from the previous section. The specimen were subjected to the original loading history at five different RMS strain levels, and similarly to three reconstructions, namely ARMA(0,0), ARMA(1,0), and ARMA(3,1), where these histories are shown in Fig. 6.1.

The number of blocks to failure, N_B, are shown for each test in Fig. 6.8. The ARMA(0,0) reconstructed history gave lives shorter than those for the original history, and the ARMA(1,0) reconstruction gave longer lives. The ARMA(3,1) reconstruction lives were closest to those for the original history at all five strain levels, being slightly longer but within a factor of two. The trends in life for the various reconstructions was in agreement with the calculated life of the previous section. However, the actual lives were shorter than predicted, especially at the lower RMS strain levels. A possible explanation for this is that cycles at the intermediate and lower levels within a given strain history often cause more fatigue damage than expected due to an interaction effect with the most sever cycles. Also, the material properties of the provided specimen may have deviated from the reported values as they were not confirmed through tests. Finally, a variation in material properties within the lot of steel bar provided is a possible cause for the deviation of prediction and test results.

The most significant result obtained, however, is that the ARMA(3,1) model and the

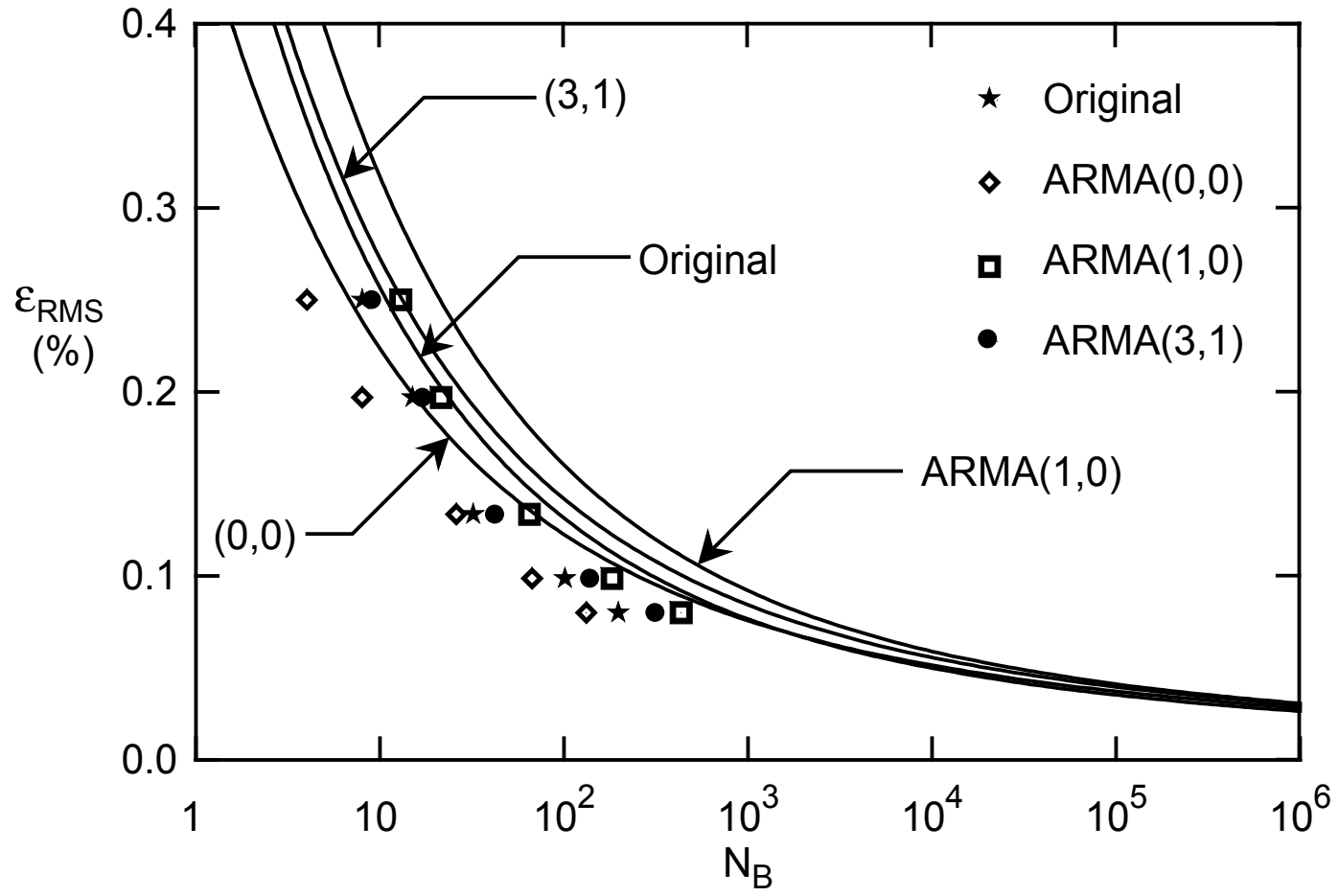

Figure 6.8. RMS strain level, ε_{RMS}, versus blocks to failure, N_B, for unnotched axial test specimen of SAE 1045 steel subjected to the original and three ARMA reconstructed histories - stationary case. Calculated lives from Fig. 6.4. are also shown as solid lines.

original loading agreed reasonably with respect to fatigue life.

6.2 Nonstationary Mean

A typical history of nonstationary strain gauge data is chosen as the random fatigue load history in this study, Fig. 6.9a, where a variation in variance was removed prior to this study. This history, containing 10240 points, constitutes one block. Its power spectral density is shown in Fig. 6.10.

According to the employed model of Eq. (5.1), the history is decomposed into its two components, m_t and n_t, where it is assumed that the scaling function, s_t, is constant. In order to model the variation of the mean, m_t, in a deterministic way various Fourier series with increasing numbers of terms are formed, giving the tentative mean descriptions. The difference, n_t, of the original record and each mean description is obtained. These differences are then analyzed for deviations from being a zero-mean process. The best mean description is chosen as the one that renders n_t stationary using the Fourier series with the least number of terms.

In order to analyze the mean-removed record, n_t, it is divided into N_I intervals each of which contains, according to Section 5.3, $N_P = 50$ points. This leads to $N_I = 204$ intervals, for each of which the interval mean is determined. As 10240 cannot be evenly divided by 50, the first and last 20 points in the series are ignored for the run tests.

Run tests based on the total number of runs, the number of runs up and down, and the length of the longest run, are performed on the sequence of interval means calculated from

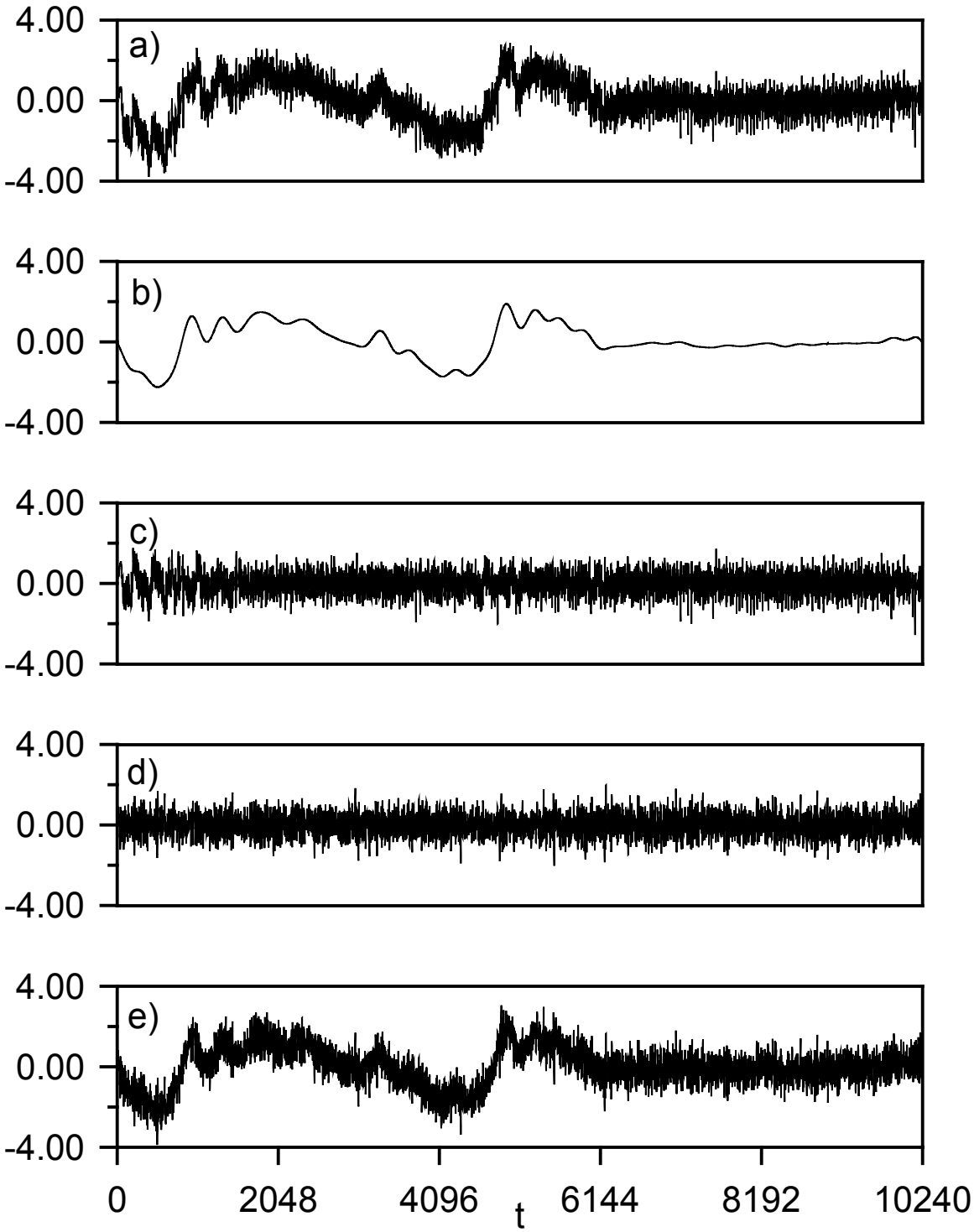

Figure 6.9. Time series plots for (a) original history, (b) deterministic mean representation with $M_m = 35$, (c) stationary series, (d) ARMA(5,0) model simulation, and (e) reconstruction - nonstationary mean case.

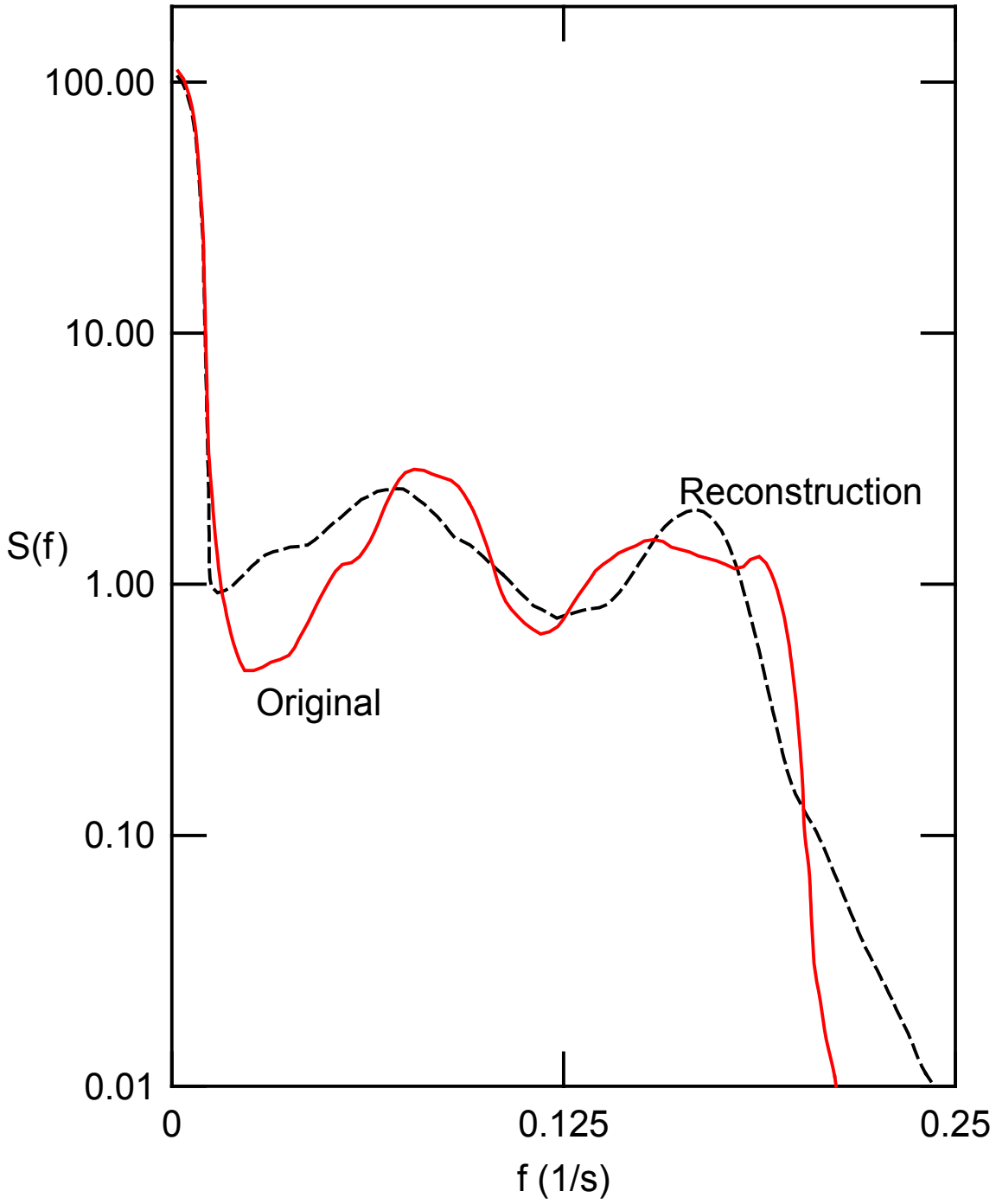

Figure 6.10. Power spectral density for original history and a history reconstructed with $M_m = 35$ and ARMA(5,0) - nonstationary mean case.

n_t. This assures that a variety of deviations from the expected random behavior of this sequence can be detected.

Confidence intervals for run tests at levels $\alpha = 0.90$, $\alpha = 0.95$, and $\alpha = 0.98$ are shown in Table 6.5, where $\alpha = 0.95$ is chosen as the level at which run tests will be performed. For the case where $N_I = 204$, the 95% $(\alpha = 0.95)$ confidence limits for the total number of runs are $(89 < \mu_{R_T} < 116)$, while the number of runs up and down covers the range $(123 < \mu_{R_{UD}} < 147)$. The length of the longest admissible run, according to Eq.(5.17) for a random sequence of length 204, is *K*=6.

The only value for which all run tests are passed is $M_m = 35$. Therefore, a total number of $M_m = 35$ Fourier series coefficients is deemed appropriate for a sufficient mean description to render the remaining signal stationary with respect to its mean value. See also Fig. 6.9b for the deterministic mean model, m_t, and Fig. 6.9c, for the mean removed record, n_t, and Fig. 6.11 for the power spectral density of the stationary series.

The stationary sequence will be presented by an ARMA model. Parameters for a number of ARMA models are estimated and the correlation coefficients between power spectra of these ARMA models and the spectrum of the stationary series are calculated, and are shown in Table 6.6. Seeking models which have correlations of $\rho_S^{(p,q)}$ greater or equal than 0.8, 0.85, 0.9, and 0.95 leads to the following choices of respective minimum order models: ARMA(5,0), ARMA(5,2), ARMA(9,0), and ARMA(10,0). Power spectral densities for ARMA(5,0) and ARMA(10,0) are shown in Fig. 6.11. The area under the PSD of both ARMA models is approximately the same as the area under the PSD of the stationary series. However, the peaks of the stationary series are much better modeled by

Table 6.5. Results of run tests for different values of M_m for $\alpha = 0.95$ (italics = failure of test, bold passed all tests) - nonstationary mean case.

$N_I = 204$			
$\alpha = 0.90$	$91 < r_T < 114$	$125 < r_{UD} < 145$	$k \leq 5$
$\alpha = 0.98$	$86 < r_T < 119$	$121 < r_{UD} < 149$	$k \leq 6$
$\alpha = 0.95$	$89 < r_T < 116$	$123 < r_{UD} < 147$	$k \leq 6$
M_m	r_T	r_{UD}	k
5	*35*	*102*	*8*
10	*67*	*100*	*8*
15	*77*	*112*	6
20	*77*	*108*	*7*
25	91	*108*	5
30	99	*114*	4
35	**109**	**132**	**4**
40	104	*116*	4
45	*130*	138	5
50	*141*	146	3

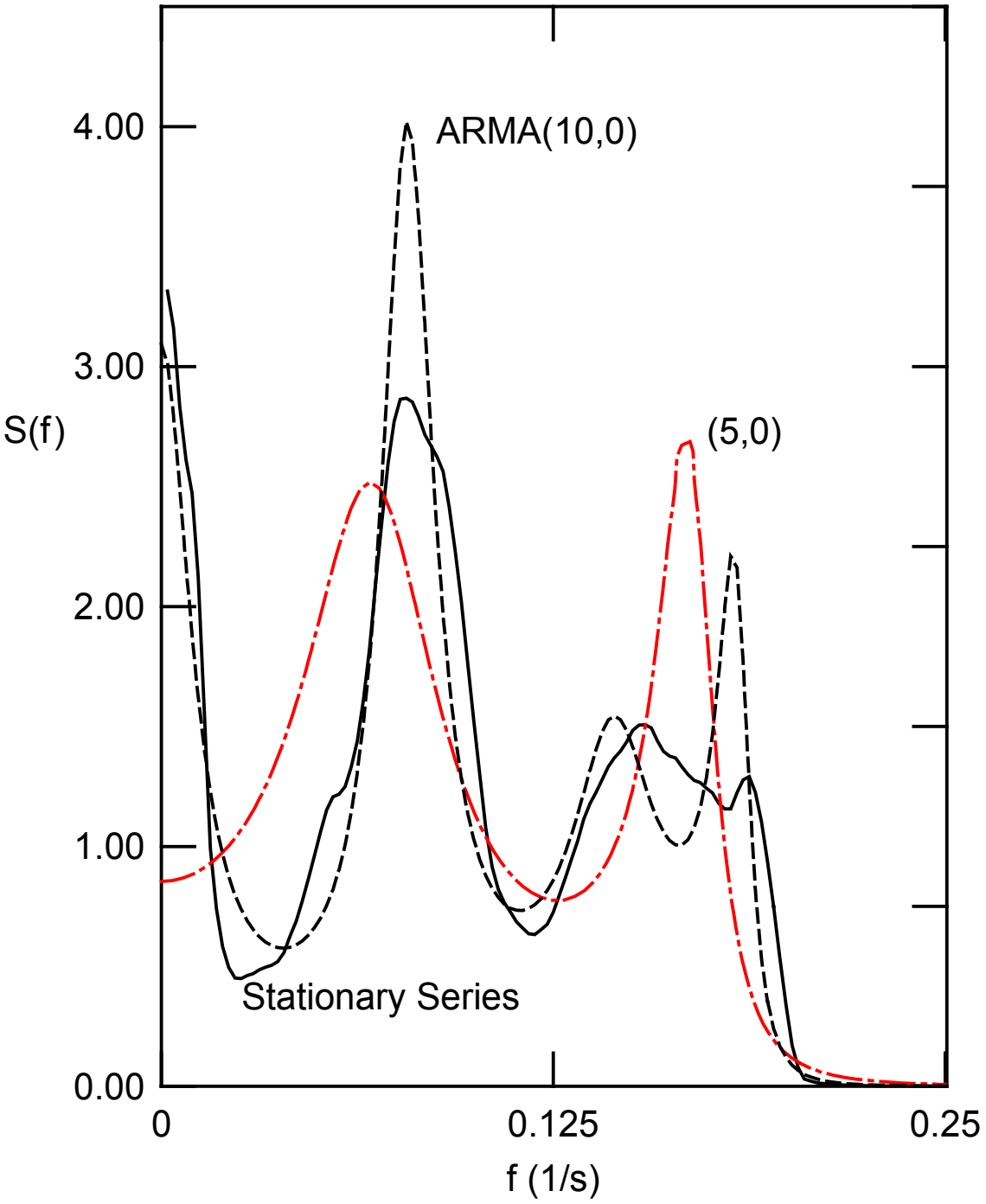

Figure 6.11. Power spectral density for the stationary series and two ARMA models, where for ARMA(5,0) $\rho_S^{(5,0)} = 0.81$ and for ARMA(10,0) $\rho_S^{(10,0)} = 0.96$ - nonstationary mean case.

Table 6.6. Correlation coefficient of power spectra, $\rho_S^{(p,q)}$, for selected ARMA(p,q) models, where the bold number indicates the minimum order model for a given correlation value - nonstationary mean case.

p \ q	0	1	2	3	4	5	6	7	8	9
1	0.52									
2	0.50	0.57								
3	0.59	0.64	0.70							
4	0.76	0.77	0.82	0.83						
5	**0.81**	0.81	**0.85**	0.85	0.84					
6	0.83	0.83	0.84	0.84	0.85	0.85				
7	0.81	0.81	0.82	0.83	0.84	0.84	0.83			
8	0.71	0.70	0.76	0.76	0.83	0.83	0.83	0.86		
9	**0.90**	0.92	0.95	0.95	0.97	0.97	0.98	0.98	0.98	
10	**0.96**	0.96	0.97	0.96	0.98	0.98	0.98	0.98	0.96	0.97
11	0.93	0.94	0.95	0.95	0.97	0.98	0.97	0.97	0.96	0.96
12	0.93	0.93	0.94	0.94	0.97	0.97	0.96	0.97	0.97	0.97

the ARMA(10,0) model than by the ARMA(5,0) model.

Reconstructions are formed for all of these ARMA models and added to the deterministic mean description. Strain life curves are obtained for the original loading, where the bounded life calculation was performed, and for various ARMA reconstructions, Fig. 6.12, where 64 independent reconstructions were performed and averaged to eliminate any bias introduced by a particular reconstruction. Note that strain life curves for reconstructions of ARMA(5,0), ARMA(5,2), ARMA(9,0), and ARMA(10,0) overlap, therefore, the lowest order model, ARMA(5,0), is deemed appropriate for load reconstruction. Strain life curves are also shown for ARMA(0,0) and ARMA(1,0), where it is noted that they constitute, as in Section 6.1, the limiting cases of all ARMA reconstructions that were studied. ARMA(0,0) leads to the shortest life, while ARMA(1,0) leads to the longest life predicted. Moreover, it is noted that ARMA(0,0) and ARMA(1,0) are closer to the bounds of the original than it is the case of the stationary loading in Section 6.1. This can be explained by the fact that, for this case, where the mean variation varies appreciably, the stationary random component's contribution to fatigue life is less than that for the case of a purely stationary loading. In other words, any bias introduced by an inappropriate ARMA model influences the reconstruction less when a deterministic mean variation is present.

The complete reconstruction, using the stationary record obtained from the selected ARMA(5,0) model shown in Fig. 6.9d, and using the deterministic mean representation, is shown in Fig. 6.9e. To demonstrate the consistency of the reconstruction, Fig. 6.13 shows five independently simulated records. The power spectral density of the reconstructed history is shown in Fig. 6.10, where it should be noted that the PSD is shown on

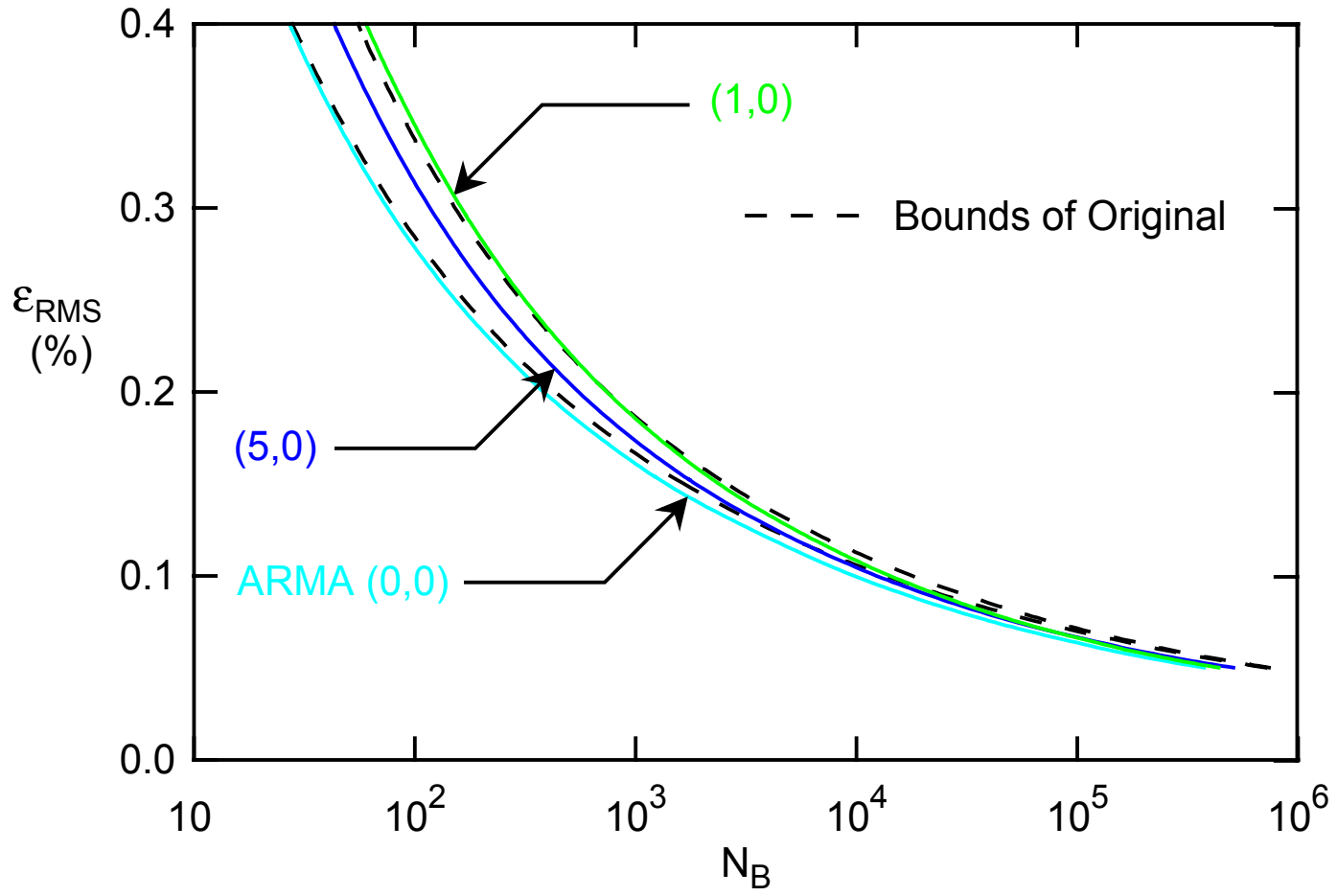

Figure 6.12. RMS strain level, ε_{RMS}, versus blocks to failure, N_B, for original and selected ARMA reconstructed histories, where $M_m = 35$ - nonstationary mean case.

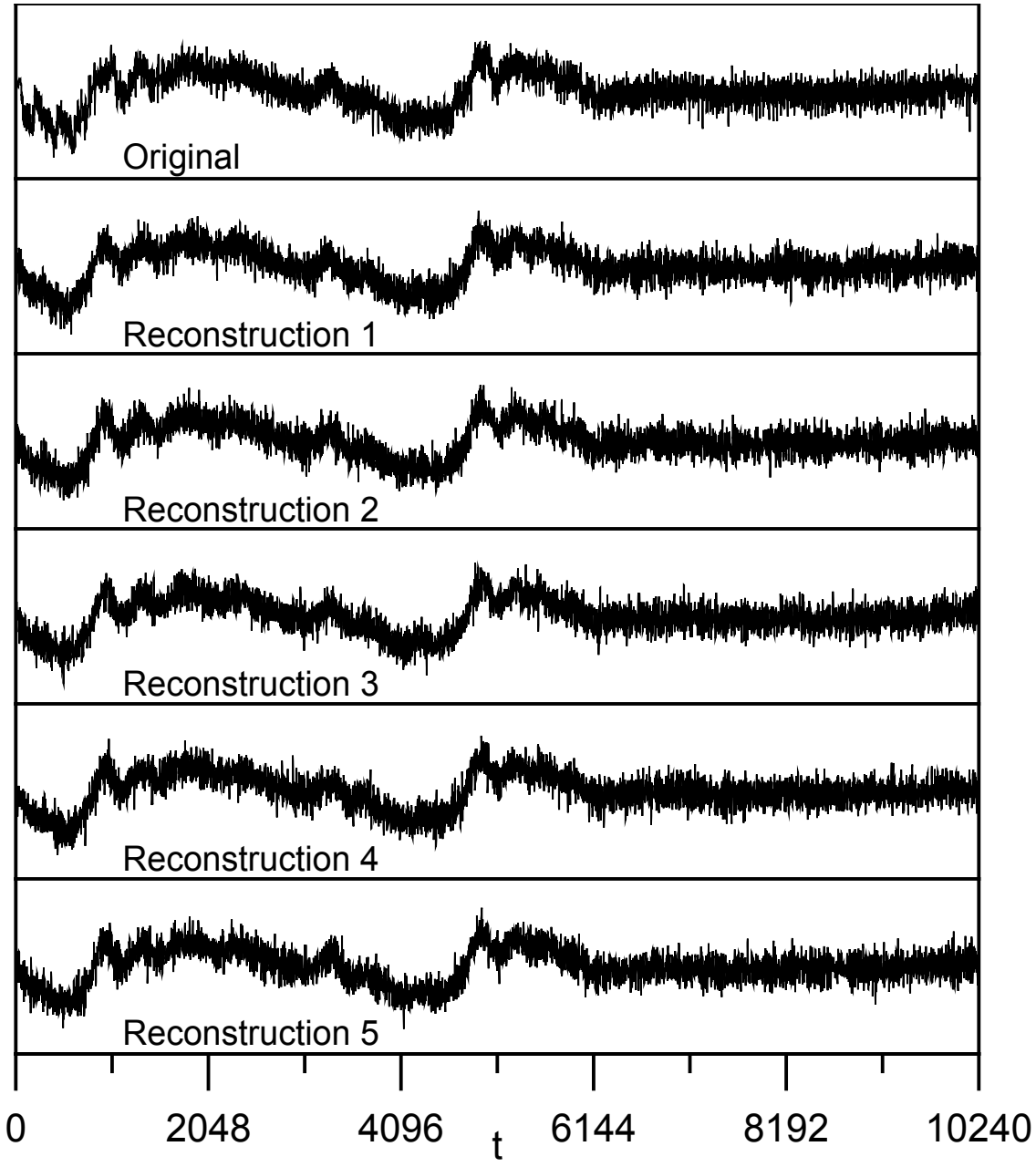

Figure 6.13. Time series plots for original history and reconstructions with deterministic mean, $M_m = 35$, where different simulations of the ARMA(5,0) model are used - nonstationary mean case.

a logarithmic scale, and the overall agreement is actually very close. Finally, for visual comparison, the rainflow and damage histograms are obtained and are shown in Figs. 6.14-6.15. The overall agreement is good; both the large number of small cycles and the small number of large cycles being well approximated.

In order to measure the correlation between the deterministic mean, m_t, and a simulated mean, $m_t^{N_Z^m}$, the correlation coefficient, $\rho_m^{N_Z^m}$, is calculated. To obtain a reliable estimate, 64 simulations are performed for each value of N_Z^m (Eq. 5.26) and averaged. Figure 6.16 shows these results, where it is seen that the correlations remain large for a range of zero phase angles between 10 and 35 and drop sharply to zero when the number of zero phase angles becomes smaller than 10. Figures 6.17 a-e show the deterministic mean variation and a set of four mean variations of different correlation with the deterministic mean. These records were obtained for correlation values of $\rho_m^{N_Z^m} = (0.95,\ 0.80,\ 0.58)$ corresponding to values for $N_Z^m = (20, 7, 4)$. Finally, a random phase angle is added to each term, $N_Z^m = 0$, so that the deterministic mean and simulated mean are uncorrelated. Figures 6.17f-g show these simulations, which are drastically different from the original. This method, therefore, allows one to obtain mean simulations with any desired closeness to the deterministic mean.

To measure the variability in fatigue life, 64 simulations are performed where both mean and random content were generated independently. The fatigue life is calculated for each simulation to obtain the mean, standard deviation, and coefficient of variation (ratio of standard deviation and mean) of fatigue life. The variability of fatigue life, expressed through the coefficient of variation, for different correlation values, $\rho_m^{N_Z^m}$, is shown in Fig. 6.18.

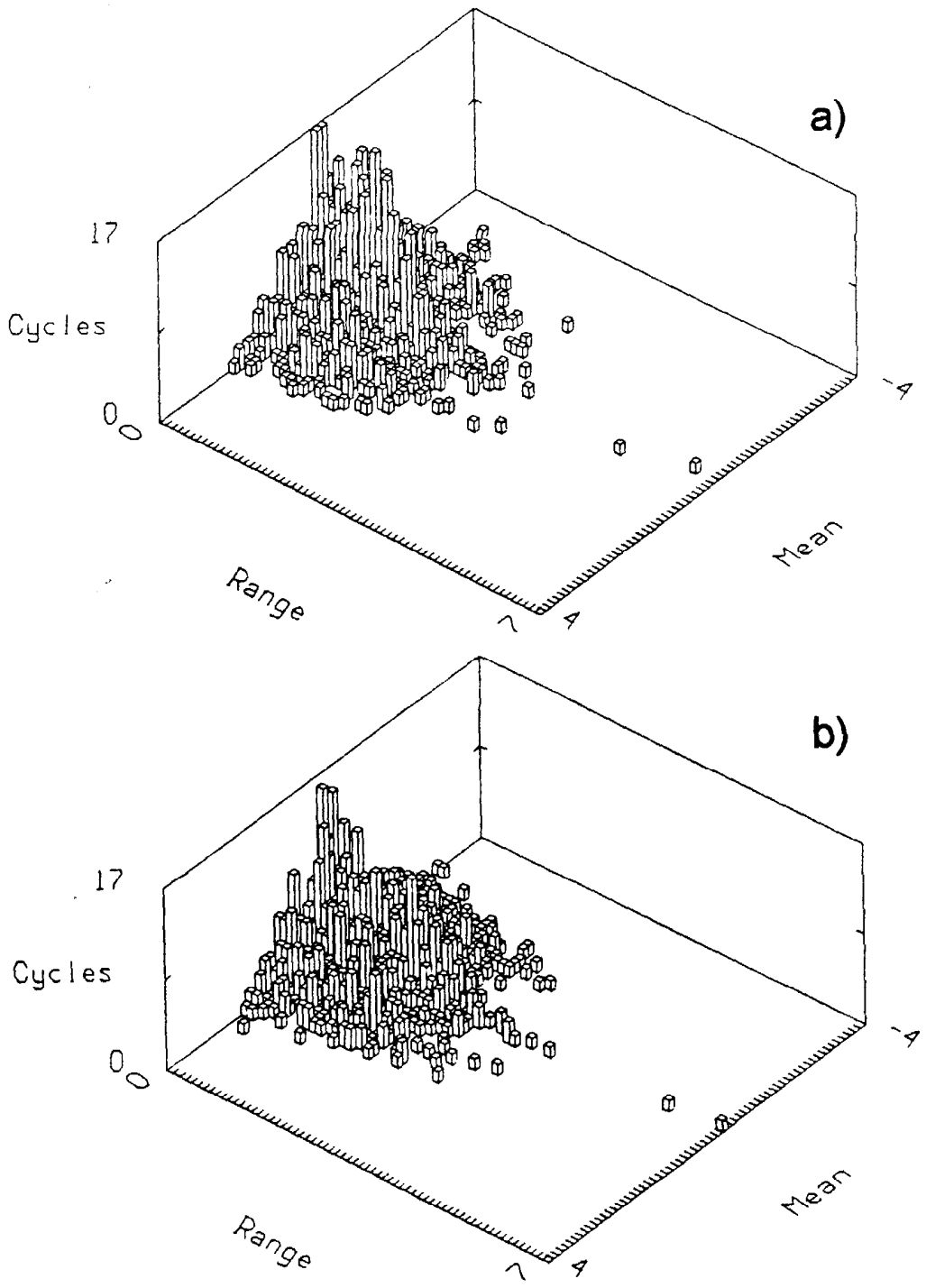

Figure 6.14. Rainflow histograms for (a) original and (b) record reconstructed with $M_m = 35$ and ARMA(5,0) - nonstationary mean case.

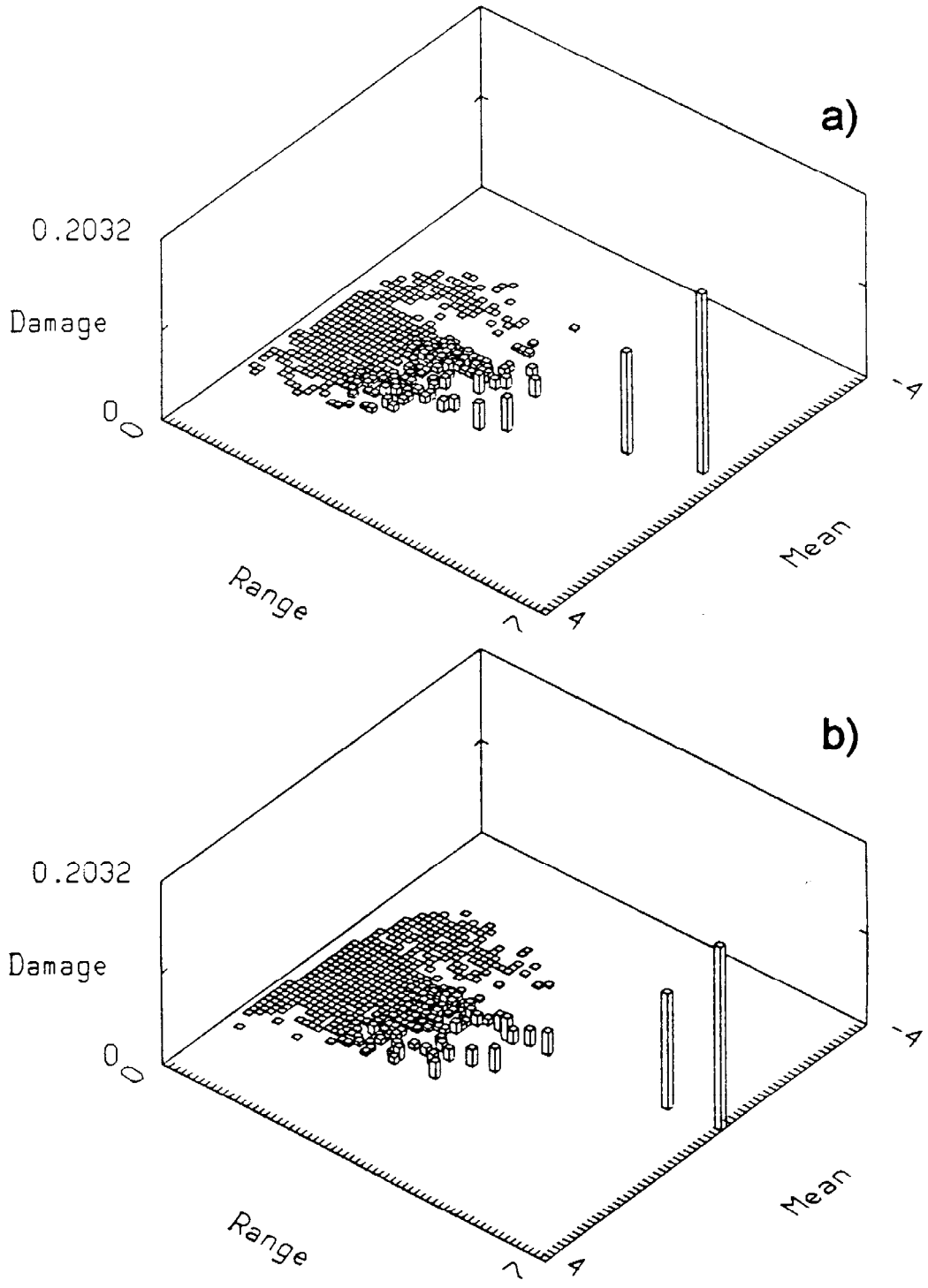

Figure 6.15. Damage histograms for (a) original and (b) record reconstructed, with $M_m = 35$ and ARMA(5,0), where $\varepsilon_{RMS} = 0.1\%$ - nonstationary mean case.

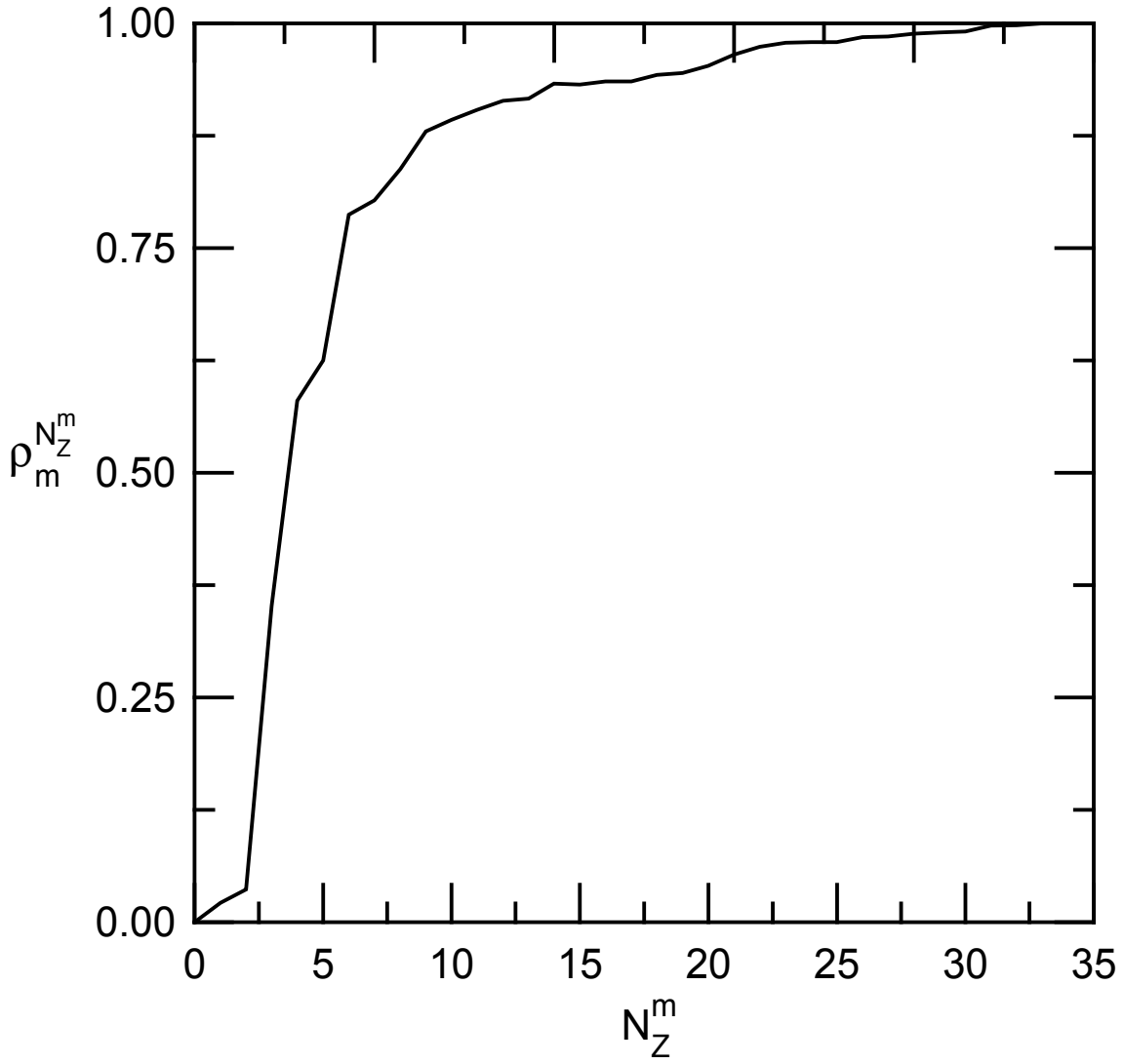

Figure 6.16. Correlation, $\rho_m^{N_Z^m}$, between deterministic and ensemble mean versus the number of zero phase shifts in ensemble mean, N_Z^m - nonstationary mean case.

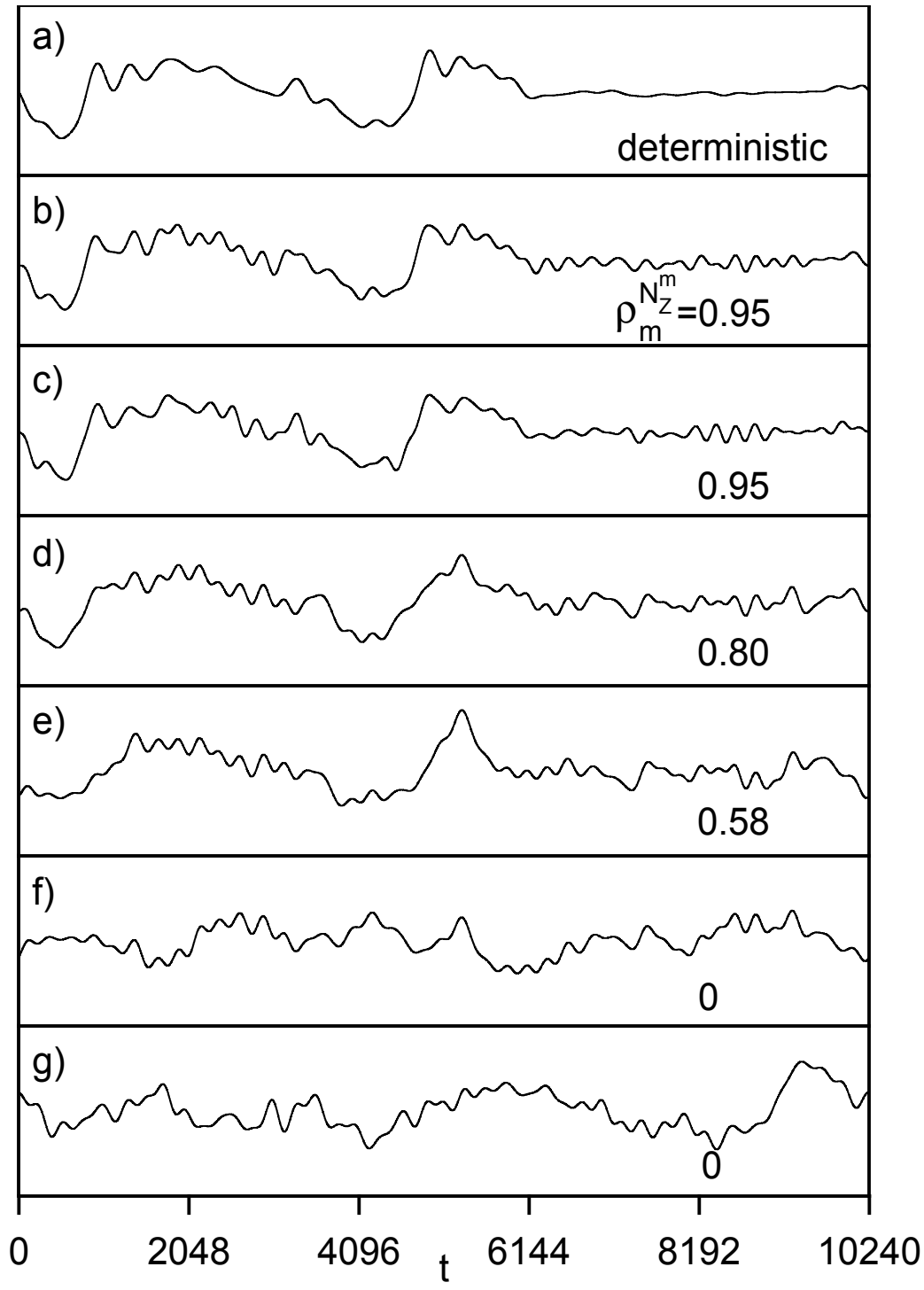

Figure 6.17. Time series plots for (a) deterministic mean description with $M_m = 35$ and mean representations correlated to the deterministic mean, with $\rho_m^{N_Z^m} = 0.95$ for $N_Z^m = 20$, $\rho_m^{N_Z^m} = 0.80$ for $N_Z^m = 7$, $\rho_m^{N_Z^m} = 0.58$ for $N_Z^m = 4$, and $\rho_m^{N_Z^m} = 0$ for $N_Z^m = 0$ - nonstationary mean case.

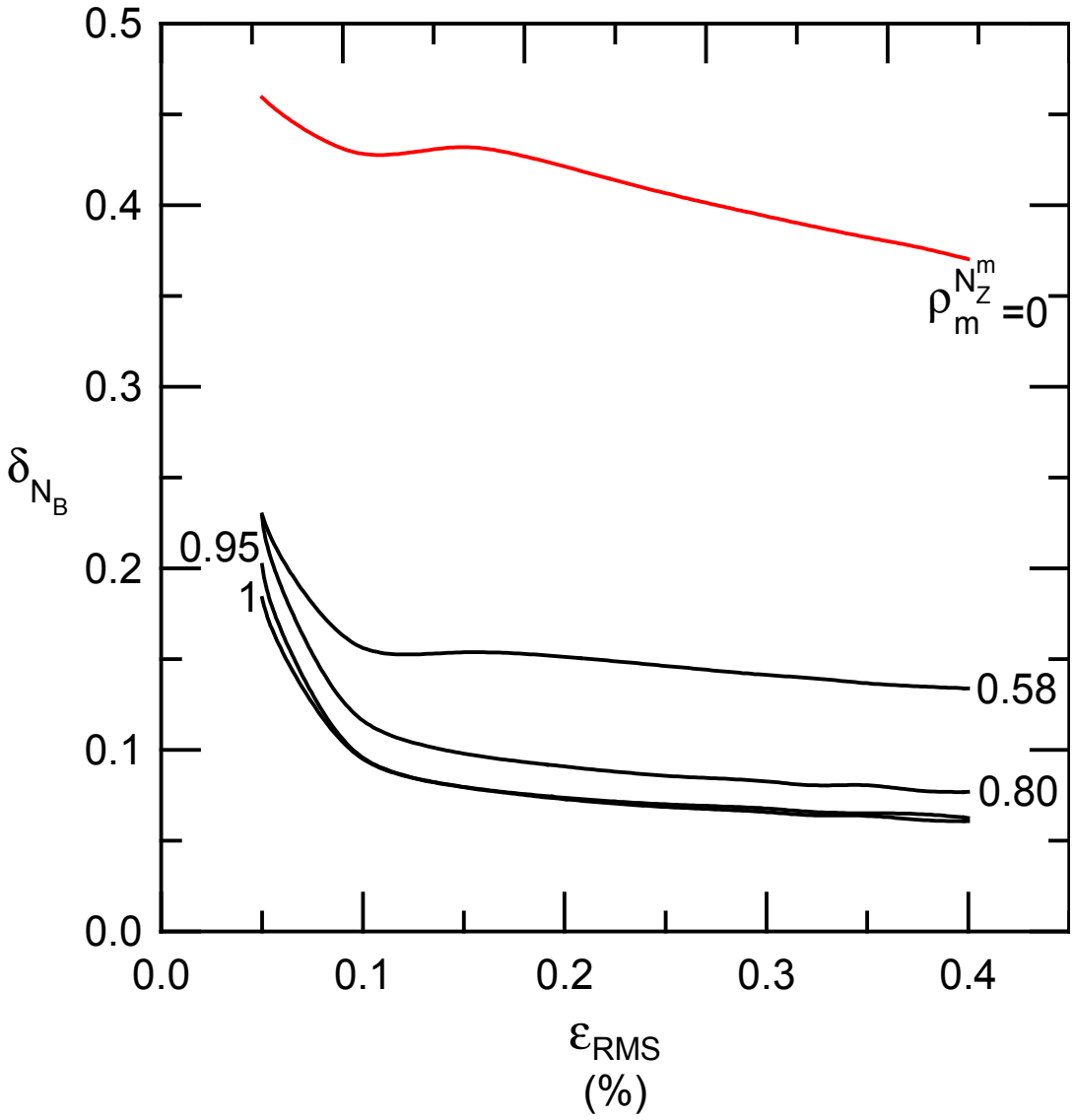

Figure 6.18. Coefficient of variation of fatigue life, δ_{N_B}, versus RMS strain, ε_{RMS}, for mean realizations of various correlations to deterministic mean, $\rho_m^{N_Z^m}$ - nonstationary mean case.

For the case of smaller values of $\rho_m^{N_Z^\mu}$ the variability in life is larger due to the contribution of the larger variations in mean. For the limiting case of $\rho_m^{N_Z^\mu}$=1, i.e. where the deterministic mean is used, the variability is smallest and entirely caused by differences in ARMA reconstructions. The variability in life for all cases of $\rho_m^{N_Z^\mu}$ is larger for smaller values of RMS strain level. This is due to the fact that, as the strain level decreases, the large number of rainflow cycles with small range contribute less to the overall damage. Therefore, only a few large range cycles contribute to fatigue damage, consequently the variability is larger.

6.3 Nonstationary Variance

A typical history of nonstationary strain gauge data is chosen as the random fatigue load history in this study, Fig. 6.19a. This history, containing 10240 points, constitutes one block. Its power spectral density is shown in Fig. 6.20.

According to the employed model of Eq. (5.1), the history is decomposed into its two components, the scaling function, s_t, and the stationary random part, n_t, where it is assumed that the mean, m_t, is constant. To model the scaling function, s_t, an estimate of the standard deviation of the time series, $\tilde{\sigma}_t$, is obtained according to Eq. (5.4), and shown in Fig. 19b. In order to concisely represent $\tilde{\sigma}_t$ the Box-Cox transformation is performed. Figure 6.21 shows the skewness coefficient of the transformed series, θ, for a range of the transformation parameter, λ, where it can be seen that two values of λ, namely $\lambda = -0.05$ and $\lambda = 0.275$, lead to symmetrically distributed series. In Fig. 6.22 the corresponding frequency histograms are shown along with their equivalent Gaussian density functions. The normalized errors between the histogram and density function, calcu-

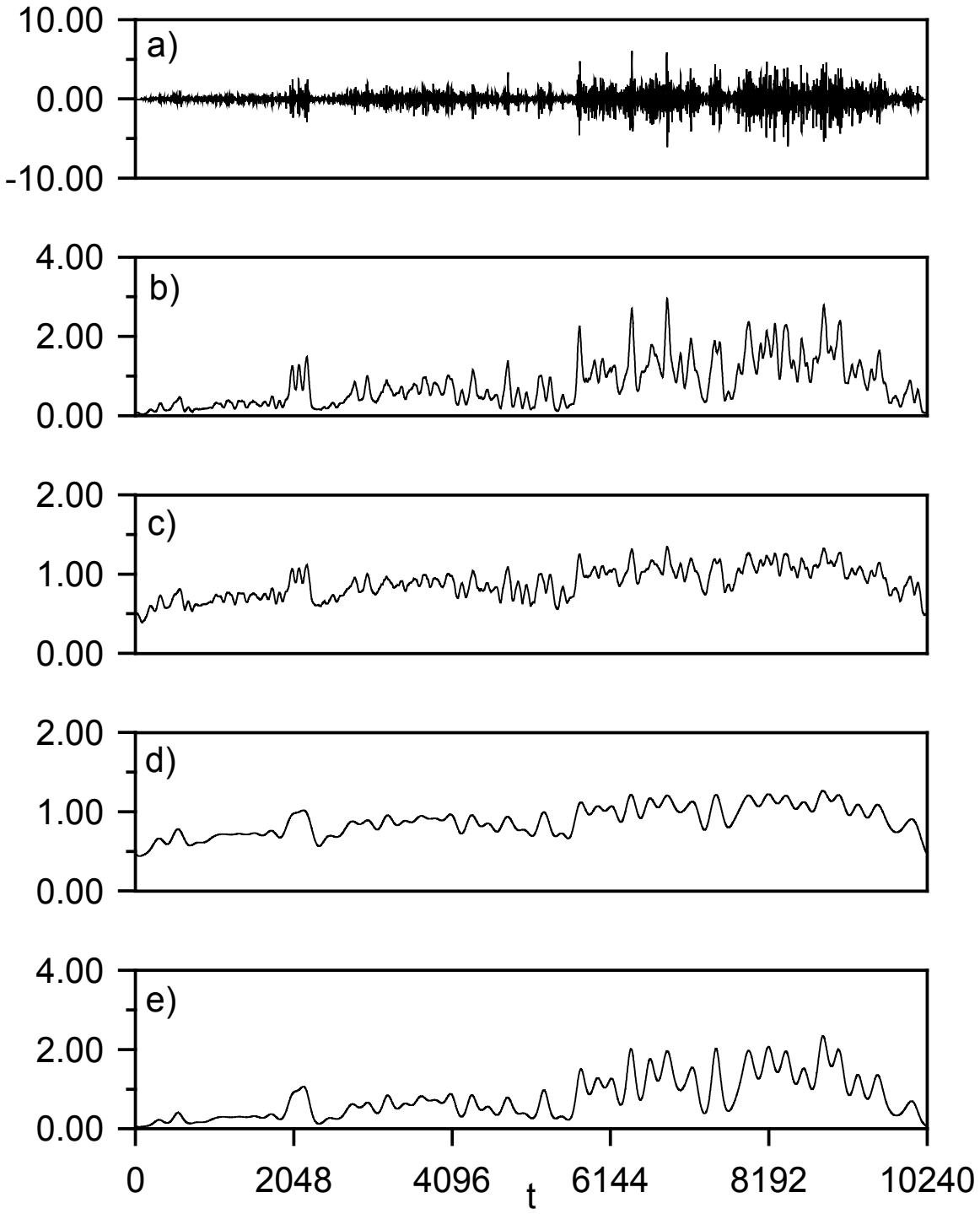

Figure 6.19. Time series plots for (a) original record, (b) estimated standard deviation, $\tilde{\sigma}_t$, (c) Box-Cox transform of $\tilde{\sigma}_t$, $\tilde{\sigma}_t^{BC}$, (d) Fourier series approximation to $\tilde{\sigma}_t^{BC}$ with $M_s = 50$, s_t^{BC}, and (e) scaling function s_t - nonstationary variance case.

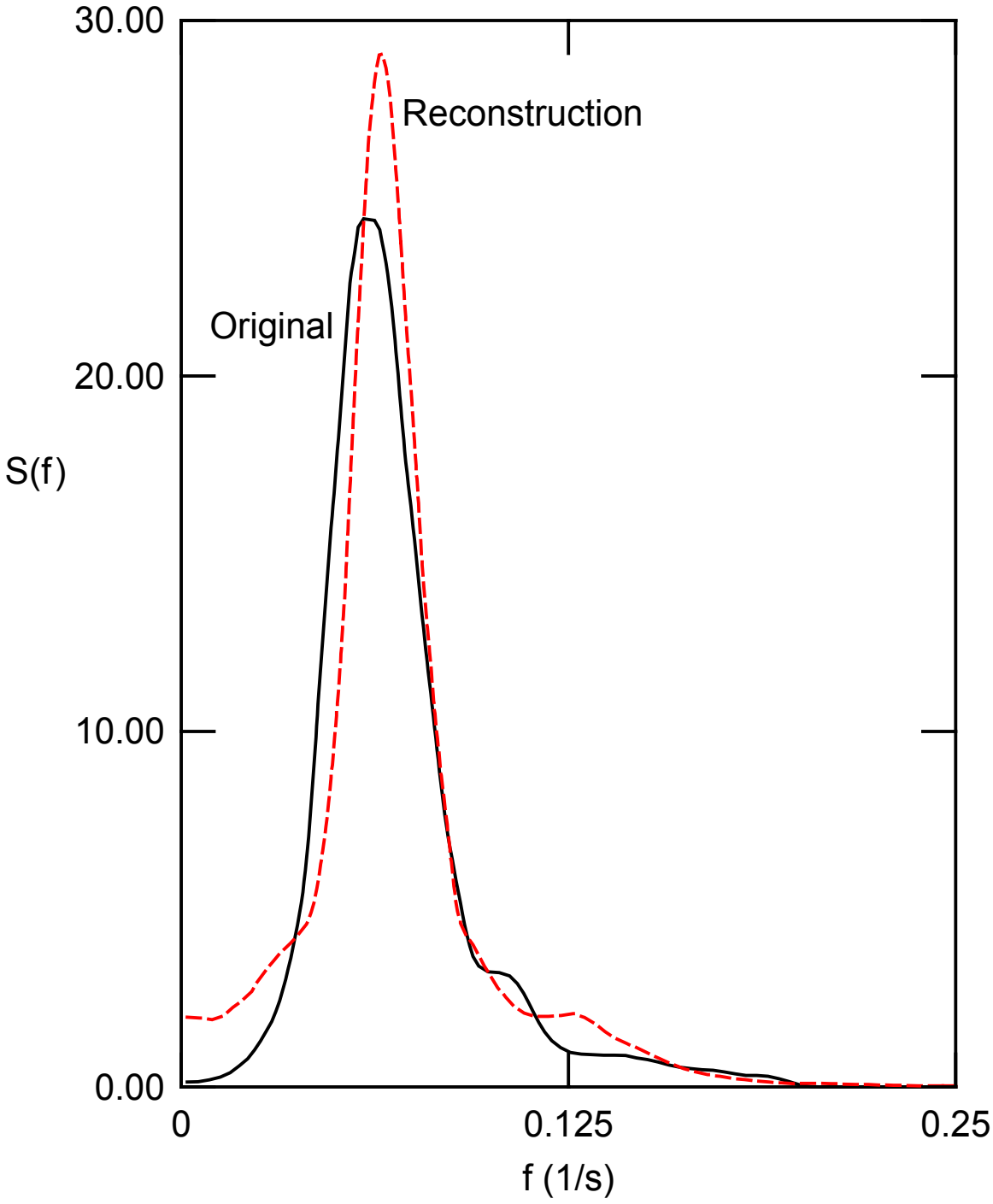

Figure 6.20. Power spectral density for the original history and a history reconstructed with $M_s = 50$ and ARMA(6,0) - nonstationary variance case.

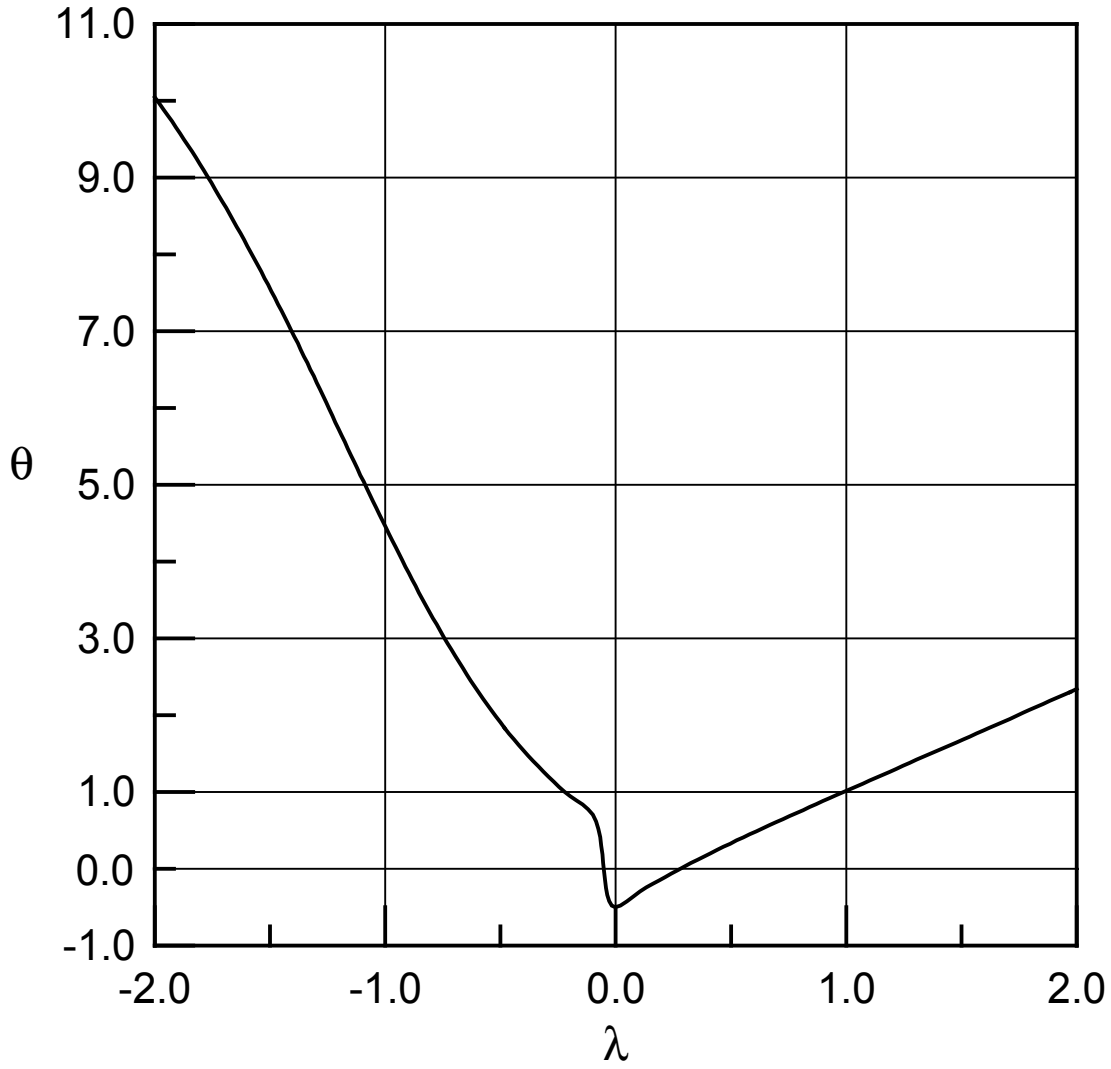

Figure 6.21. Box-Cox transformation parameter, λ, versus skewness coefficient, θ, of transformed series - nonstationary variance case.

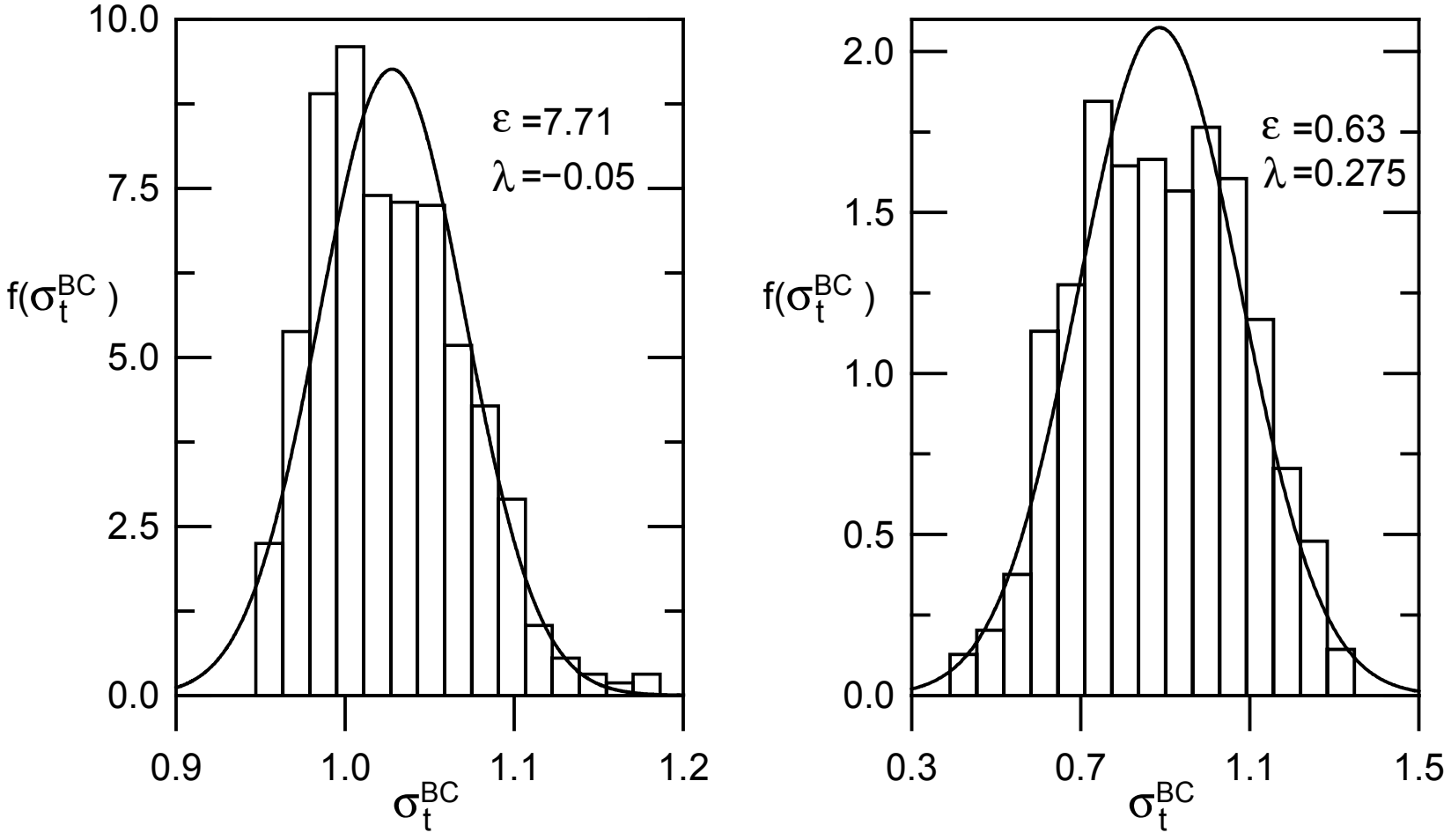

Figure 6.22. Frequency histogram (bar chart) of Box-Cox transformed series, σ_t^{BC}, and probability density function (smooth curve) of corresponding normal distribution for two values of transformation parameter λ, where ε denotes the normalized error between the histogram and the probability density function - nonstationary variance case.

lated according to Eq. (5.9), are $\varepsilon = 7.71$ for $\lambda = -0.05$ and $\varepsilon = 0.63$ for $\lambda = 0.275$. The optimal transformation parameter, therefore, is $\lambda = 0.275$, and the transformed variable, $\tilde{\sigma}_t^{BC}$, is shown in Fig. 6.19c. A number of Fourier series with an increasing number of terms are formed according to Eq. (5.10), giving the tentative scaling functions. The series, s_t^{BC}, with the fewest number of terms that is correlated at 95% to $\tilde{\sigma}_t^{BC}$ has $M_s = 50$ terms and is shown in Fig. 6.19d. The inverse Box-Cox transformation of s_t^{BC}, s_t, is the scaling function used to render the original series stationary with respect to variance and shown in Fig. 6.19e. This stationary series, the quotient of x_t and s_t, is shown in Fig. 6.23a.

The stationary series will be presented by an ARMA model. Parameters for a number of ARMA models are estimated and the correlation coefficients between power spectra of these ARMA models and the spectrum of the stationary series are calculated and are shown in Table 6.7. Seeking models which have correlations of $\rho_S^{(p,q)}$ greater or equal than 0.8, 0.85, 0.9, and 0.95 leads to the following choices of respective minimum order models: ARMA(2,0), ARMA(2,1), and ARMA(6,0). Power spectral densities of the stationary series, ARMA(2,0), and ARMA(6,0) are shown in Fig. 6.24. The area under the PSD of both ARMA models is approximately the same as the area under the PSD of the stationary series. However, the peak of the stationary series is closer approximated by the ARMA(2,0) than by the ARMA(6,0) model. In the very low frequency range, however, the ARMA(6,0) approximates the PSD of the stationary series better. Moreover, the area under the PSD of the stationary series is about the same as the are under the PSD for the original loading. This can be explained by the fact that the original series was of unit variance, while the stationary series was obtained by dividing the original series by an estimate of it's standard deviation. Such division leads by definition to a series of unit variance,

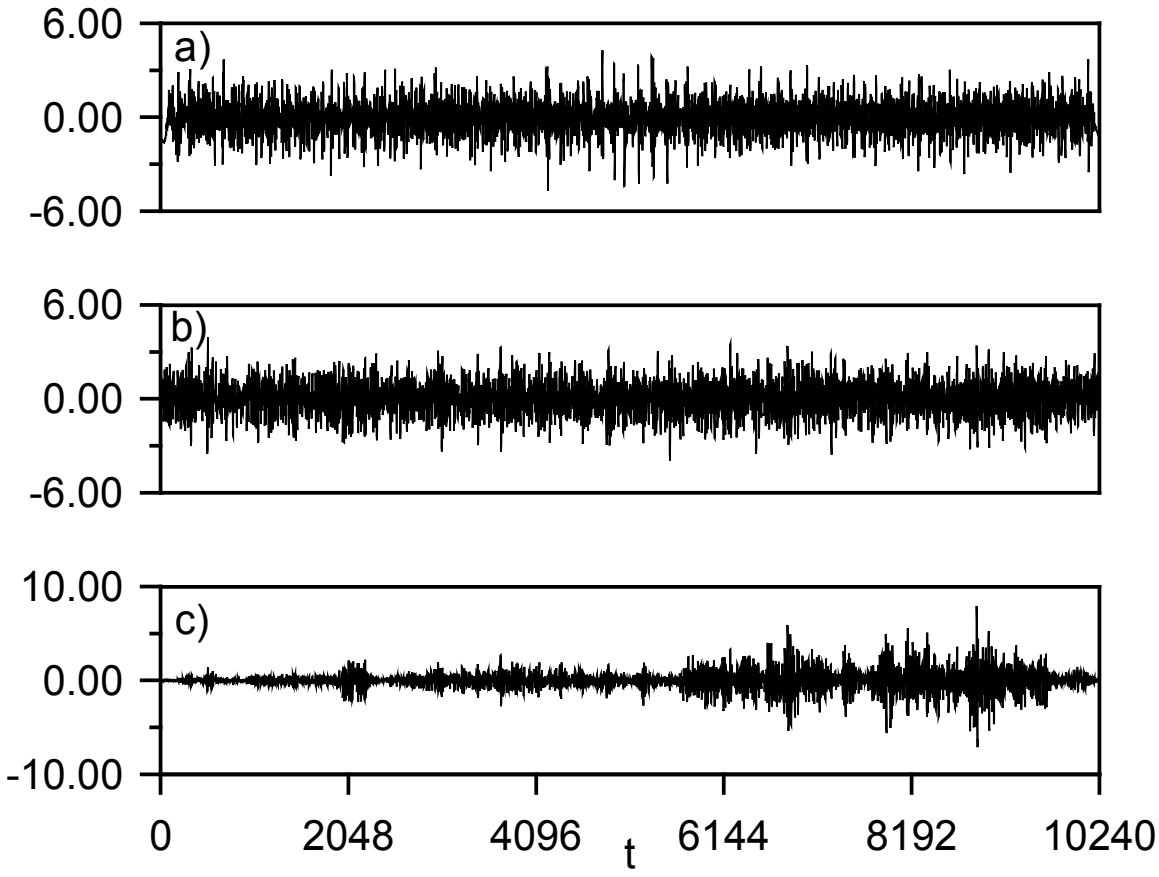

Figure 6.23. Time series plots for (a) stationary series, (b) ARMA(6,0) model simulation, and (c) reconstruction - nonstationary variance case.

Table 6.7. Correlation coefficient of power spectra, $\rho_S^{(p,q)}$, for selected ARMA(p,q) models, where the bold number indicates the minimum order model for a given correlation value - nonstationary variance case.

p \ q	0	1	2	3	4	5	6	7
1	0.08							
2	**0.84**	**0.86**						
3	0.84	0.86	0.88					
4	0.89	0.88	0.87	0.85				
5	0.88	0.89	0.90	0.89	0.97			
6	**0.95**	0.95	0.96	0.93	0.96	0.97		
7	0.94	0.95	0.95	0.93	0.96	0.98	0.99	
8	0.97	0.96	0.96	0.95	0.97	0.98	0.99	0.99

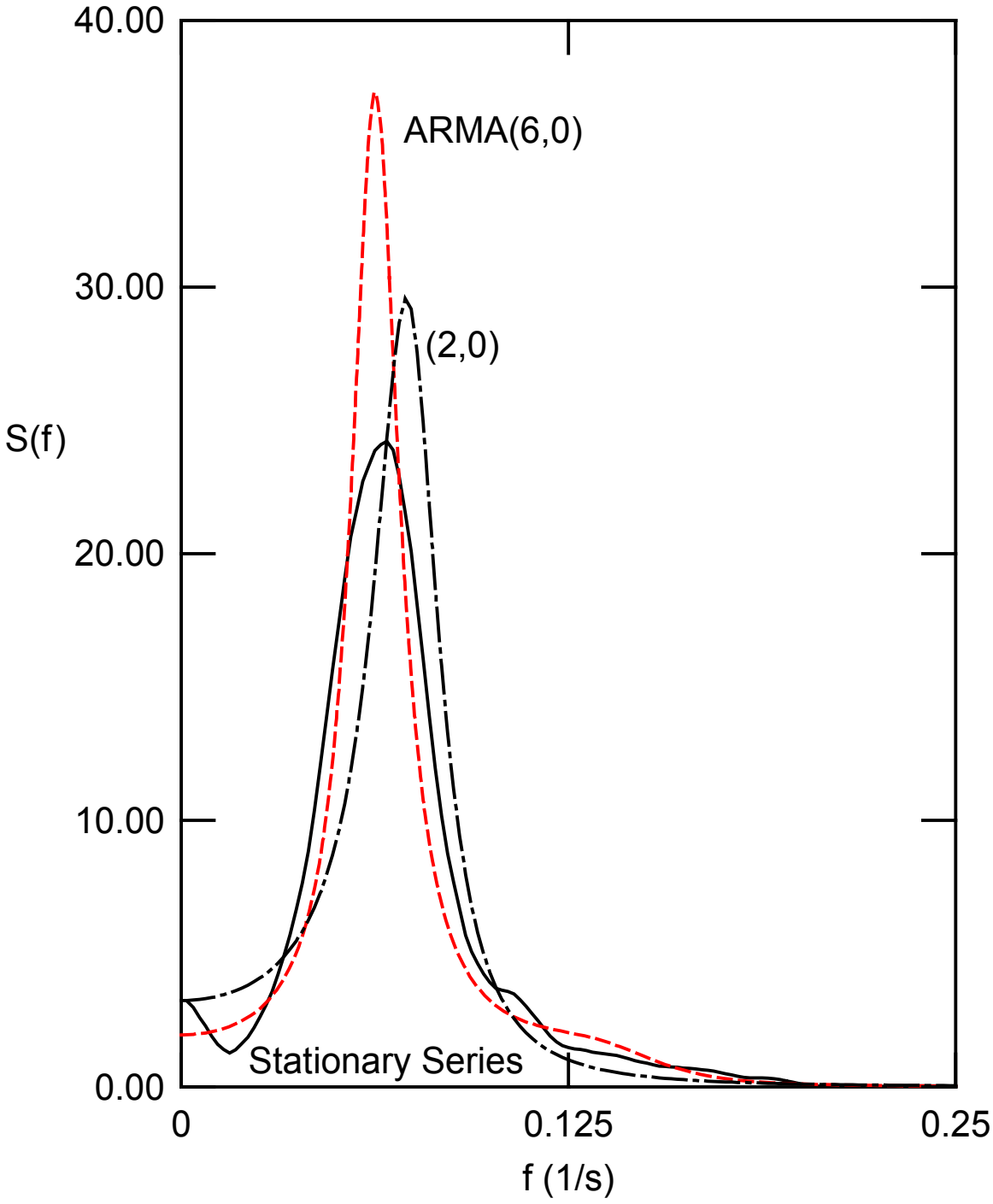

Figure 6.24. Power spectral density for the stationary series and two ARMA models, where for ARMA(2,0) $\rho_S^{(2,0)} = 0.84$ and for ARMA(6,0) $\rho_S^{(6,0)} = 0.95$ - non-stationary variance case.

therefore, the areas under the respective power spectral densities have to be identical.

Reconstructions are formed for all of these ARMA models and multiplied by the deterministic scaling function. Strain life curves are obtained for the original loading, where the bounded life calculation is performed, and for various ARMA reconstructions, Fig. 6.25, where 64 independent reconstructions were performed and averaged to eliminate any bias introduced by a particular reconstruction. Note that strain life curves for the ARMA(2,0), ARMA(2,1), and ARMA(6,0) reconstructions are very close, but only the highest order model, i.e. ARMA(6,0) model is deemed appropriate as its strain life curve falls, at least partially, inside the bounds of the original. As before strain life curves are also shown for ARMA(0,0) and ARMA(1,0), the limiting cases. Here, it is noted that ARMA(0,0) and ARMA(1,0) life predictions are about as far from the bounds of the original than it is the case of the stationary loading in Section 6.1. As the mean variation is zero, it is the stationary random component that governs fatigue life. The scaling function, s_t, determines the variance of the process, but the ARMA model determines the correlation, and therefore rainflow cycles, of the series. Therefore, any bias introduced by an inappropriate ARMA model influences the reconstruction as it was the case in Section 6.1.

A complete reconstruction, using the stationary record obtained from the selected ARMA(6,0) model, shown in Fig. 6.23b, is shown in Fig. 6.23c. The power spectral density of the reconstructed history is shown in Fig. 6.20. Finally, for visual comparison, the rainflow and damage histograms are obtained and are shown in Figs. 6.26-6.27. The overall agreement is good; both the large number of small cycles and the small number of large cycles being well approximated. To demonstrate the consistency of the reconstruc-

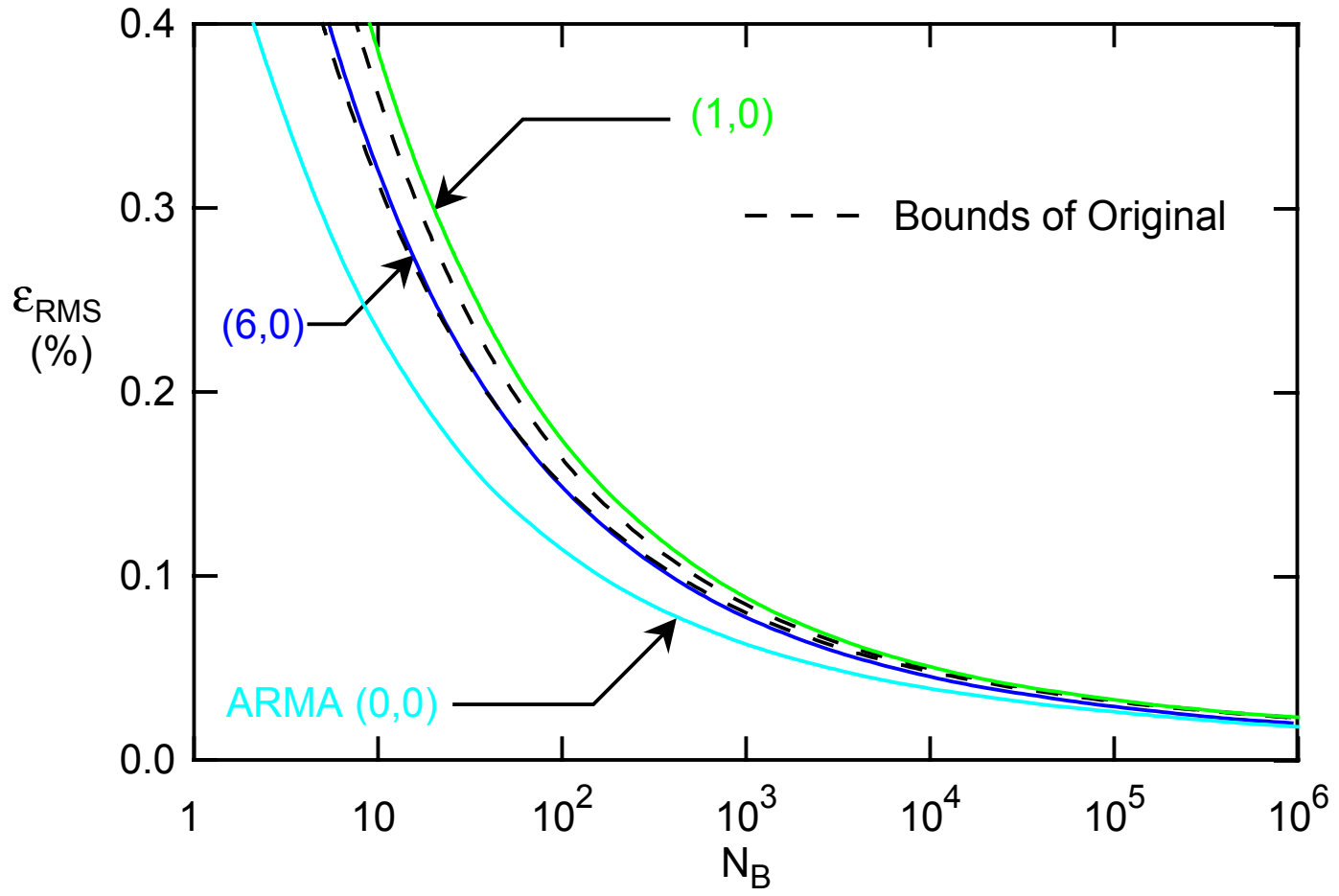

Figure 6.25. RMS strain level, ε_{RMS}, versus blocks to failure, N_B, for the original and reconstructed history with ARMA(6,0) and $M_s = 50$ - nonstationary variance case.

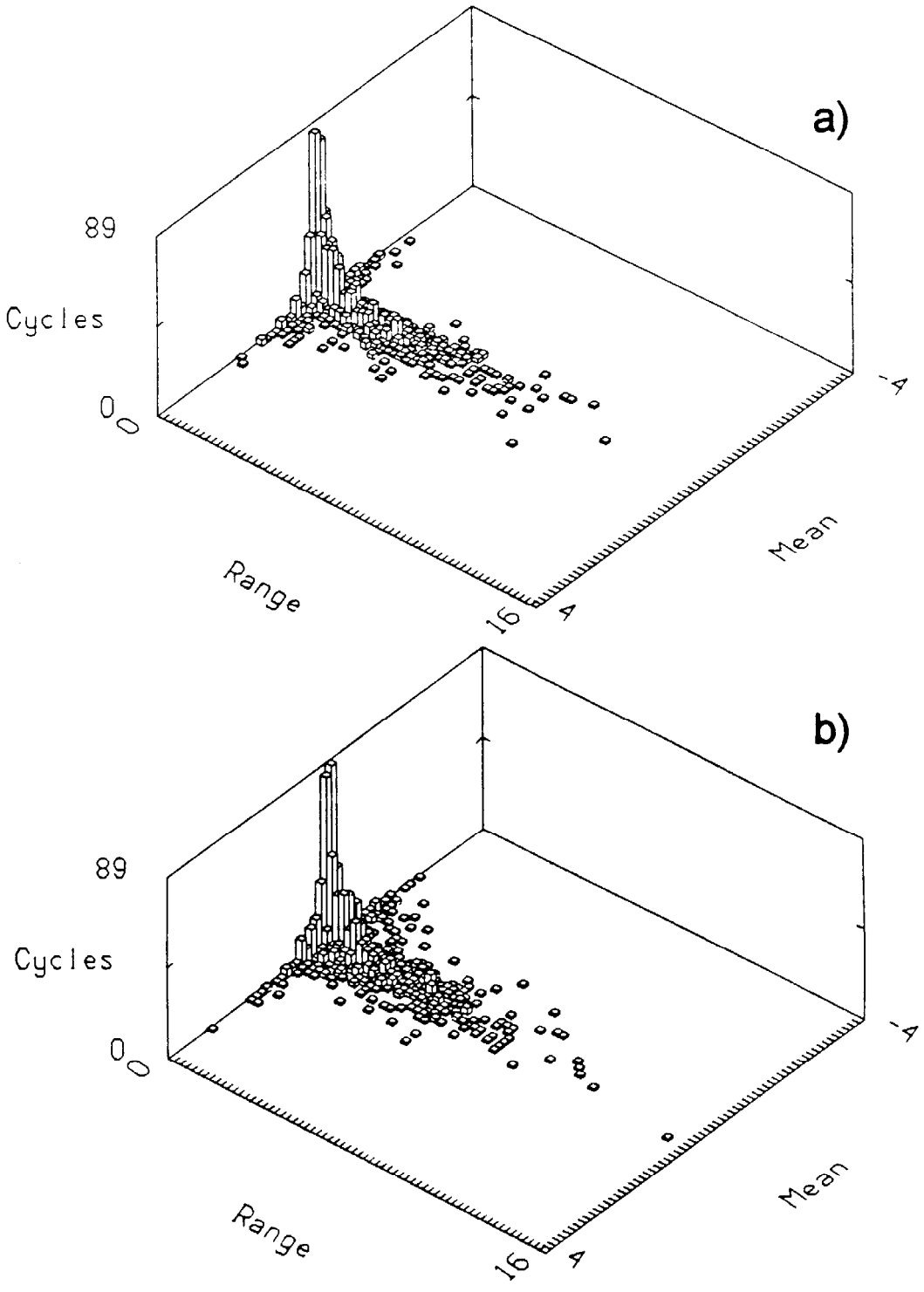

Figure 6.26. Rainflow histograms for (a) original and (b) reconstruction with $M_s = 50$ and ARMA(6,0) - nonstationary variance case.

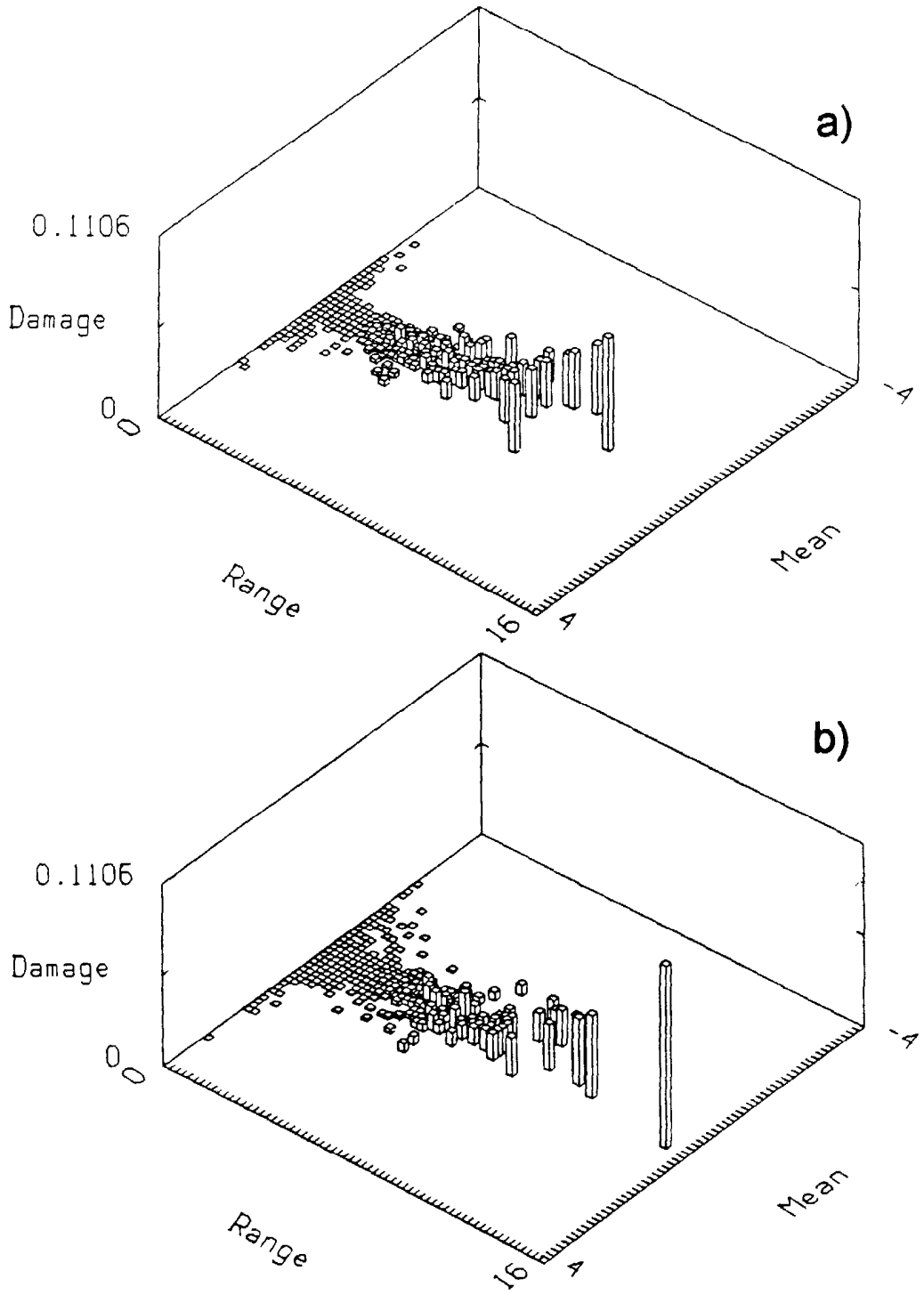

Figure 6.27. Damage histograms for (a) original and (b) reconstruction with $M_s = 50$ and ARMA(6,0), where $\varepsilon_{RMS} = 0.1\%$ - nonstationary variance case.

tion, Fig. 6.28 shows five independently simulated records.

6.4 Nonstationary Mean and Variance

A typical history of nonstationary strain gauge data is chosen as the random fatigue load history in this study, Fig. 6.29a, where it is noted that this is the history used in Section 6.2, but no manipulation prior to this study was performed. This history, containing 10240 points, constitutes one block. Its power spectral density is shown in Fig. 6.30.

According to the employed model of Eq. (5.1), the history is decomposed into its three components, the mean component, m_t, the scaling function, s_t, and the stationary random part, n_t. In order to model the variation of the mean in a deterministic way, m_t, various Fourier series with increasing numbers of terms are formed, giving the tentative mean descriptions. The difference, $n_t \cdot s_t$, of the original record, x_t, and each mean description, m_t, is obtained. These differences are then analyzed for deviations from being a zero-mean process. The best mean description is chosen as the one that renders $n_t \cdot s_t$ stationary with respect to its mean, using the Fourier series with the least number of terms.

In order to analyze the mean-removed record, $n_t \cdot s_t$, it is divided into N_I intervals each of which contains, according to Section 5.3, $N_P = 50$ points. This leads to $N_I = 204$ intervals, for each of which the interval mean is determined. As 10240 can not be evenly divided by 50, the first and last 20 points in the series are ignored for the run tests.

Run tests based on the total number of runs, the number of runs up and down, and the

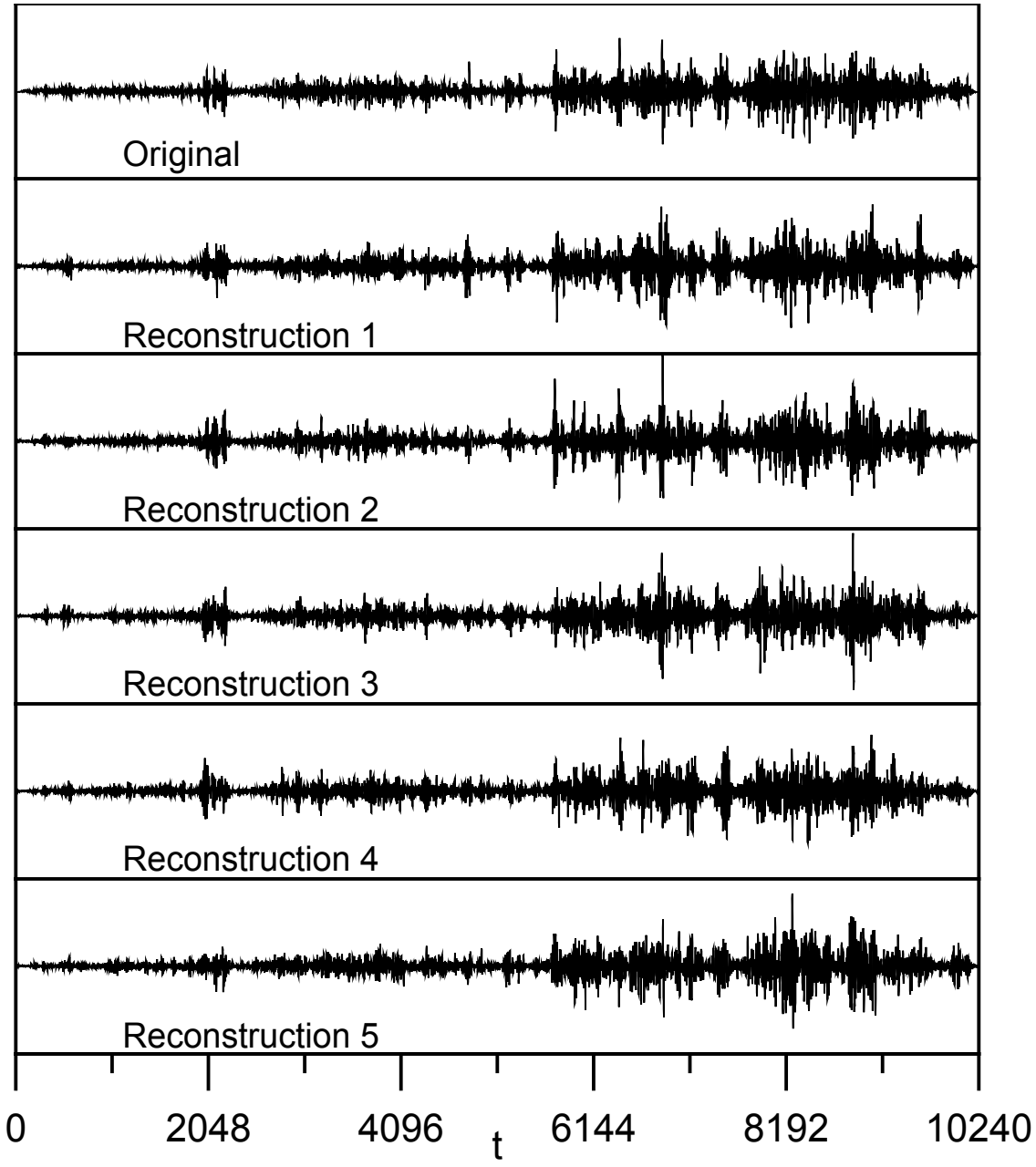

Figure 6.28. Time series plots for original history and reconstructions with the deterministic scaling function, $M_s = 50$, where different simulations of the ARMA(6,0) model are used - nonstationary variance case.

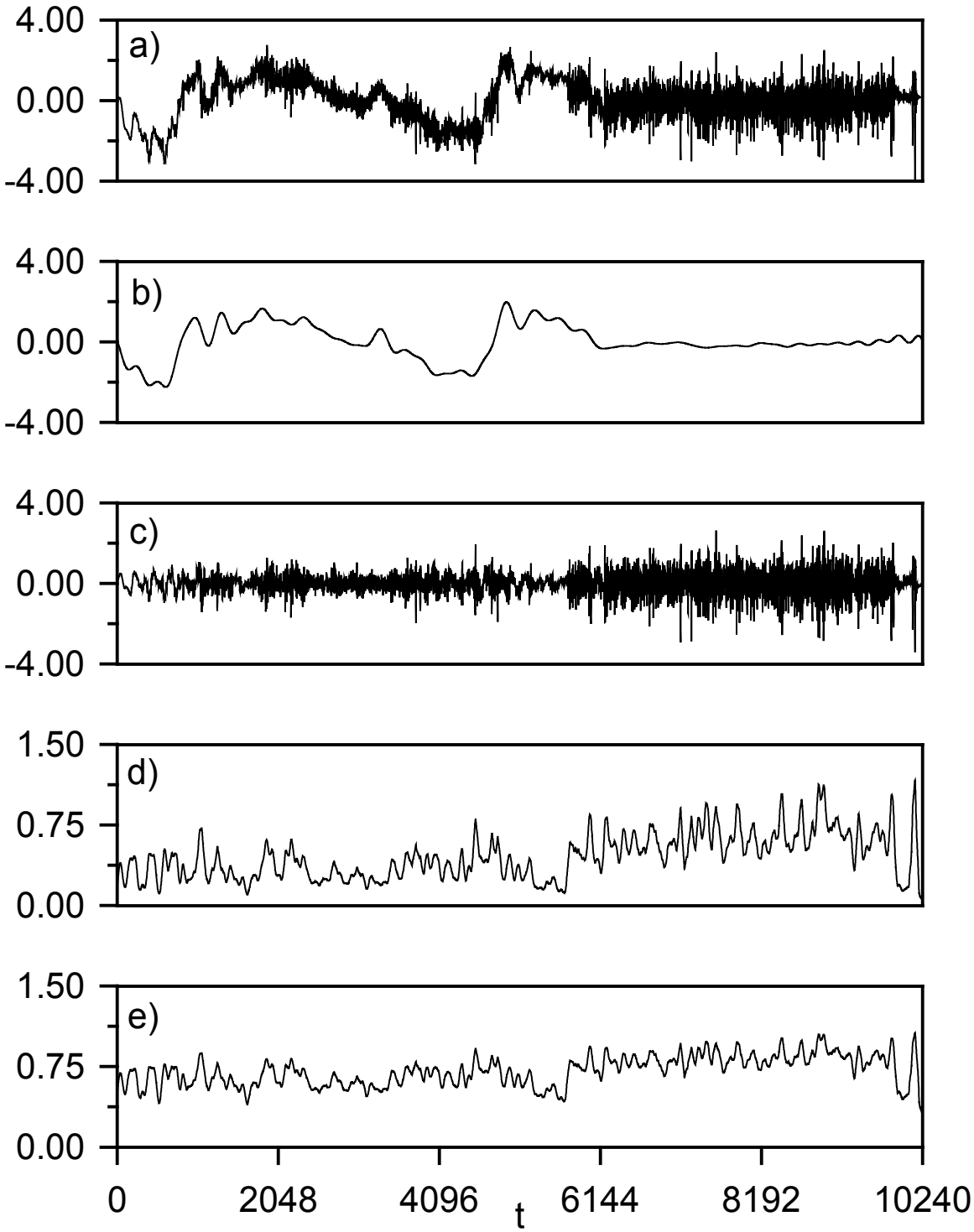

Figure 6.29. Time series plots for (a) original history, (b) deterministic mean with $M_m = 41$, (c) mean-removed series, (d) estimated standard deviation, $\tilde{\sigma}_t$, (e) Box-Cox transform of $\tilde{\sigma}_t$, $\tilde{\sigma}_t^{BC}$ - nonstationary mean and variance.

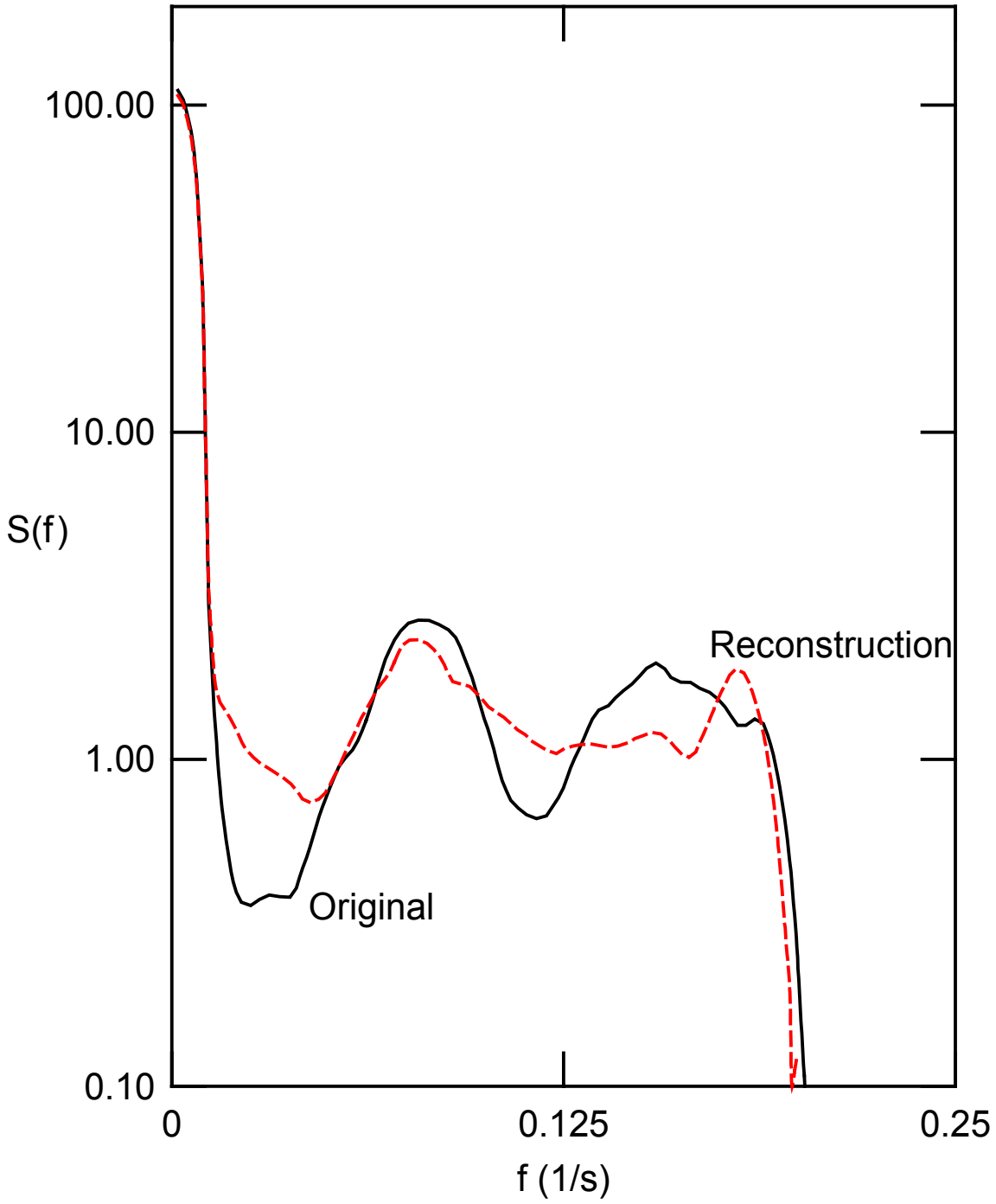

Figure 6.30. Power spectral density for the original history and a history reconstructed with $M_m = 41$, $M_s = 70$, and ARMA(8,0) - nonstationary mean and variance case.

length of the longest run, are performed on the sequence of interval means calculated from $n_t \cdot s_t$. This assures that a variety of deviations from the expected random behavior of this sequence can be detected.

For the case where $N_I = 204$, the 95% $(a = 0.95)$ confidence limits for the total number of runs are $(89 < m_{R_T} < 116)$, while the number of runs up and down covers the range $(123 < m_{R_{UD}} < 147)$. The length of the longest admissible run, according to Eq. (5.17) for a random sequence of length 204, is *K*=6.

Table 6.8 shows the results of these run tests. There is no value for which all run tests are passed. However, for $M_m = 41$ the total number of runs, r_T, is within the allowable range and the number or runs up and down, r_{UD}, is only slightly outside the allowable range. Therefore, a total number of $M_m = 41$ Fourier series coefficients is deemed appropriate for a sufficient mean description to render the remaining signal approximately stationary with respect to its mean value. See also Fig. 6.30b for the deterministic mean model, m_t, and Fig. 6.30c, for the mean removed record, $n_t \cdot s_t$,

In order to model the scaling function, s_t, an estimate of the standard deviation, $\tilde{s}_t$, of the time series is obtained according to Eq. (5.4), and shown in Fig. 6.30d. In order to concisely represent $\tilde{s}_t$ the Box-Cox transformation is performed, where $l = 0.403$ is the optimal transformation parameter, and the transformed variable, $\tilde{s}_t^{BC}$, is shown in Fig. 6.30e. A number of Fourier series with increasing number of terms are formed according to Eq. (5.9), giving the tentative scaling functions. The series, s_t^{BC}, with the fewest number of terms that is correlated at 95% to $\tilde{s}_t^{BC}$ has $M_s = 70$ terms and is shown in Fig. 6.31a. The inverse Box-Cox transformation of s_t^{BC}, s_t, is the scaling function used to ren-

Table 6.8. Results of run tests for different values of M_m for $\alpha = 0.95$ (italics = failure of test, bold accepted as stationary) - nonstationary mean and variance case.

$N_l = 204$			
$\alpha = 0.90$	$91 < r_T < 114$	$125 < r_{UD} < 145$	$k \leq 5$
$\alpha = 0.98$	$86 < r_T < 119$	$121 < r_{UD} < 149$	$k \leq 6$
$\alpha = 0.95$	$89 < r_T < 116$	$123 < r_{UD} < 147$	$k \leq 6$
M_m	r_T	r_{UD}	k
20	*77*	*108*	6
30	103	*118*	4
40	109	*116*	4
41	**108**	***118***	**5**
42	*122*	134	4
50	*143*	142	3
60	*147*	*150*	3
70	*157*	*162*	3
80	*162*	*166*	4
90	*156*	*166*	3

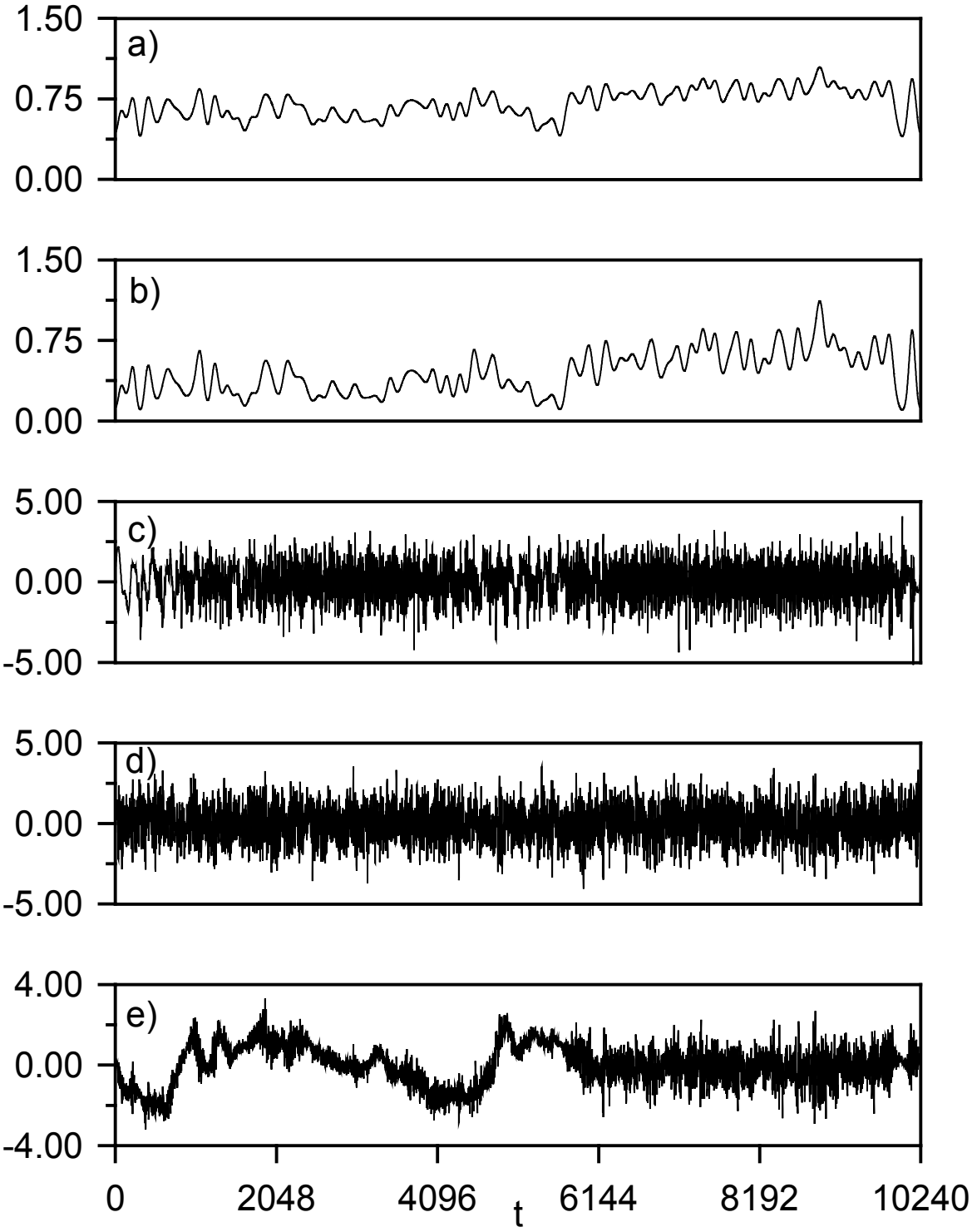

Figure 6.31. Time series plots for (a) Fourier series fit to $\widetilde{\sigma}_t^{BC}$ with $M_s = 70$, s_t^{BC}, (b) scaling function s_t, (c) stationary series, (d) ARMA(8,0) model simulation, and (e) reconstruction - nonstationary mean and variance case.

der the mean-removed series stationary with respect to variance and shown in Fig. 6.31b. This stationary series, the quotient of $n_t \cdot s_t$ and s_t, is shown in Fig. 6.31c.

The stationary series will be presented by an ARMA model. Parameters for a number of ARMA models are estimated, and the correlation coefficient between power spectra of these ARMA models and the spectrum of the stationary series is calculated, Table 6.9. Seeking models which have correlations of $r_S^{(p,q)}$ greater or equal than 0.8, 0.85, 0.9, and 0.95 leads to the choice of ARMA(8,0) as the model with least number of parameters that is correlated to the stationary series at more than 80%. The corresponding value of the correlation coefficient is $r_S^{(8,0)} = 0.96$. Power spectral densities of the stationary series and ARMA(8,0) are shown in Fig. 6.32. It is noted that the relative extrema of the stationary series are very closely approximated by the ARMA model, as it is the case for the area under the PSD of the original.

Reconstructions are formed for this ARMA model and multiplied by the deterministic scaling function. After adding the deterministic mean variation, m_t, strain life curves are obtained for the original loading, where the bounded life calculation is performed, and for the reconstruction, Fig. 6.33, where 64 independent reconstructions were performed and averaged to eliminate any bias introduced by a particular reconstruction. This reconstruction is deemed appropriate as its strain life curve falls, at least partially, inside the bounds of the original. A complete reconstruction, using the stationary record obtained from the selected ARMA(8,0) model, shown in Fig. 6.31d, is shown in Fig. 6.31e. Strain life curves are also shown for ARMA(0,0) and ARMA(1,0), where it is noted that they constitute, as in Section 6.1, the limiting cases of all ARMA reconstructions. ARMA(0,0) leads to the shortest life, while ARMA(1,0) leads to the longest life predicted. Moreover, it is

Table 6.9. Correlation coefficient of power spectra, $\rho_S^{(p,q)}$, for selected ARMA(p,q) models, where the bold number indicates the minimum order model for a given correlation value - nonstationary mean and variance case.

p \ q	0	1	2	3	4	5	6	7	8	9
1	0.62									
2	0.48	0.50								
3	0.69	0.71	0.73							
4	0.46	0.52	0.62	0.68						
5	0.73	0.74	0.74	0.74	0.75					
6	0.75	0.71	0.68	0.58	0.58	0.59				
7	0.56	0.54	0.80	0.93	0.94	0.95	0.93			
8	**0.96**	0.95	0.94	0.95	0.95	0.95	0.93	0.93		
9	0.89	0.89	0.94	0.96	0.96	0.94	0.91	0.94	0.95	
10	0.95	0.92	0.93	0.94	0.94	0.94	0.91	0.95	0.94	0.94

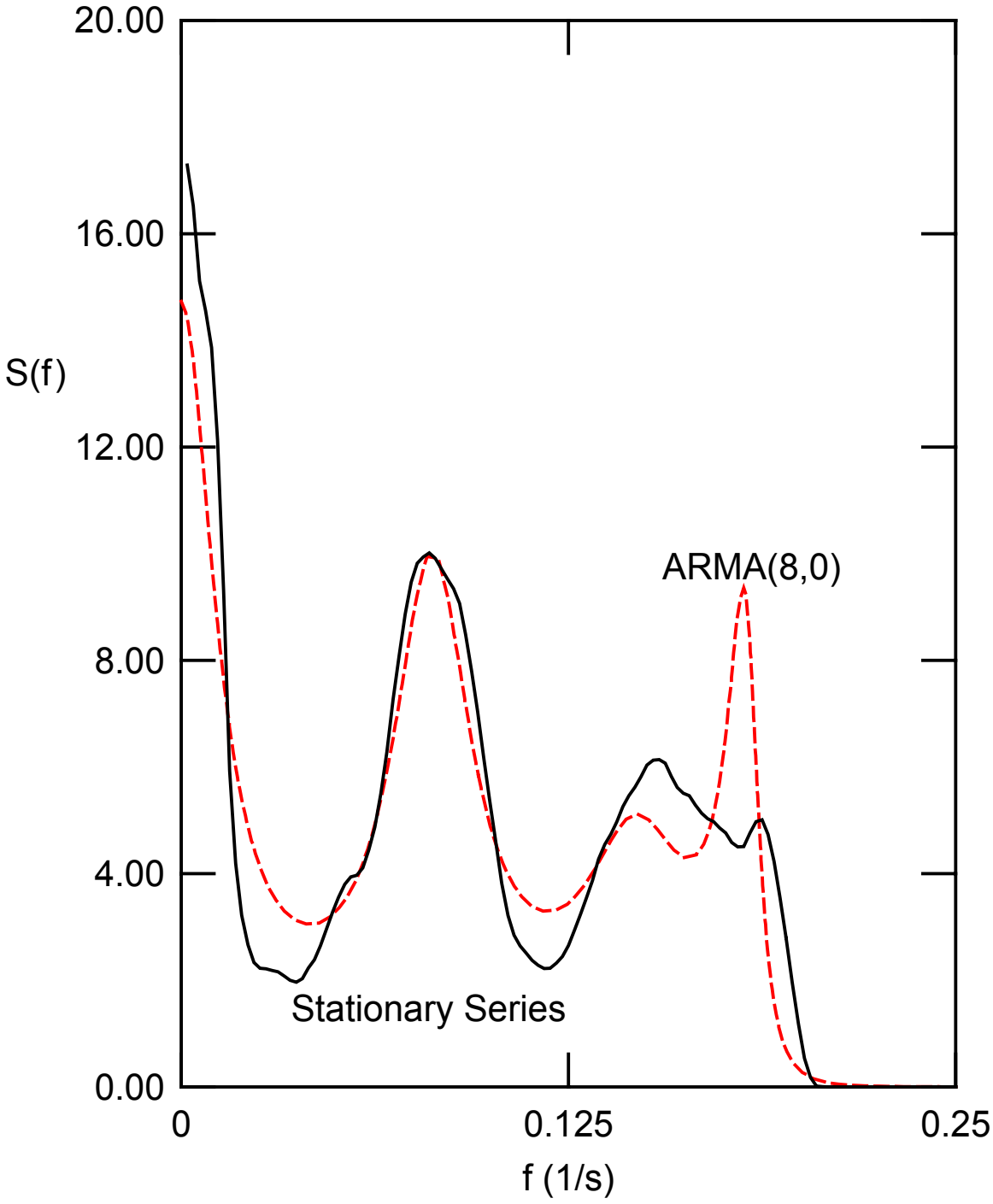

Figure 6.32. Power spectral density for the stationary series and for ARMA(8,0) with $\rho_S^{(8,0)} = 0.96$ - nonstationary mean and variance case.

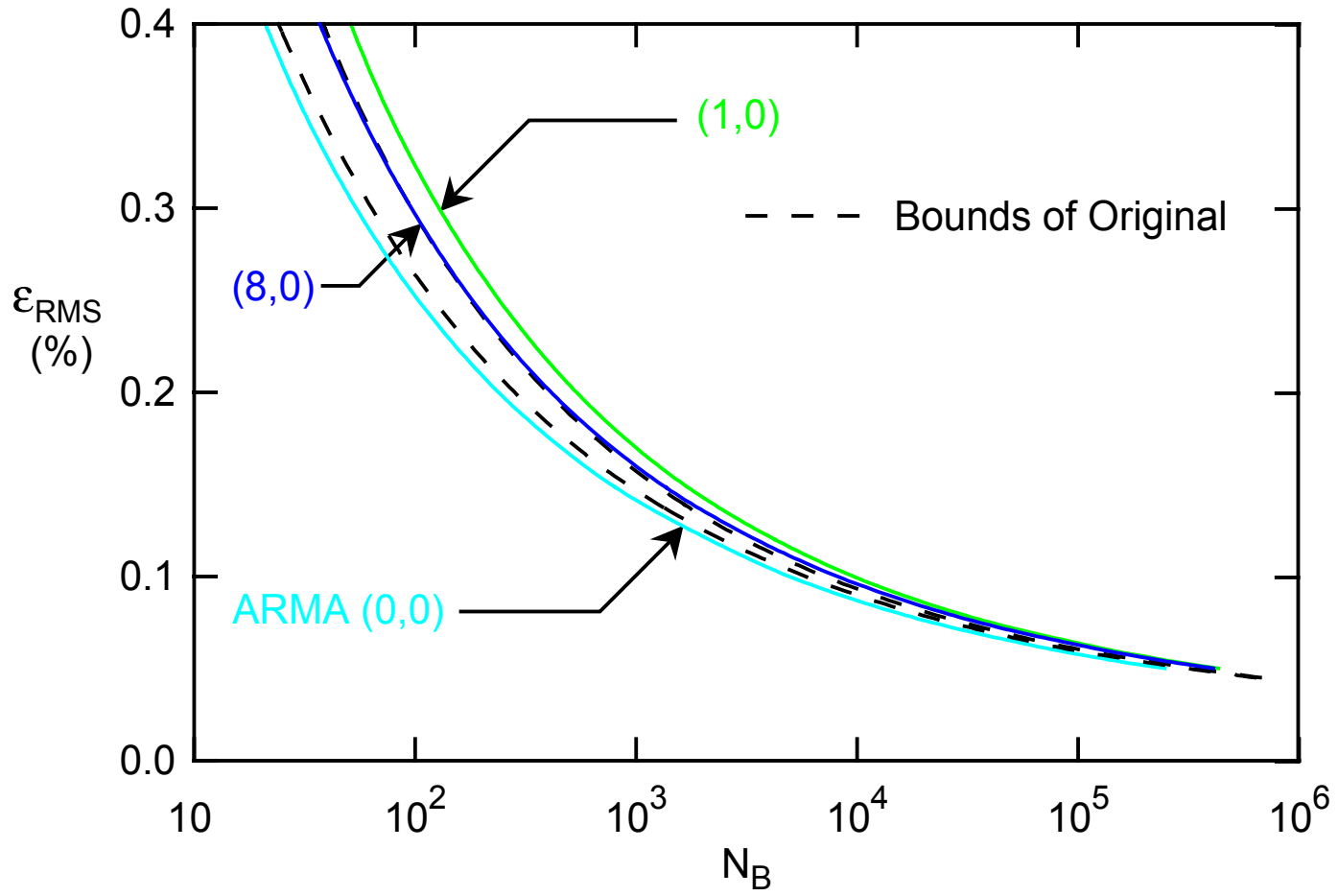

Figure 6.33. RMS strain level, ε_{RMS}, versus blocks to failure, N_B, for original history and a history reconstructed with $M_m = 41$, $M_s = 70$, and ARMA(8,0) - nonstationary mean and variance case.

noted that, as for the case of a nonstationary mean variation in Section 6.2, ARMA(0,0) and ARMA(1,0) are closer to the bounds of the original than is the case of the stationary loading in Section 6.1. Again, this can be explained by the presence of the mean variation.

The power spectral density of the reconstructed history is shown in Fig. 6.30, where it should be noted that the PSD is shown on a logarithmic scale and the overall agreement is actually very close. Finally, for visual comparison, the rainflow and damage histograms are obtained and shown in Figs. 6.34-6.35. The overall agreement is good; both the large number of small cycles and the small number of large cycles being well approximated. To demonstrate the consistency of the reconstruction, Fig. 6.36 shows five independently simulated records.

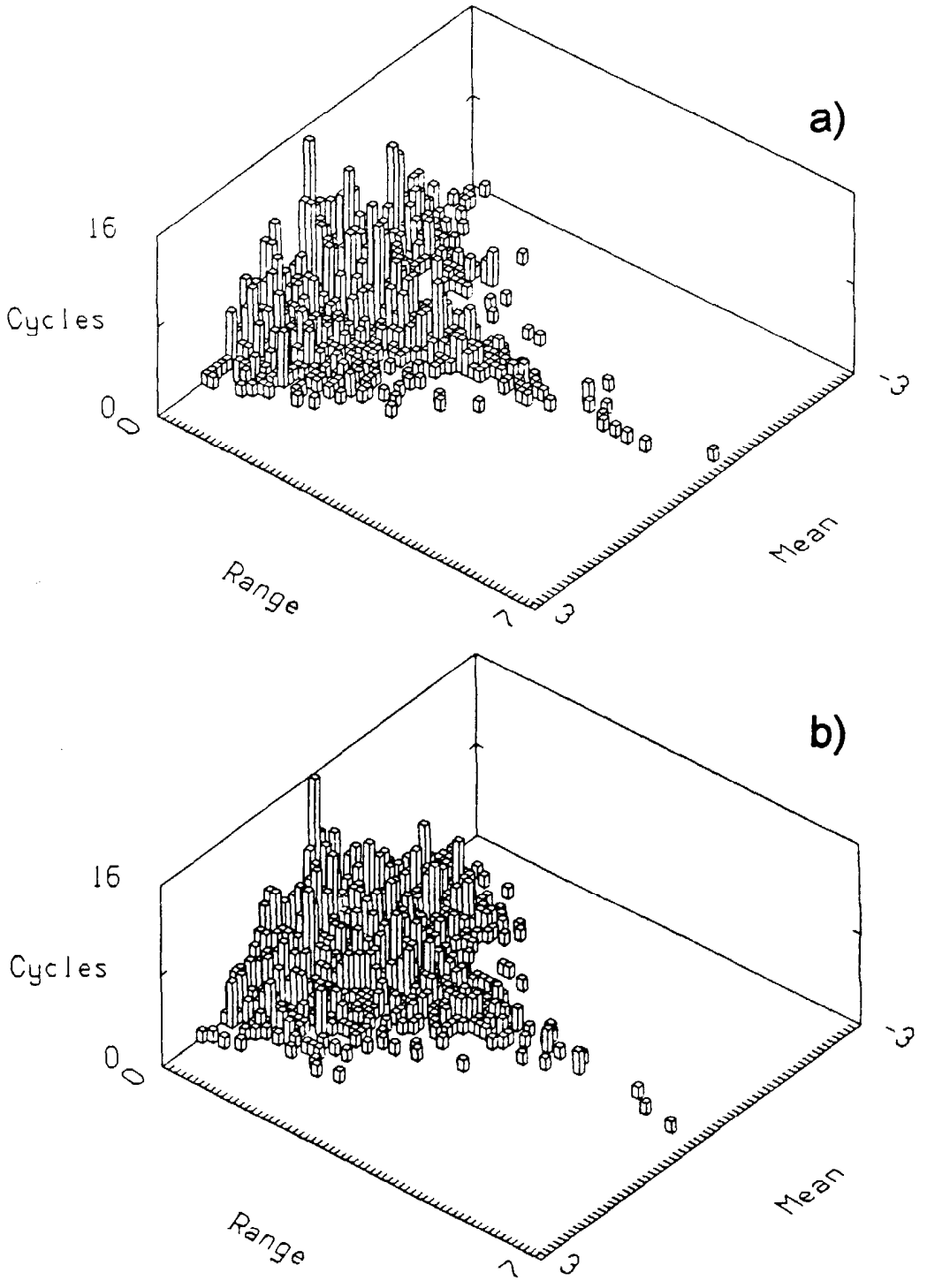

Figure 6.34. Rainflow histograms for (a) original and (b) reconstruction, with $M_m = 41$, $M_s = 70$, and ARMA(8,0) - nonstationary mean and variance case.

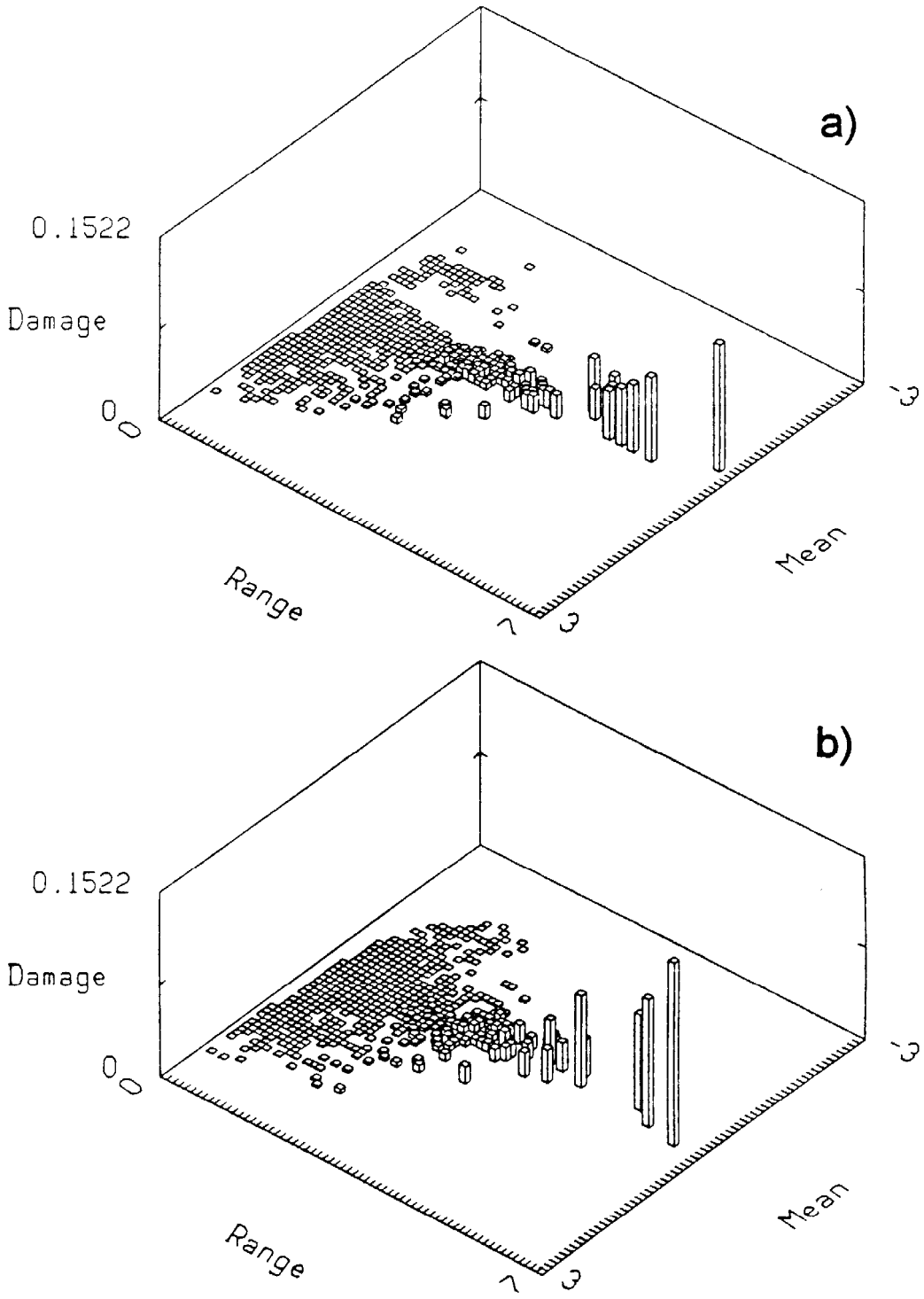

Figure 6.35. Damage histograms for (a) original and (b) reconstruction, with $M_m = 41$, $M_s = 70$, ARMA(8,0), $\varepsilon_{RMS} = 0.1\%$ - nonstationary mean and variance case.

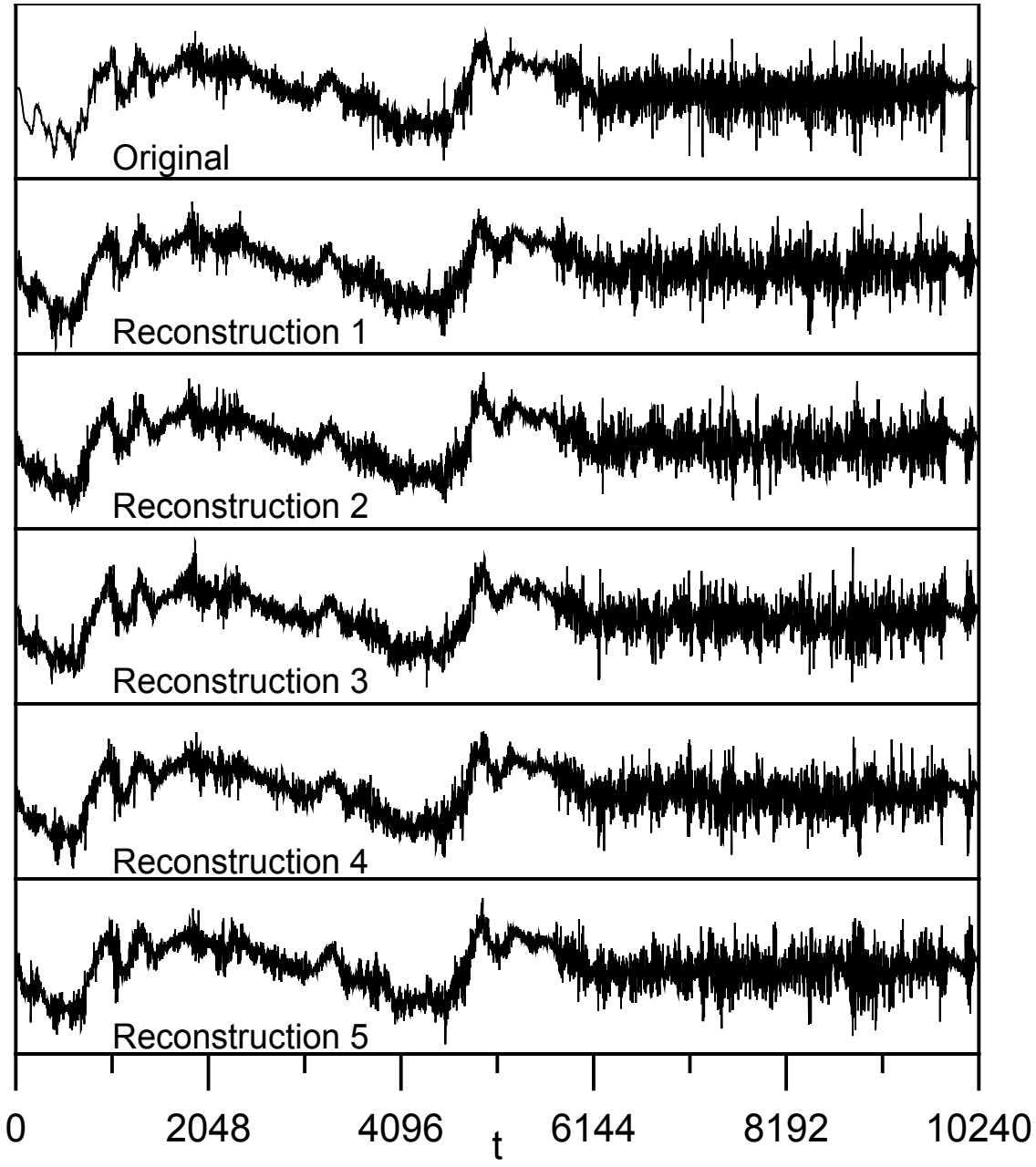

Figure 6.36. Time series plots for original history and reconstructions with the deterministic mean, $M_m = 41$, and the deterministic scaling function, $M_s = 70$, where different simulations of the ARMA(8,0) model are used - nonstationary variance case.

CHAPTER 7. STUDIES OF MULTIAXIAL LOADINGS

A strain gauge rosette history was obtained from an automotive front suspension component driven through proving ground maneuvers. This history was provided by General Motors Corporation, MI, to the Society of Automotive Engineers, SAE, Fatigue Design and Evaluation Committee. This set constitutes three channels, where channels 1 and 3 measure strain in directions perpendicular to each other and channel 2 measures strain along a direction which is half between channels 1 and 3. All fatigue life calculations were performed by Lokesh Juneja (according to aforementioned multiaxial fatigue model, Juneja, 1992) and are based on the material properties of SAE 1045 steel, stated in Table 6.1.

7.1 Stationary Mean and Variance

The history, Fig. 7.1, containing 12500 points, constitutes one block. The auto- and cross- spectral densities, $S_{ij}(f)$, where $i, j = 1, 2, 3$ refer to channels 1, 2, 3, are shown in Figs. 7.2-7.7. As the history consists of three channels, no meaningful normalization with respect to mean or variance can be achieved. The basic statistics of all three channels, for original and reconstructed record, are shown in Table 7.1.

According to the employed model of Eq. (5.1), the history is decomposed into its

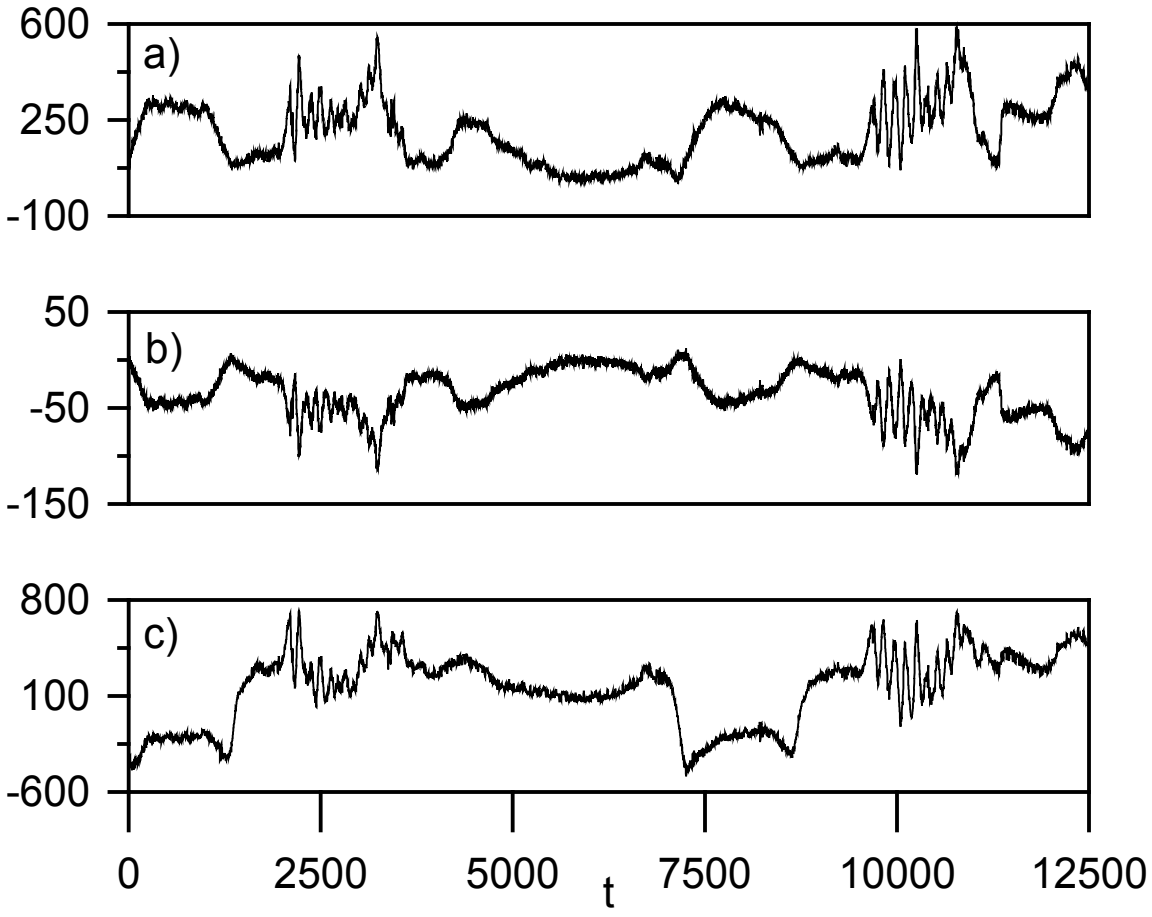

Figure 7.1. Time series plots for strain gauge data (a) channel 1, (b) channel 2, and (c) channel 3.

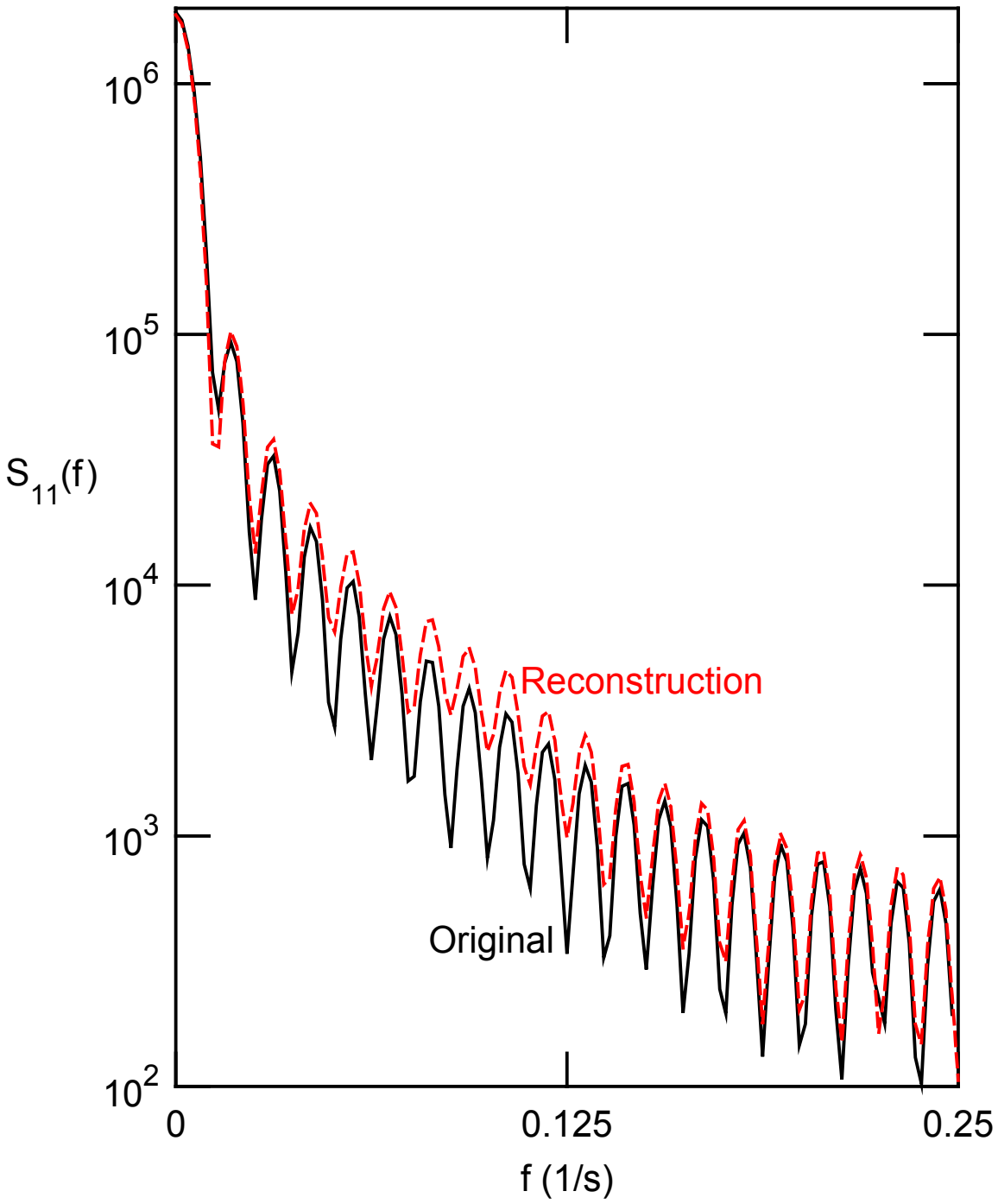

Figure 7.2. Power spectral density, $S_{11}(f)$, for the original history and a reconstructed history.

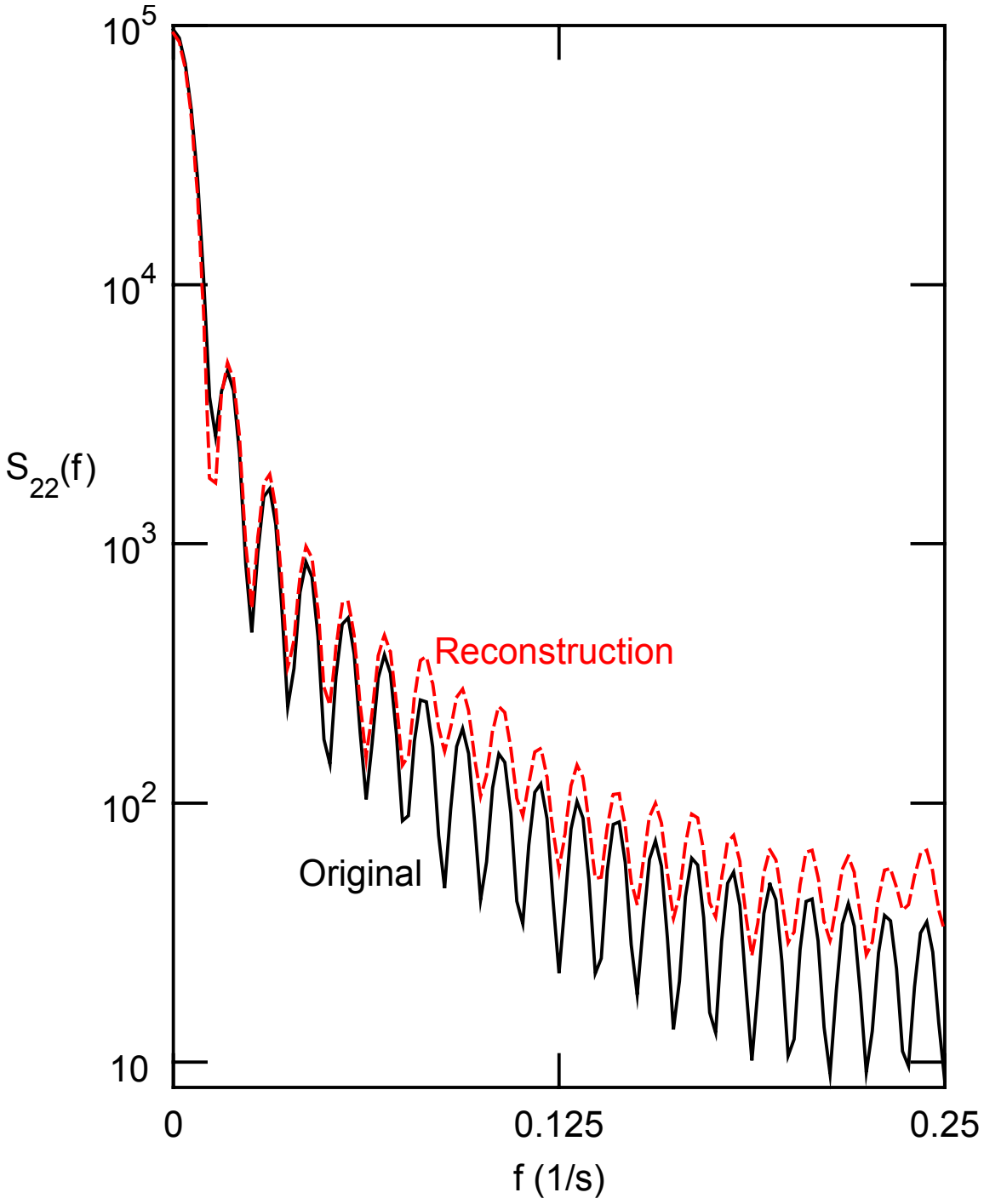

Figure 7.3. Power spectral density, $S_{22}(f)$, for the original history and a reconstructed history.

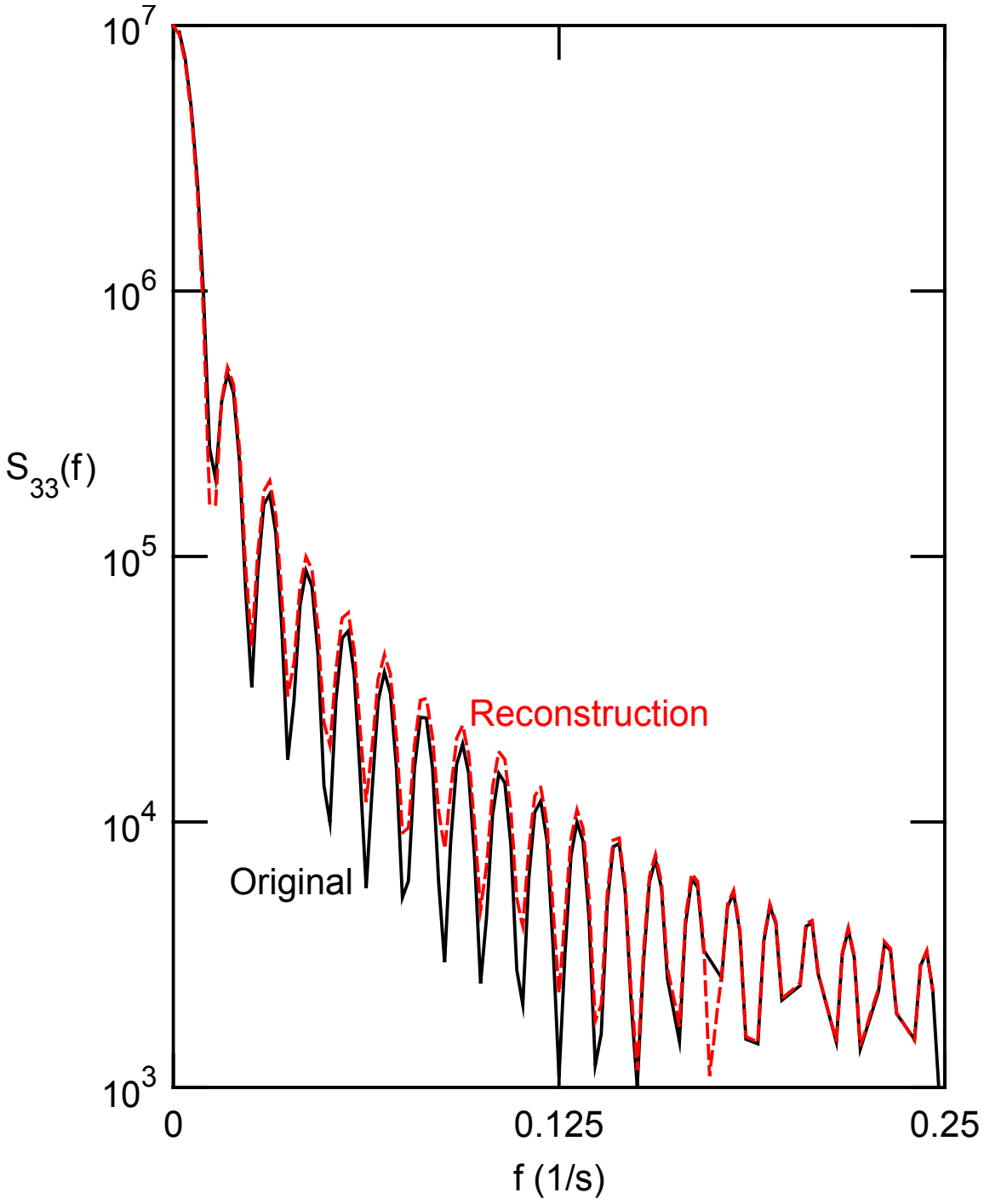

Figure 7.4. Power spectral density, $S_{33}(f)$, for the original history and a reconstructed history.

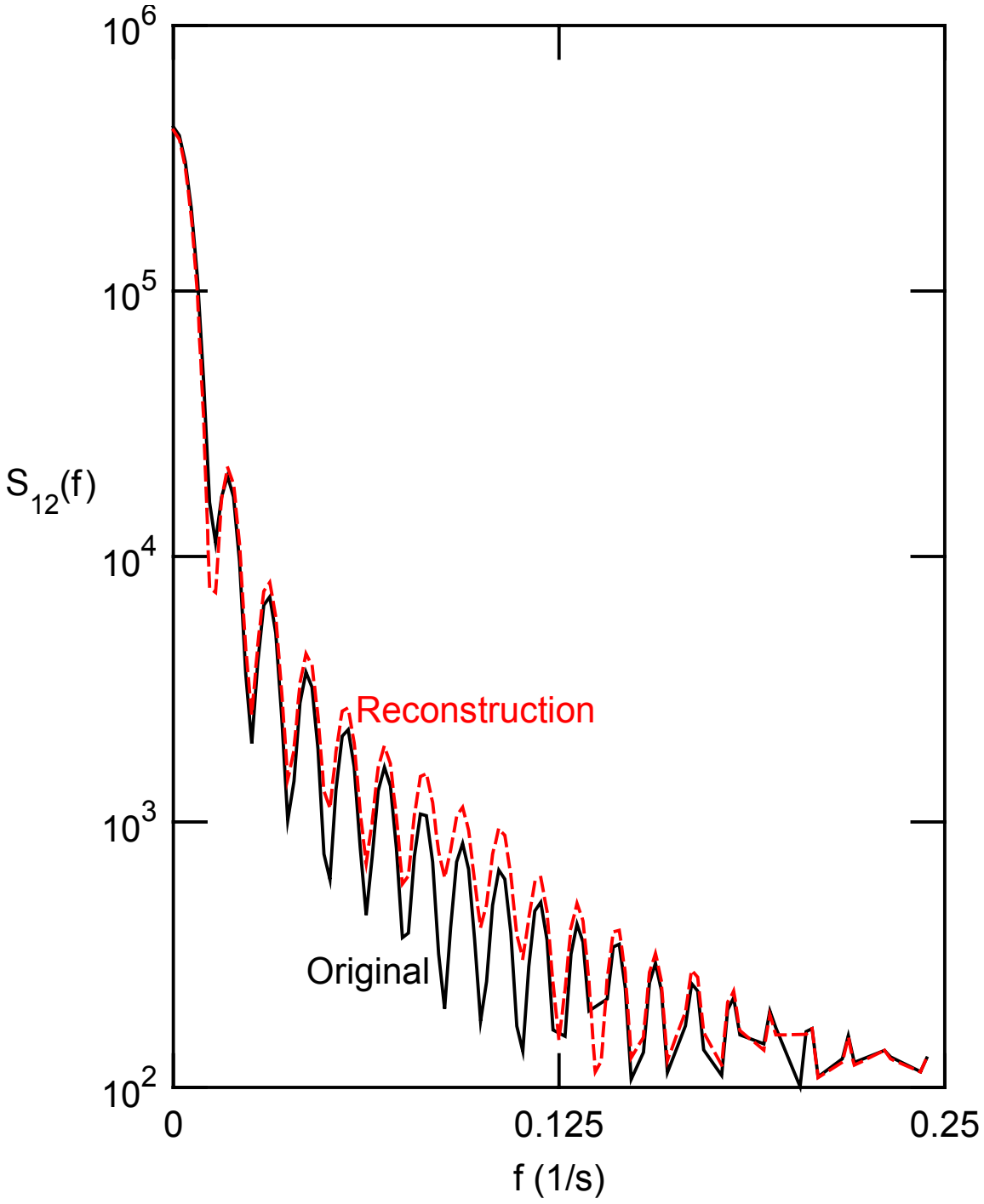

Figure 7.5. Power spectral density, $S_{12}(f)$, for the original history and a reconstructed history.

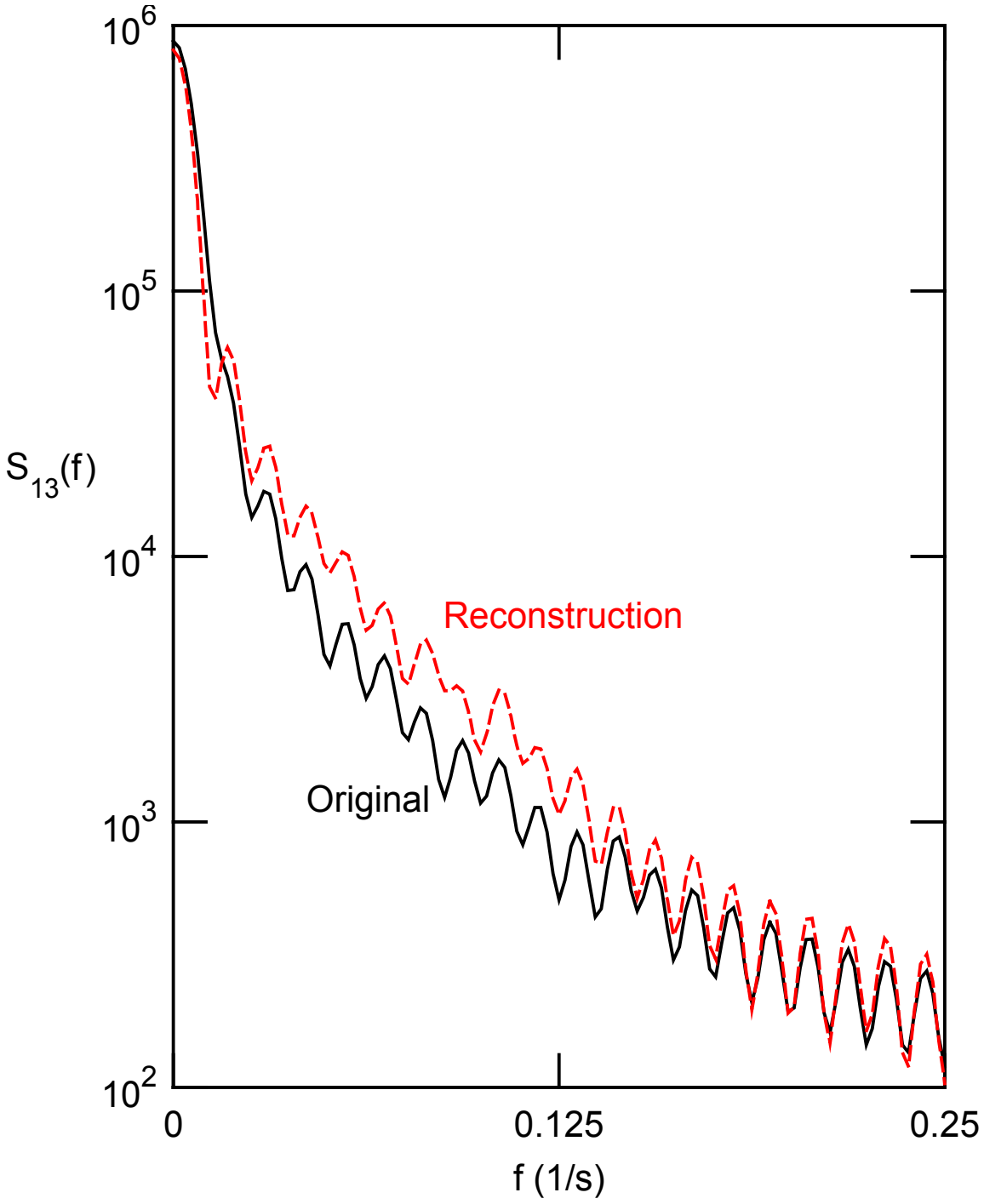

Figure 7.6. Power spectral density, $S_{13}(f)$, for the original history and a reconstructed history.

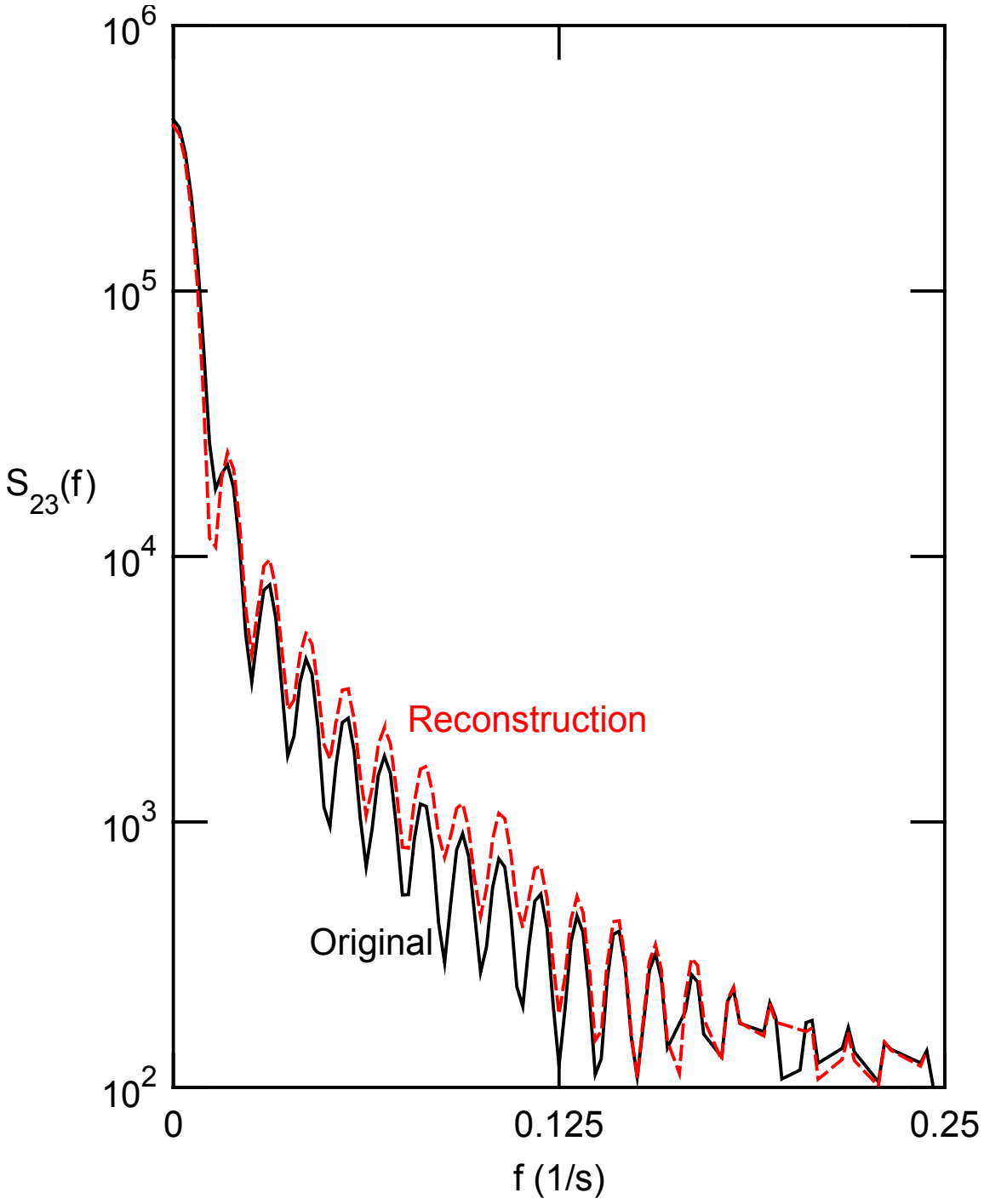

Figure 7.7. Power spectral density, $S_{23}(f)$, for the original history and a reconstructed history.

Table 7.1. Basic statistics for original and reconstructed 3 channel history.

	Channel 1		Channel 2		Channel3	
	Original	Reconstruction	Original	Reconstruction	Original	Reconstruction
Mean	205.478	204.782	– 34.603	– 34.494	158.532	159.480
Standard Deviation	114.104	112.579	25.561	25.199	258.937	255.718
Skewness	0.456	0.380	– 0.650	– 0.590	– 0.467	– 0.458
Minimum	16.950	– 57.213	– 119.768	– 127.471	– 485.613	510.565
Maximum	589.808	582.593	12.046	22.738	722.396	– 738.664

three components, the mean component, $\mathbf{m}_t$, the scaling function, $\mathbf{s}_t$, and the stationary random part, $\mathbf{n}_t$, where it is understood that the three channels, such as $m_t^{(1)}$, $m_t^{(2)}$, and $m_t^{(3)}$ constitute the respective vector, $\mathbf{m}_t$, and will from now on be referred to as $m_t^{(i)}$. In order to model the variation of the mean, $m_t^{(i)}$, in a deterministic way, various Fourier series with increasing numbers of terms are formed, giving the tentative mean descriptions. The differences of the original records and each mean description, $n_t^{(i)} \cdot s_t^{(i)}$, are obtained. These differences are then analyzed for deviations from being a zero-mean process. The best mean description is chosen as the one that renders $n_t^{(i)} \cdot s_t^{(i)}$ stationary, with respect to its mean, using the Fourier series with the least number of terms.

In order to analyze the mean-removed records, $n_t^{(i)} \cdot s_t^{(i)}$, the same analysis as for the uniaxial cases is performed. Each channel is divided into N_I intervals each of which contains, according to Section 5.3, $N_P = 50$ points. This leads to $N_I = 250$ intervals, for each of which the interval mean is determined.

Run tests based on the total number of runs, the number of runs up and down, and the length of the longest run, are performed on the sequence of interval means calculated from $n_t^{(i)} \cdot s_t^{(i)}$. This assures that a variety of deviations from the expected random behavior of this sequence can be detected.

Confidence intervals for run tests at levels $\alpha = 0.90$, $\alpha = 0.95$, and $\alpha = 0.98$ are shown in Table 7.2, where $\alpha = 0.95$ is chosen as the level at which run tests will be performed. For the case where $N_I = 250$, the 95% $(\alpha = 0.95)$ confidence limits for the total number of runs are $(110 < \mu_{R_T} < 141)$, while the number of runs up and down covers the range $(153 < \mu_{R_{UD}} < 179)$. The length of the longest admissible run, according to Eq. (5.16) for a

Table 7.2. Results of run tests of channels 1, 2, and 3 for different values of M_m for $\alpha = 0.95$ (italics = failure of test, bold accepted as stationary).

	$N_I = 250$								
	Channel 1			Channel 2			Channel 3		
$\alpha = 0.98$	$107<r_T<144$	$150<r_{UD}<181$	$k\leq 6$	$107<r_T<144$	$150<r_{UD}<181$	$k\leq 6$	$107<r_T<144$	$150<r_{UD}<181$	$k\leq 6$
$\alpha = 0.90$	$113<r_T<138$	$155<r_{UD}<177$	$k\leq 6$	$113<r_T<138$	$155<r_{UD}<177$	$k\leq 6$	$113<r_T<138$	$155<r_{UD}<177$	$k\leq 6$
$\alpha = 0.95$	$110<r_T<141$	$153<r_{UD}<179$	$k\leq 6$	$110<r_T<141$	$153<r_{UD}<179$	$k\leq 6$	$110<r_T<141$	$153<r_{UD}<179$	$k\leq 6$
M_m	r_T	r_{UD}	k	r_T	r_{UD}	k	r_T	r_{UD}	k
25	*96*	*119*	6	*98*	*113*	6	*108*	*123*	6
30	*106*	*129*	5	*104*	*129*	5	114	*129*	4
35	114	*137*	5	110	*133*	5	110	*123*	5
40	120	*141*	4	122	*143*	4	120	*135*	4
45	128	*139*	4	128	*141*	4	132	*143*	4
50	**140**	**155**	**4**	**136**	**153**	**4**	***142***	***147***	**4**
55	*152*	153	4	*150*	155	4	*150*	157	4
60	*158*	167	3	*156*	161	4	*156*	165	3
65	*164*	169	3	*156*	163	3	*164*	169	3
70	*164*	173	3	*164*	169	3	*168*	175	3

random sequence of length 250 is K=6.

It can be seen that for both channels 1 and 2 a value of $M_m = 50$ renders the series $n_t^{(1)} \cdot s_t^{(1)}$ and $n_t^{(2)} \cdot s_t^{(2)}$ stationary with respect to their mean. For channel 3, however, there is no value for which all run tests are passed. For $M_m = 50$ the total number of runs, r_T, is just above the allowable range and the number or runs up and down, r_{UD}, is slightly below the allowable range. Other values of M_m would possibly lead to a series that would pass at least one of the two tests. However, it is believed that failing both tests by a slim margin is preferable. Therefore, a total number of $M_m = 50$ Fourier series coefficients is deemed appropriate for a sufficient mean description to render the series $n_t^{(3)} \cdot s_t^{(3)}$ approximately stationary with respect to its mean value. See also Figs. 7.8b, 7.10b, and 7.12b for the deterministic mean models, $m_i(t)$, and Figs. 7.8c, 7.10c, and 7.12c for the mean removed records, $n_t^{(i)} \cdot s_t^{(i)}$.

In order to model the scaling functions, $s_t^{(i)}$, an estimate of the standard deviation of the time series, $\tilde{\sigma}_t^{(i)}$, is obtained according to Eq. (5.4), and shown in Figs. 7.8d, 7.10d, and 7.12d, respectively. In order to concisely represent $\tilde{\sigma}_t^{(i)}$ the Box-Cox transformations are performed, where $\lambda_1 = -0.613$, $\lambda_2 = -1.318$, and $\lambda_3 = -0.524$ are the optimal transformation parameters, and the transformed series, $\tilde{\sigma}_t^{(i)BC}$, are shown in Figs. 7.8e, 7.10e, and 7.12e. A number of Fourier series with an increasing number of terms are formed according to Eq. (5.9) giving the tentative scaling functions. The series with the fewest number of terms that is correlated at 95% to $\tilde{\sigma}_t^{(i)BC}$, $s_t^{(i)BC}$, has $M_s = 40$ terms for channel 1, $M_s = 90$ terms for channel 2, and $M_s = 80$ terms for channel 3. These series are shown in is shown in Figs. 7.9a, 7.11a, and 7.13a. The inverse Box-Cox transformations of $s_t^{(i)BC}$, $s_t^{(i)}$, are the scaling functions used to render the mean- removed

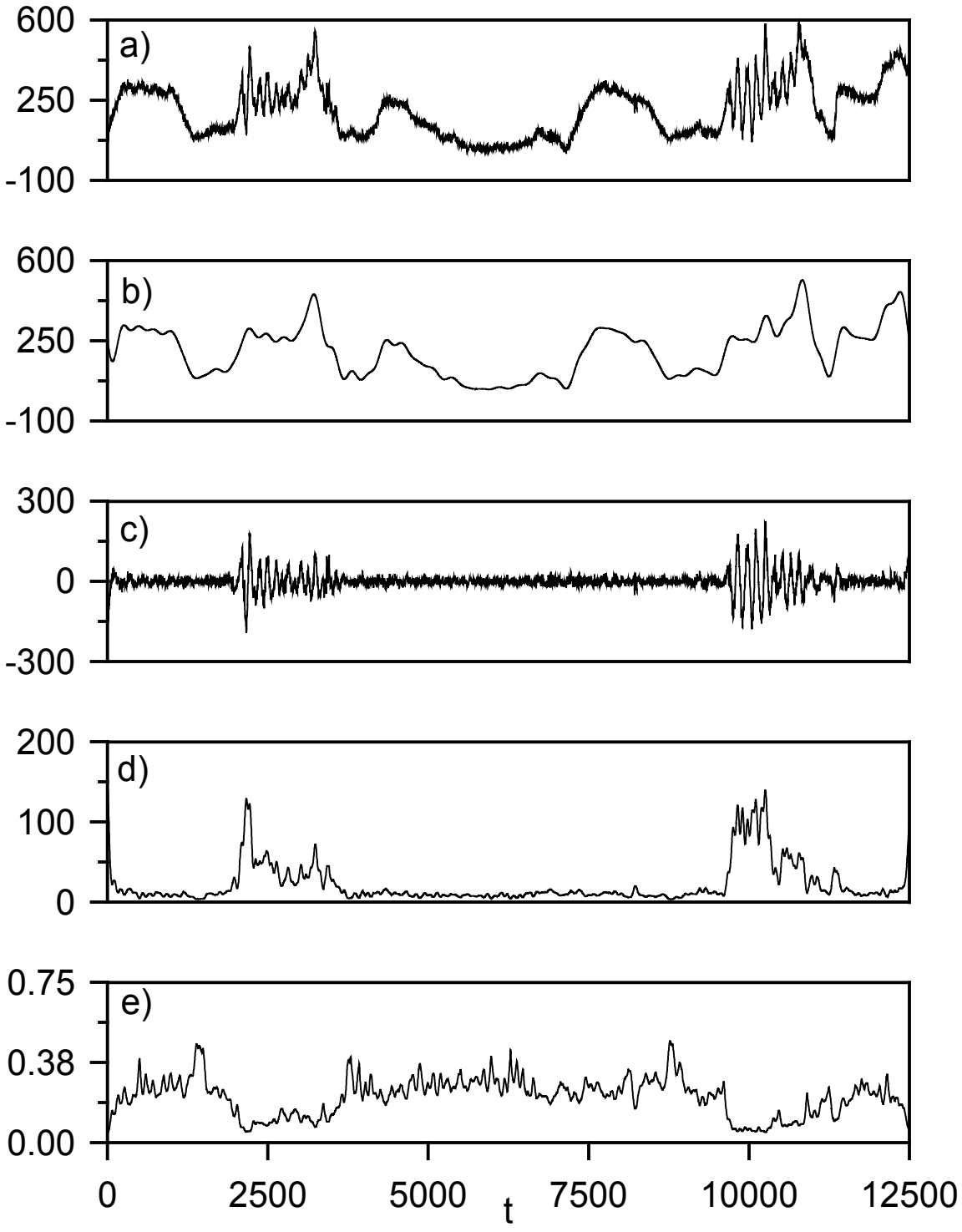

Figure 7.8. Time series plots for (a) original history, (b) deterministic mean with $M_\mu = 50$, (c) mean-removed series, (d) estimated standard deviation, $\tilde{\sigma}_t$, (e) Box-Cox transformation of $\tilde{\sigma}_t$, $\tilde{\sigma}_t^{BC}$ - channel 1.

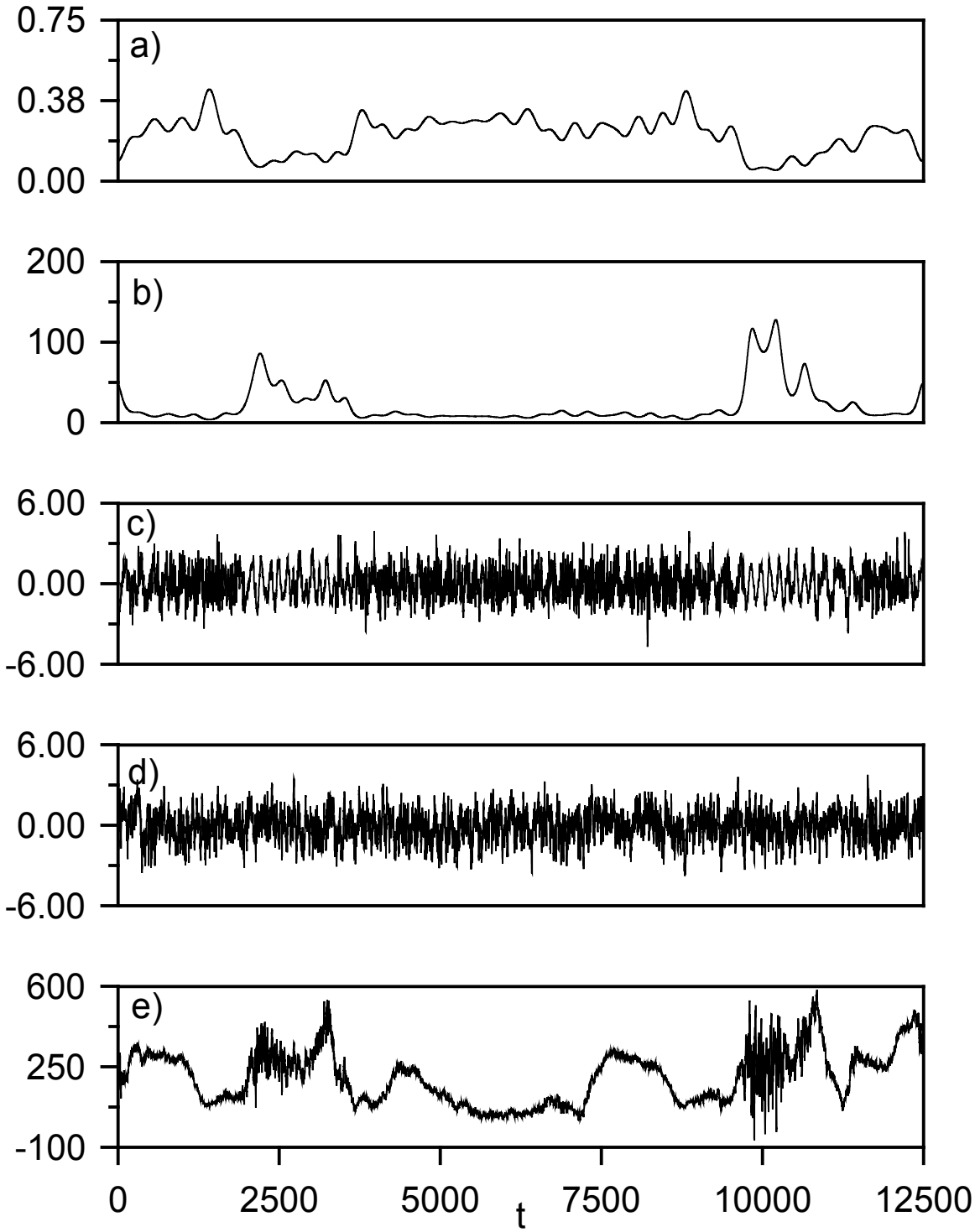

Figure 7.9. Time series plots for (a) Fourier series approximation to $\tilde{\sigma}_t^{BC}$ with $M_s = 40$, s_t^{BC}, (b) scaling function, s_t, (c) stationary series, (d) ARMA(6,5) model simulation, and (e) reconstruction - channel 1.

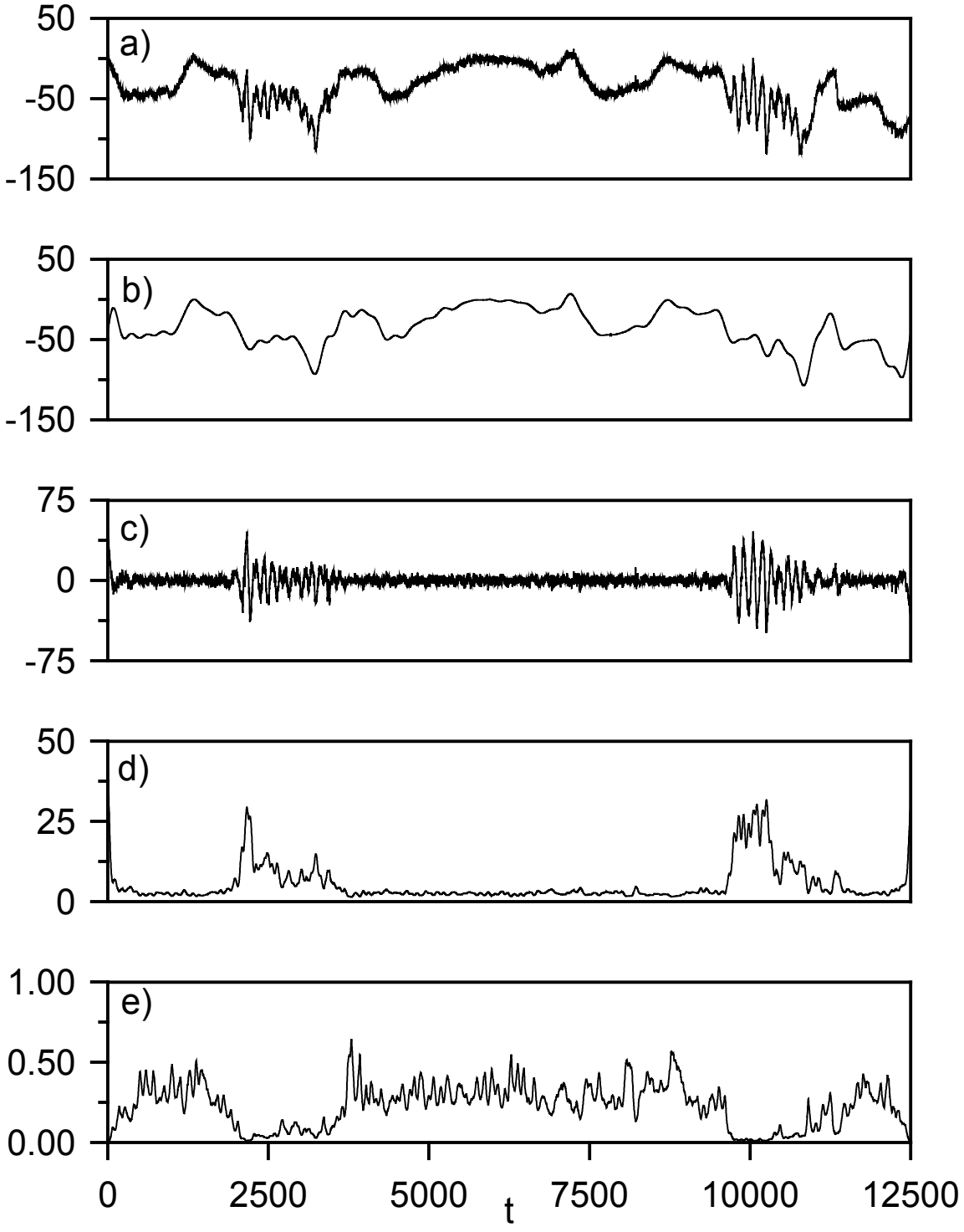

Figure 7.10. Time series plots for (a) original history, (b) deterministic mean with $M_\mu = 50$, (c) mean-removed series, (d) estimated standard deviation, $\widetilde{\sigma}_t$, (e) Box-Cox transformation of $\widetilde{\sigma}_t$, $\widetilde{\sigma}_t^{BC}$ - channel 2.

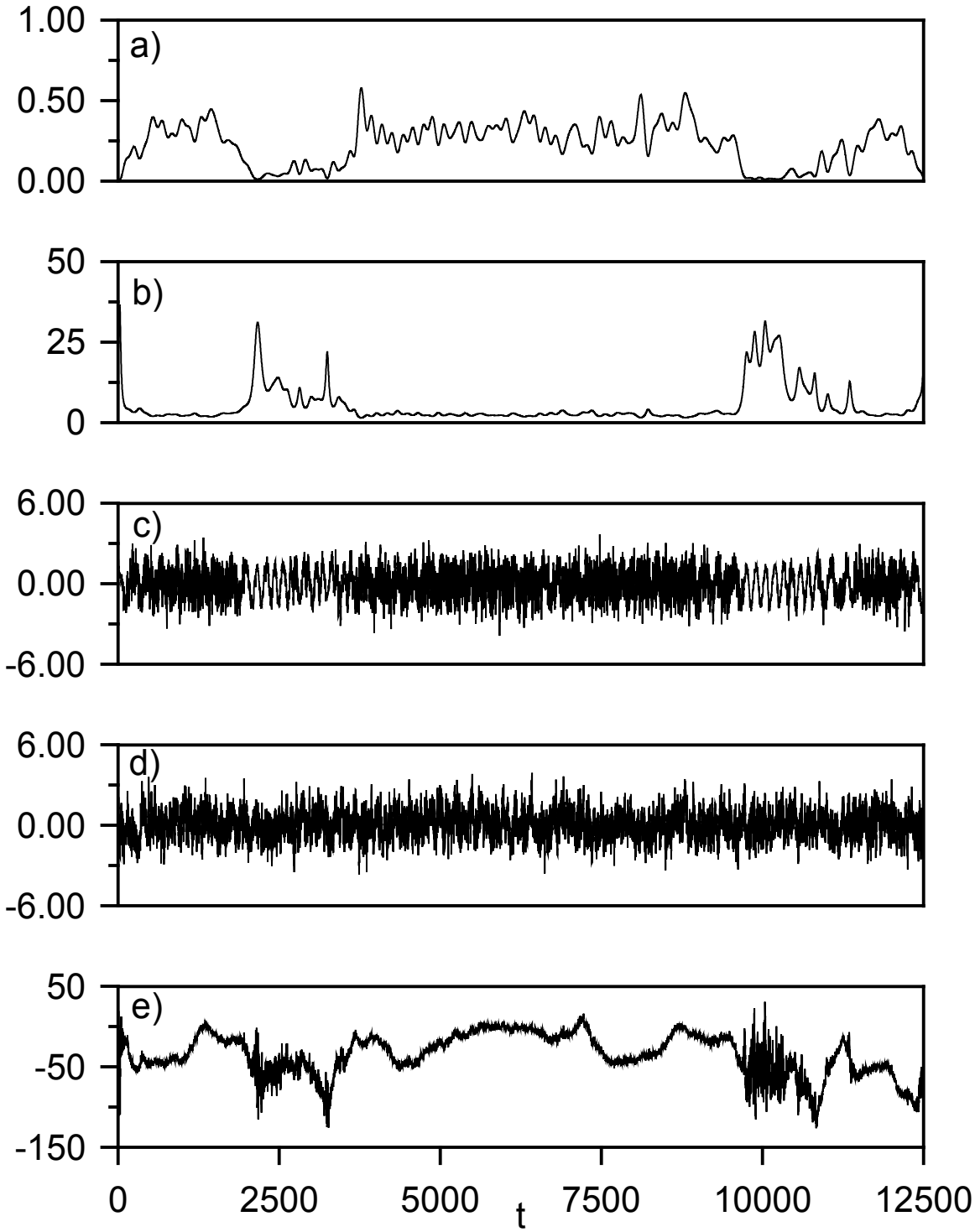

Figure 7.11. Time series plots for (a) Fourier series approximation to $\tilde{\sigma}_t^{BC}$ with $M_s = 90$, s_t^{BC}, (b) scaling function, s_t, (c) stationary series, (d) ARMA(6,5) model simulation, and (e) reconstruction - channel 2.

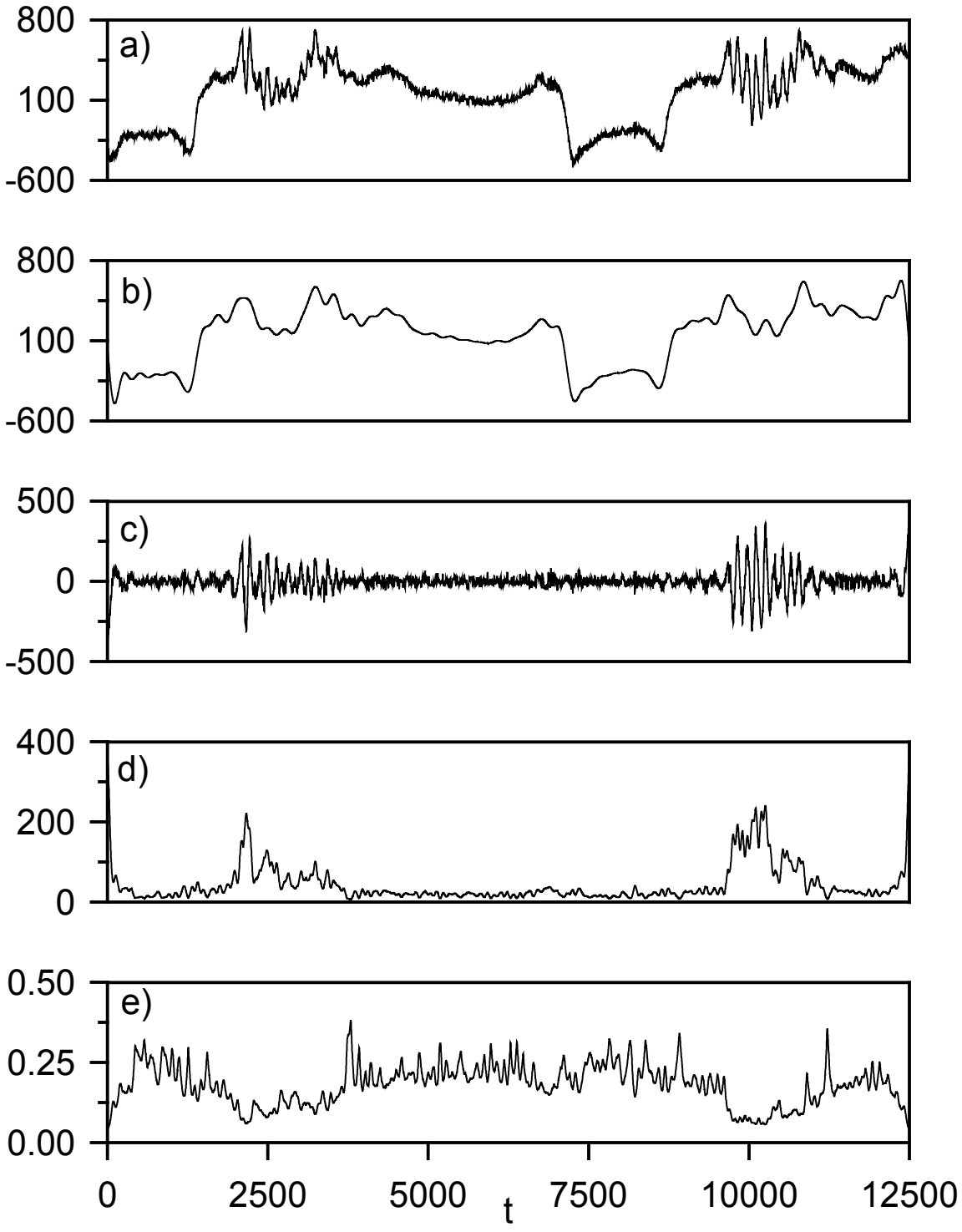

Figure 7.12. Time series plots for (a) original history, (b) deterministic mean with $M_\mu = 50$, (c) mean-removed series, (d) estimated standard deviation, $\widetilde{\sigma}_t$, (e) Box-Cox transformation of $\widetilde{\sigma}_t$ $\widetilde{\sigma}_t^{BC}$ - channel 3.

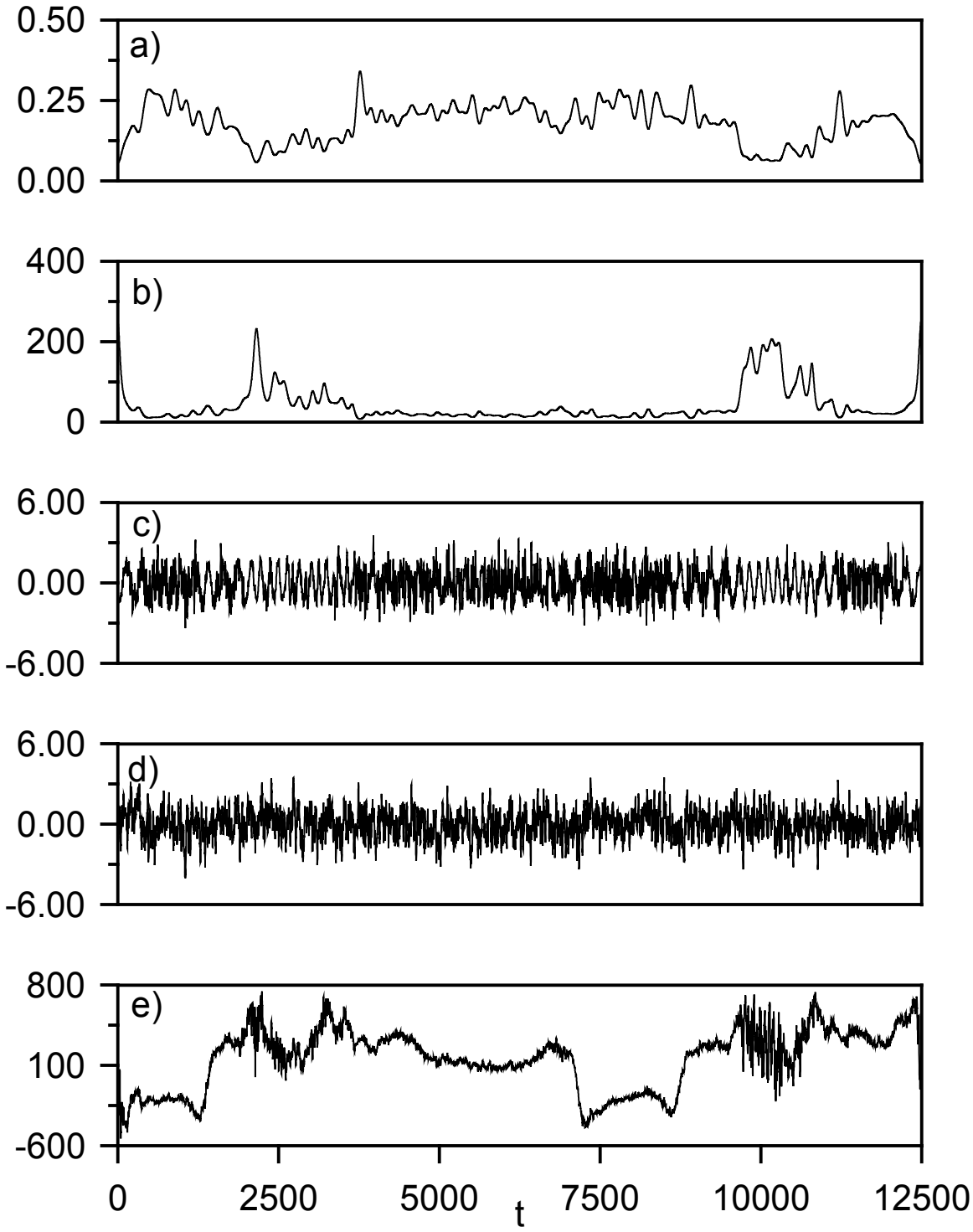

Figure 7.13. Time series plots for (a) Fourier series approximation to $\tilde{\sigma}_t^{BC}$ with $M_s = 80$, s_t^{BC}, (b) scaling function, s_t, (c) stationary series, (d) ARMA(6,5) model simulation, and (e) reconstruction - channel 3.

series, $n_t^{(i)} \cdot s_t^{(i)}$, stationary with respect to variance and are shown in Figs. 7.9b, 7.11b, and 7.13b. The stationary series, i.e. the quotient of $n_t^{(i)} \cdot s_t^{(i)}$ and $s_t^{(i)}$, are shown in Figs. 7.9c, 7.11c, and 7.13c.

The stationary series are represented by a three dimensional ARMA model. Parameters for a number of ARMA models are estimated, where Tables 7.3-7.5 show parameters for a few selected models, and the correlation coefficient between power spectra of these ARMA models and the spectrum of the stationary series is calculated, Table 7.6. Because the auto- and cross-spectra of the stationary series are relatively simple, low order ARMA models fit these spectra well. Therefore, models are sought where all of the spectra, $S_{ij}(f)$ have a minimum correlation of $\rho_{S_{ij}}^{(p,q)}$ greater than 0.9, 0.95, 0.97, and 0.98 to the respective spectra obtained for the stationary series. This leads to the choice of ARMA(2,0), ARMA(2,1), ARMA(3,0), and ARMA(6,5). It is noted that increasing the model order beyond ARMA(6,5) does not increase the correlation coefficients. Auto- and cross-spectral densities for ARMA(2,0) and ARMA(6,5) are shown in Figs. 7.14-7.19. The area under the spectral densities is well approximated by both models, but the higher order model traces the peaks better. Moreover, as all spectra are shown on a logarithmic scale, the agreement is actually quite good.

Time series are generated for all ARMA models, shown in Figs. 7.9d, 7.11d, and 7.13d, are multiplied by the deterministic scaling functions, $s_t^{(i)}$, and are added to the deterministic mean variations, $m_t^{(i)}$. A complete reconstruction, using a realization of the selected ARMA(6,5) model is shown in Figs. 7.9e, 7.11e, and 7.13e. It is noted that the original time series for all three channels exhibit, in the regions of t=2500 and t=10000, a distinctly different pattern. It is presumed that a maneuver was executed that induced a

Table 7.3. ARMA parameters, $\boldsymbol{\phi}_i$, and correlation matrix, $\mathbf{V}$, of white noise input for selected ARMA models.

ARMA(p,q)	(0,0)	(1,0)	(2,0)
$\boldsymbol{\phi}_i$; i= 1		$\begin{bmatrix} 0.83 & -0.16 & -2.9\text{E}-2 \\ -0.57 & 0.10 & -0.16 \\ 6.9\text{E}-4 & -5.6\text{E}-2 & 0.93 \end{bmatrix}$	$\begin{bmatrix} 0.94 & -0.20 & 0.34 \\ -0.72 & 0.14 & -0.40 \\ -7.1\text{E}-2 & -8.4\text{E}-2 & 1.60 \end{bmatrix}$
2			$\begin{bmatrix} -0.16 & 1.8\text{E}-2 & -0.35 \\ 5.7\text{E}-2 & -0.24 & 0.18 \\ 2.4\text{E}-2 & 8.7\text{E}-3 & -0.64 \end{bmatrix}$
$\mathbf{V}$	$\begin{bmatrix} 1.18 & -0.91 & 0.92 \\ -0.91 & 1.07 & -0.82 \\ 0.92 & -0.82 & 1.14 \end{bmatrix}$	$\begin{bmatrix} 0.14 & -0.05 & 0.07 \\ -0.05 & 0.35 & -4.1\text{E}-2 \\ 0.07 & -4.1\text{E}-2 & 7.2\text{E}-2 \end{bmatrix}$	$\begin{bmatrix} 0.12 & -3.4\text{E}-2 & 4.8\text{E}-2 \\ -3.4\text{E}-2 & 0.32 & -2.4\text{E}-2 \\ 4.8\text{E}-2 & -2.4\text{E}-2 & 4.5\text{E}-2 \end{bmatrix}$

Table 7.4. ARMA parameters, $\boldsymbol{\phi}_i$ and $\boldsymbol{\theta}_i$, and correlation matrix, $\mathbf{V}$, of white noise input for selected ARMA models.

ARMA(p,q)	(2,1)	(3,0)
$\boldsymbol{\phi}_i$; i= 1	$\begin{bmatrix} 0.73 & -0.31 & 0.29 \\ -0.82 & -7.5\text{E}-2 & -0.41 \\ -7.4\text{E}-2 & -9.3\text{E}-2 & 1.5 \end{bmatrix}$	$\begin{bmatrix} 1.18 & -0.91 & 0.92 \\ -0.91 & 1.07 & -0.82 \\ 0.92 & -0.82 & 1.14 \end{bmatrix}$
2	$\begin{bmatrix} -5.3\text{E}-2 & -6.2\text{E}-2 & -0.33 \\ 1.3\text{E}-2 & -0.23 & 0.16 \\ 2.1\text{E}-2 & 3.3\text{E}-3 & 0.54 \end{bmatrix}$	$\begin{bmatrix} -0.14 & -3.6\text{E}-2 & -0.67 \\ -6.7\text{E}-2 & -0.23 & 0.59 \\ 6.8\text{E}-2 & 1.8\text{E}-2 & -0.90 \end{bmatrix}$
3		$\begin{bmatrix} 5.8\text{E}-2 & -6.1\text{E}-2 & 0.20 \\ 0.32 & 0.31 & -0.24 \\ -9.3\text{E}-2 & -1.4\text{E}-2 & 0.17 \end{bmatrix}$
$\boldsymbol{\theta}_i$; i=1	$\begin{bmatrix} -0.31 & -0.15 & -0.12 \\ -0.17 & -0.31 & -7.4\text{E}-2 \\ -1.2\text{E}-2 & -9.8\text{E}-3 & -0.23 \end{bmatrix}$	
$\mathbf{V}$	$\begin{bmatrix} -8.8\text{E}-2 & -2.9\text{E}-2 & 3.8\text{E}-2 \\ -2.9\text{E}-2 & 0.23 & -1.7\text{E}-2 \\ 3.8\text{E}-2 & -1.7\text{E}-2 & 3.5\text{E}-2 \end{bmatrix}$	$\begin{bmatrix} 0.12 & -0.04 & 4.6\text{E}-2 \\ -0.04 & 0.28 & -2.5\text{E}-2 \\ 4.6\text{E}-2 & -2.5\text{E}-2 & 4.4\text{E}-2 \end{bmatrix}$

Table 7.5. ARMA parameters, $\boldsymbol{\phi}_i$ and $\boldsymbol{\theta}_i$, and correlation matrix, $\mathbf{V}$, of white noise input for ARMA(6,5) model.

ARMA(6,5)	$\boldsymbol{\phi}_i$	$\boldsymbol{\theta}_i$
i= 1	$\begin{bmatrix} 0.88 & -0.17 & 0.91 \\ -0.80 & 0.19 & -0.83 \\ -0.22 & -3.4\text{E}-2 & 2.20 \end{bmatrix}$	$\begin{bmatrix} -0.16 & -1.8\text{E}-2 & 0.50 \\ -0.16 & -5.2\text{E}-2 & -0.34 \\ -0.13 & 4.9\text{E}-2 & 0.47 \end{bmatrix}$
2	$\begin{bmatrix} -3.3\text{E}-2 & 3.5\text{E}-2 & -1.50 \\ -0.11 & -0.23 & 1.50 \\ 0.26 & 5.9\text{E}-3 & -1.70 \end{bmatrix}$	$\begin{bmatrix} 0.17 & -7.6\text{E}-3 & -0.17 \\ -0.18 & 0.13 & 0.33 \\ -1.8\text{E}-2 & -2.5\text{E}-2 & 6.0\text{E}-3 \end{bmatrix}$
3	$\begin{bmatrix} 0.37 & -8.4\text{E}-3 & 0.20 \\ 0.68 & 0.65 & -0.85 \\ -4.2\text{E}-2 & -2.9\text{E}-2 & 0.53 \end{bmatrix}$	$\begin{bmatrix} 0.24 & -2.2\text{E}-2 & -0.52 \\ 0.33 & 0.33 & 0.18 \\ 4.5\text{E}-2 & -4.5\text{E}-2 & -0.31 \end{bmatrix}$
4	$\begin{bmatrix} -0.73 & -9.3\text{E}-3 & 0.59 \\ 0.23 & 0.17 & 0.09 \\ 1.2\text{E}-2 & -1.8\text{E}-2 & -0.27 \end{bmatrix}$	$\begin{bmatrix} 3.4\text{E}-2 & -4.7\text{E}-2 & 0.06 \\ 0.21 & 0.34 & -0.18 \\ 2.6\text{E}-2 & -1.1\text{E}-2 & 9.2\text{E}-2 \end{bmatrix}$
5	$\begin{bmatrix} 3.5\text{E}-2 & 1.3\text{E}-2 & 0.20 \\ 4.4\text{E}-2 & 9.6\text{E}-3 & -2.6\text{E}-2 \\ -0.18 & -1.4\text{E}-2 & 0.47 \end{bmatrix}$	$\begin{bmatrix} -0.17 & 6.3\text{E}-3 & 0.08 \\ -8.6\text{E}-2 & -0.21 & 0.13 \\ -0.06 & -1.5\text{E}-2 & -5.2\text{E}-3 \end{bmatrix}$
6	$\begin{bmatrix} 0.26 & -2.4\text{E}-2 & -0.42 \\ -0.18 & -2.8\text{E}-2 & 0.12 \\ 0.11 & 3.6\text{E}-3 & -0.25 \end{bmatrix}$	
$\mathbf{V}$	$\begin{bmatrix} 8.8\text{E}-2 & -2.9\text{E}-2 & 3.8\text{E}-2 \\ -2.9\text{E}-2 & 0.23 & -1.7\text{E}-2 \\ 3.8\text{E}-2 & -1.7\text{E}-2 & 3.5\text{E}-2 \end{bmatrix}$	

Table 7.6. Correlation coefficient of power spectra, $\rho_{S_{ij}}^{(p,q)}$, for selected ARMA(p,q) models, where the subscript indicates the auto- or cross-spectrum with minimal correlation coefficient and the bold number indicates the minimum order model for a given correlation value.

p \ q	0	1	2	3	4	5	6	7
1	0.86_{13}							
2	$\mathbf{0.93}_{22}$	$\mathbf{0.96}_{22}$						
3	$\mathbf{0.97}_{22}$	0.97_{22}	0.97_{22}					
4	0.96_{22}	0.96_{22}	0.97_{22}	0.96_{13}				
5	0.95_{13}	0.96_{13}	0.96_{13}	0.97_{33}	$\mathbf{0.88}_{33}$			
6	0.95_{22}	0.95_{22}	0.95_{22}	0.94_{22}	0.86_{13}	$\mathbf{0.98}_{33}$		
7	0.97_{22}	0.97_{22}	0.97_{22}	0.97_{22}	0.86_{13}	$\mathbf{0.88}_{33}$	0.97_{11}	
8	0.94_{22}	0.94_{22}	0.94_{22}	0.96_{22}	0.86_{13}	$\mathbf{0.88}_{33}$	0.98_{22}	0.97_{22}

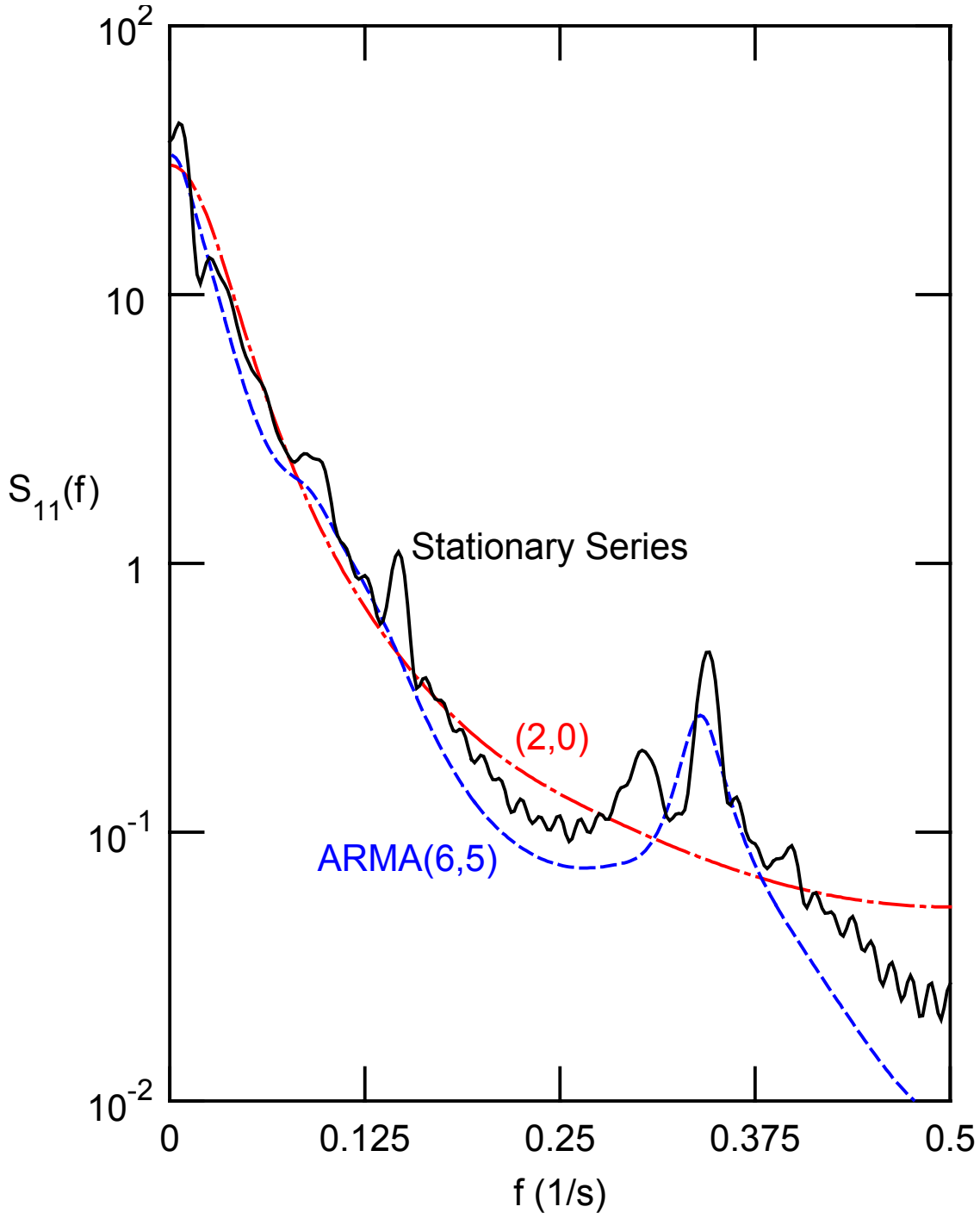

Figure 7.14. Power spectral density, $S_{11}(f)$, for the stationary series, for ARMA(2,0) with $\rho_{S_{33}}^{(2,0)} = 0.93$, and for ARMA(6,5) with $\rho_{S_{22}}^{(6,5)} = 0.98$.

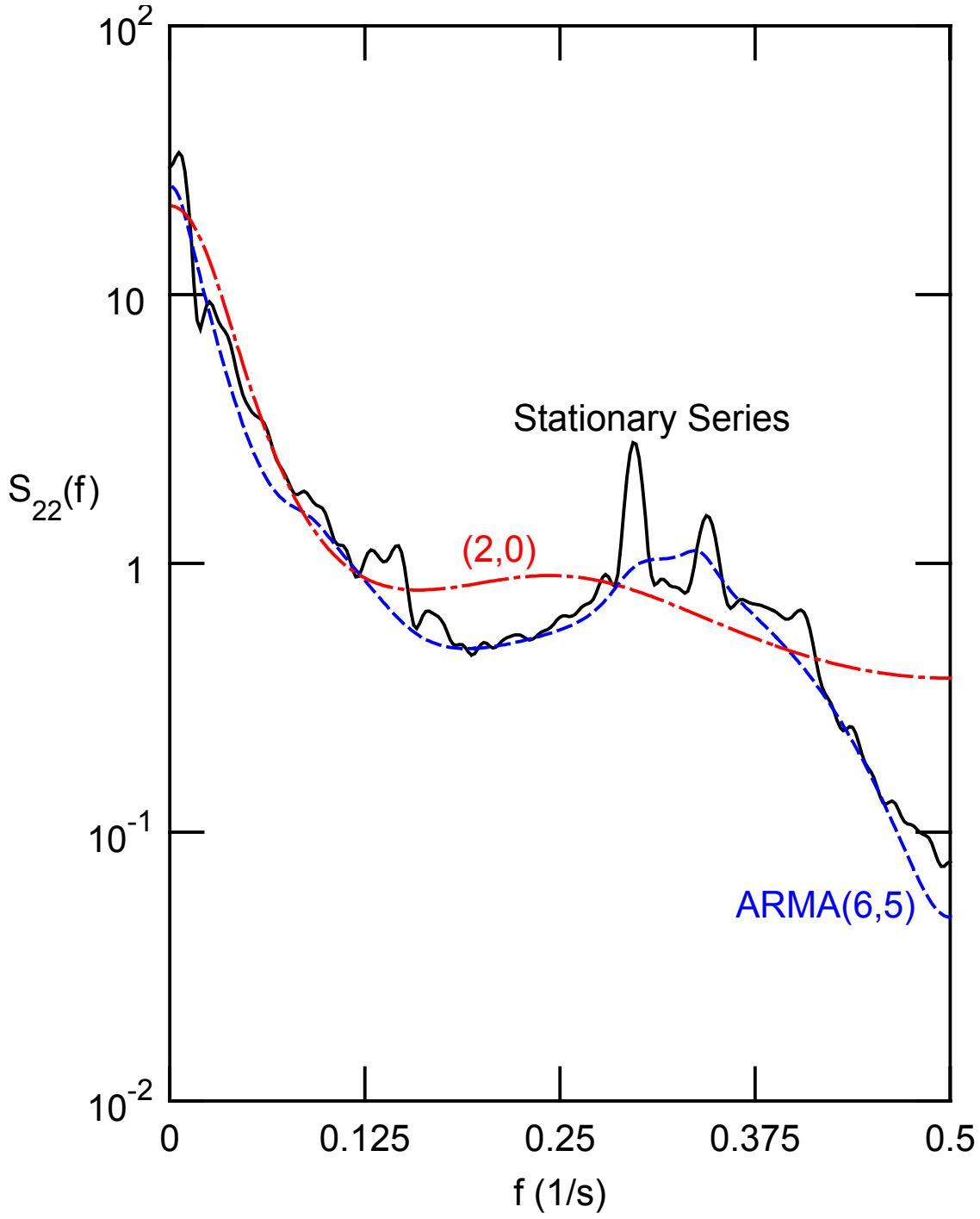

Figure 7.15. Power spectral density, $S_{22}(f)$, for the stationary series, for ARMA(2,0) with $\rho_{S_{33}}^{(2,0)} = 0.93$, and for ARMA(6,5) with $\rho_{S_{22}}^{(6,5)} = 0.98$.

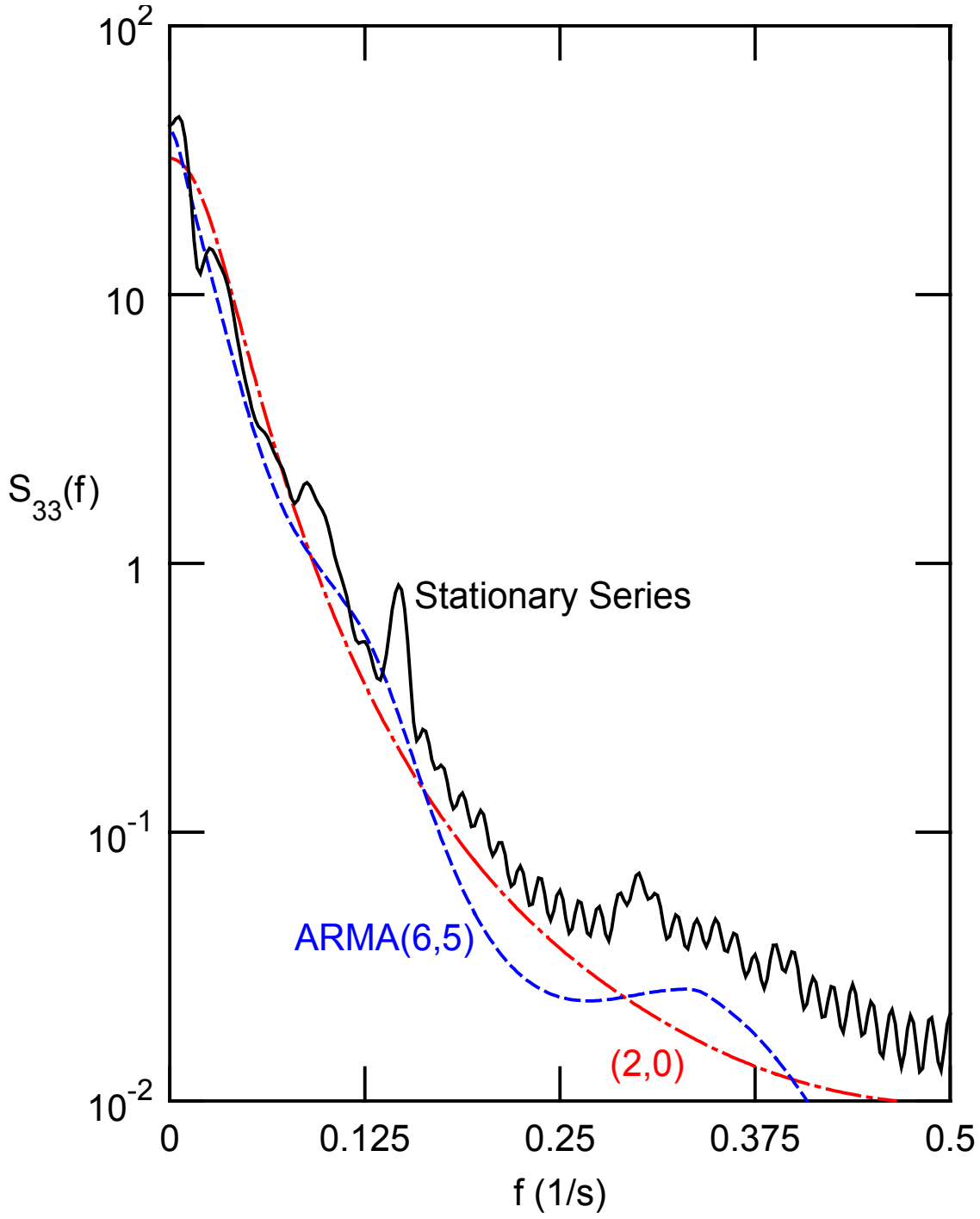

Figure 7.16. Power spectral density, $S_{33}(f)$, for the stationary series, for ARMA(2,0) with $\rho_{S_{33}}^{(2,0)} = 0.93$, and for ARMA(6,5) with $\rho_{S_{22}}^{(6,5)} = 0.98$.

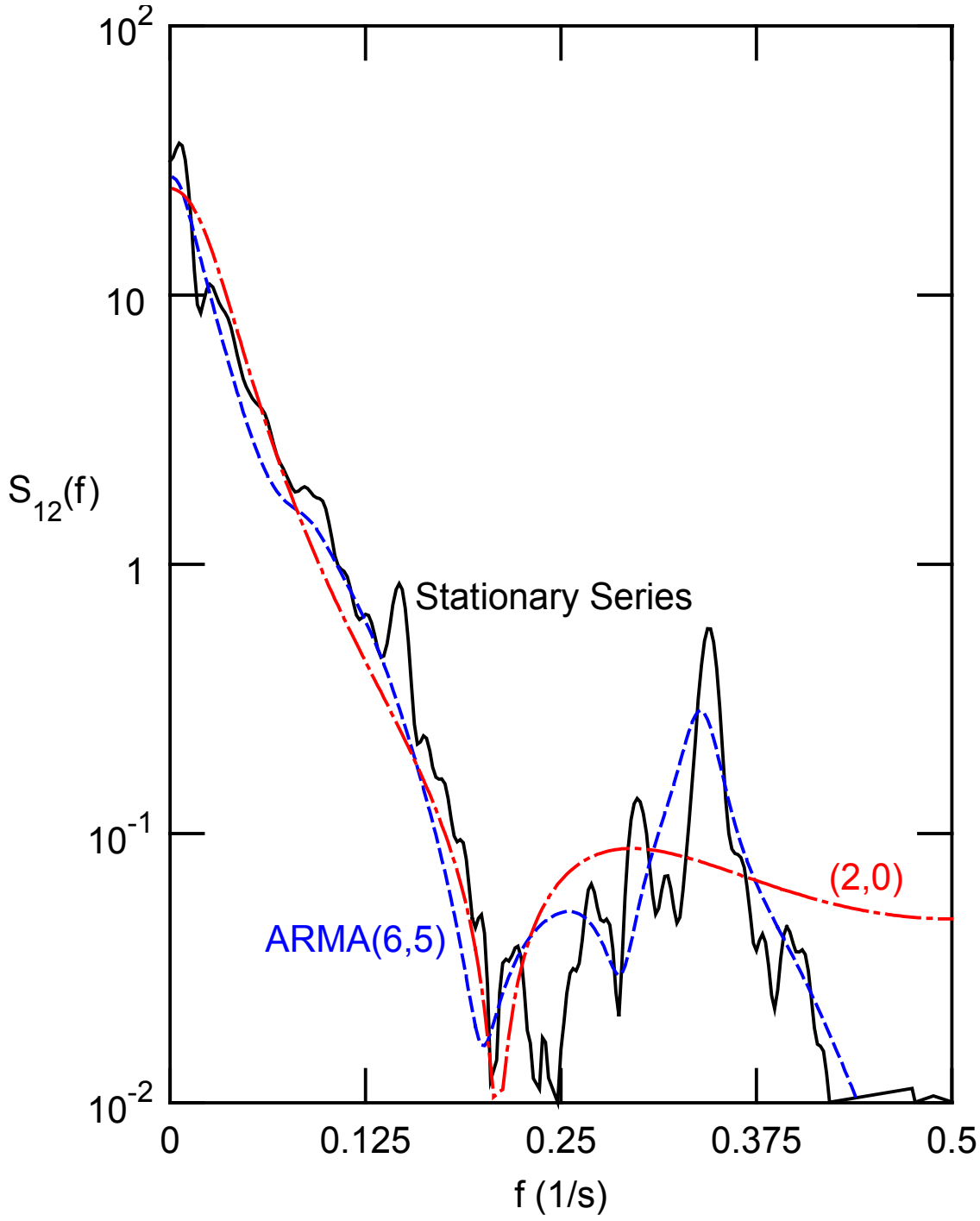

Figure 7.17. Power spectral density, $S_{12}(f)$, for the stationary series, for ARMA(2,0) with $\rho_{S_{33}}^{(2,0)} = 0.93$, and for ARMA(6,5) with $\rho_{S_{22}}^{(6,5)} = 0.98$.

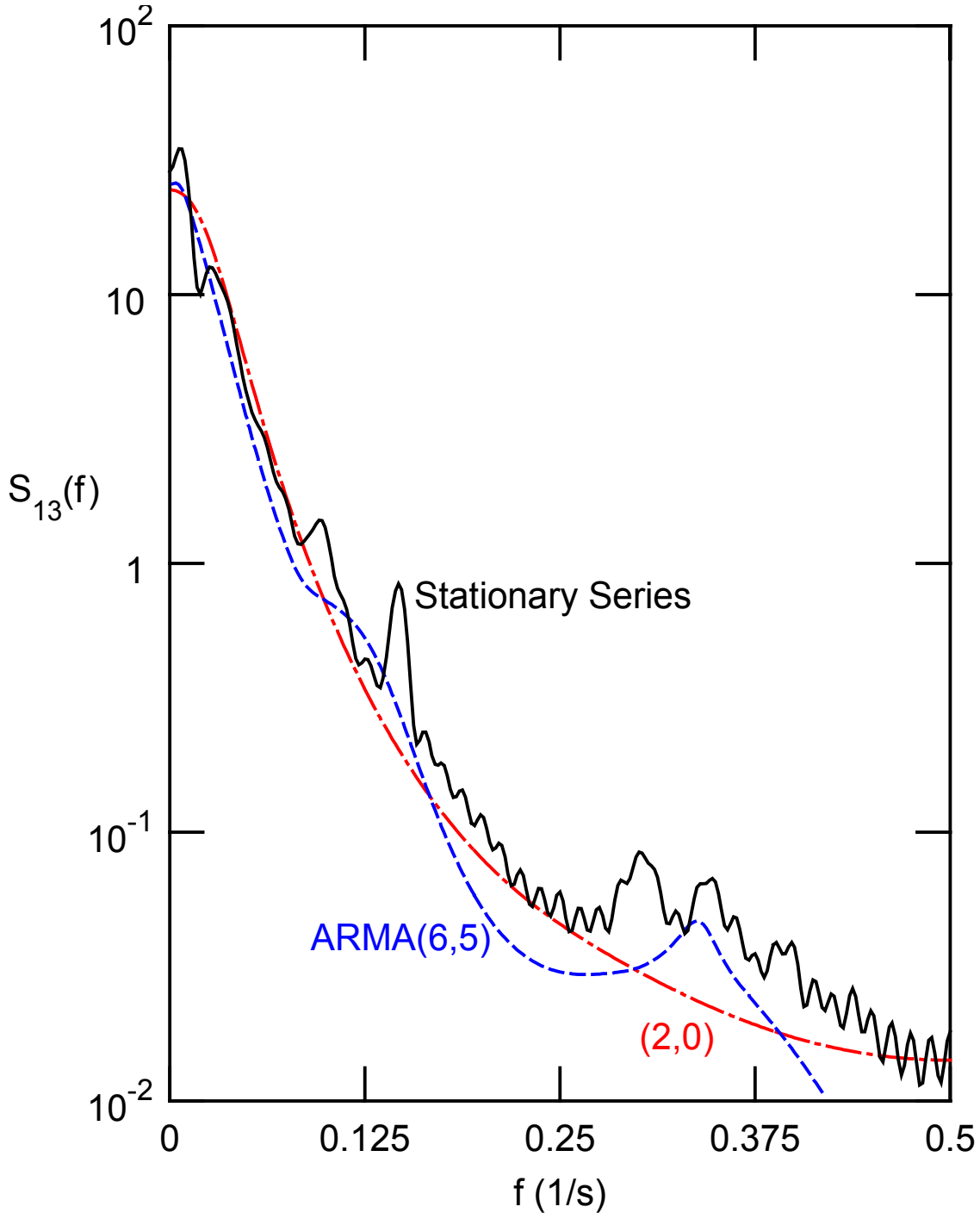

Figure 7.18. Power spectral density, $S_{13}(f)$, for the stationary series, for ARMA(2,0) with $\rho_{S_{33}}^{(2,0)} = 0.93$, and for ARMA(6,5) with $\rho_{S_{22}}^{(6,5)} = 0.98$.

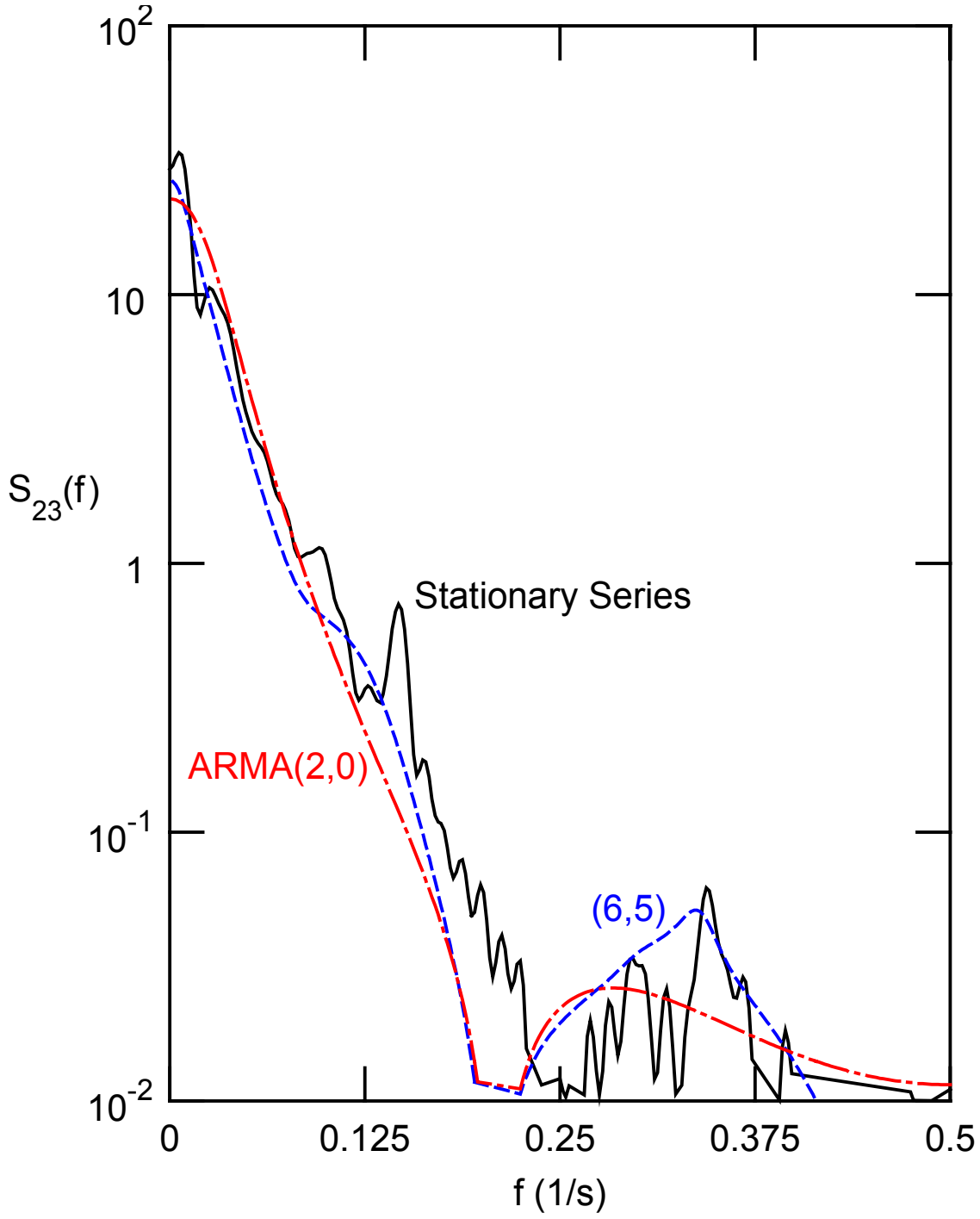

Figure 7.19. Power spectral density, $S_{23}(f)$, for the stationary series, for ARMA(2,0) with $\rho_{S_{33}}^{(2,0)} = 0.93$, and for ARMA(6,5) with $\rho_{S_{22}}^{(6,5)} = 0.98$.

few large amplitude short duration (spike) events. The spectral content of this part of the series is therefore distinctly different from the remaining series. Consequently, the reconstruction will perform poorly in that region. It can be seen in the reconstruction that for these regions a much larger number of large amplitude cycles are predicted than were present in the original loading. This will affect fatigue life predictions.

The power spectral densities, $S_{ij}(f)$, of the reconstructed histories are shown in Figs. 7.2-7.7., where again it is noted that the spectra are shown on a logarithmic scale. As the spectra are calculated for the record as a whole, any of the above stated variations in spectral content, as they are of short duration, are averaged and cannot be observed.

Fatigue lives are calculated according to the simplified critical plane approach described in Section 4.2.1, and these are shown in Fig. 7.20. Reconstructions using ARMA(2,0), ARMA(2,1), ARMA(3,0), and ARMA(6,5) predict fatigue lives that are very close to each other, such that strain life curves partially overlapped. As before, the ARMA(0,0) and ARMA(1,0) models constitute the limiting cases on fatigue life. Because the reconstruction introduced a number of large cycles that are not present in the original loading, all reconstructions tend to be biased toward shorter lives. In fact, the limiting case of the ARMA(1,0) reconstruction that predicts the longest life is the one that is closest to the life predicted for the original record. However, of all reconstructions with a minimum correlation for the power spectra, $\rho_{S_{ij}}^{(p,q)} \geq 0.90$, the strain life curve obtained from the ARMA(6,5) model was closest to the one obtained from the original loading. The ARMA(6,5) model was, therefore, deemed appropriate for reconstruction as both spectral shape and fatigue life agreed reasonably well with the original.

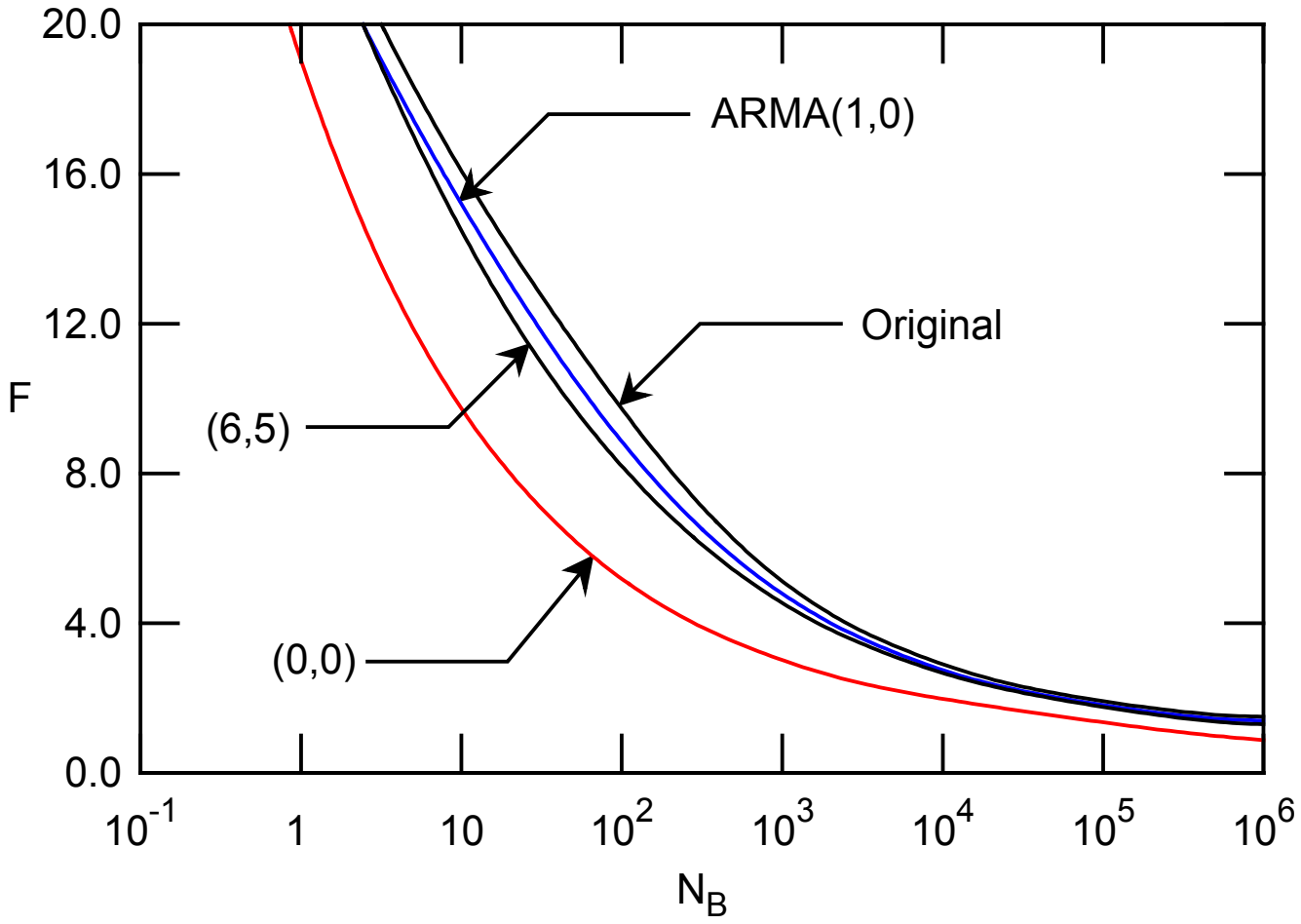

Figure 7.20. Scaling factor, F, versus blocks to failure, N_B, for the original and selected ARMA reconstructed histories.

CHAPTER 8. CONCLUSIONS AND RECOMMENDATIONS

The proposed method presents an efficient and effective solution to the modeling of non-stationary random fatigue loadings. As the time base of the original loading is preserved, it is applicable wherever a concise load description, preserving information regarding frequency content, is desired. The method, therefore, can be used in a diversity of fields, such as random vibration, Monte Carlo studies, and Finite Element Methods.

For all studied cases, the ARMA(0,0) reconstruction predicted a shorter fatigue life than higher order models, while the ARMA(1,0) model predicted a fatigue life longer than higher order model reconstructions.

The ability of to generate a loading ensemble is useful in generalizing observed loadings. Statistically equivalent variations of an observed loading can be obtained, with the option of specifying, separately for the mean and variance content, the degree of correlation between original and reconstructed loadings.

The traditional procedure of ARMA model building needs adjustment for large data sets, specifically in specifying criteria of model order selection that do not depend on the series of residuals after fitting a model. The criteria presented in the literature demand models of very large order, when a lower order model is sufficient for representing all

relevant dynamics of the original loading. The criterion, proposed herein, is a first attempt to the solution of this problem.

To measure the success of removing nonstationarity with respect to the mean value, nonparametric tests were proposed. While these tests are useful in detecting trends and cyclical patterns, they did not always allow one to uniquely identify an optimal mean description.

Further study of the following aspects is proposed:

To take fully advantage of the stochastic nature of the model, the method of fatigue life prediction should be adjusted. Calculating the life from a short record, by assuming that this record would be applied repeatedly until failure occurs, does not reflect realistic variations in loadings. It is proposed that generating nonrepeating infinitely long histories could be used to calculate a more realistic fatigue life estimate.

For the case of multiaxial loadings, correlations between channels should be considered not only for the random variations, but also for mean content and scaling functions. This objective can be achieved by using vector Fourier series, where the Fourier coefficients can account for correlations between channels.

The proposed method of ensemble generation could be verified if more data were collected for a particular record. In general, it can be said that, for a meaningful stochastic analysis, a field test should be repeated for a number of times before reliable information about the underlying ensemble can be inferred.

Considering nonstationarities with respect to mean and variance only is not always sufficient. Loadings of short duration and large amplitude, so called spikes or pothole events, are not included in the current description of loadings. Moreover, as seen in Chapter 7, the power spectral density may change over time even for a record for which the mean variation has been removed, and a scaling function applied, such that the variance is constant. Further study in identifying and modeling such nonstationarities, therefore, is needed.

REFERENCES

Akaike, H., "Maximum Likelihood Identification of Gaussian Autoregressive Moving Average Models", *Biometrika*, Vol. 60, No. 2, 1973, pp. 255-265.

Akaike, H., "A New Look at the Statistical Model Identification", *IEEE Transactions on Automatic Control*, Vol. AC-19, No. 6, Dec., 1974, pp. 716-723.

Ang, A. H-S., and Tang, W. H., *Probability Concepts in Engineering Planning and Design*, Vol. 1, John Wiley & Sons, New York, 1975.

ASTM, "Standard Practices for Cycle Counting in Fatigue Analysis," *Annual Book of ASTM Standards*, Vol. 03.01, American Society for Testing and Materials, Philadelphia, PA, Standard No. E 1045, 1987, pp. 1079-1092.

Bannantine, J. A., Comer, J. J., and Handrock, J. L., *Fundamentals of Metal Fatigue Analysis*, Prentice Hall, Inc., Englewood Cliffs, 1990.

Bartlett, M. S., "On the Theoretical Specification and Sampling Properties of Autocorrelated Time Series," *Journal of the Royal Statistical Society*, Series B, Vol. 8, 1946, pp. 27-40.

Bendat, J. S. and Piersol, A. G., *Random Data: Analysis and Measurement Procedures*, Second Edition, Wiley-Interscience, New York, 1986.

Beste, A., Dreßler, K., Kötzle, H., Krüger, W., Maier, B., and Petersen, J., "Multiaxial Rainflow A Consequent Continuation of Professor Tatsuo Endo's Work" *The Rainflow Method in Fatigue*, Y. Murakami, ed., Butterworth-Heinemann, Oxford, 1991.

Bílý, M., Bukoveczky, J., "Digital Simulation of Environmental Processes with Respect to Fatigue," *Journal of Sound and Vibration*, Vol. 49, No. 4, 1976, pp. 551-568.

Bishop, N. W. M. and Sherratt, F., "A Theoretical Solution for the Estimation of "Rainflow" Ranges from Power Spectral Density Data," *Fatigue Fracture Engineering Material Structure*, Vol. 13, No. 4, 1990, pp. 311-326.

Bonnen, J. J., Conle, F. A., and Chu, C. C., "Biaxial Torsion-Bending Fatigue of SAE Axle Shafts," *Society of Automotive Engineers*, Warrendale, PA, No. 910164, 1991.

Box, G. E. P. and Cox, D. R., "An Analysis of Transformation," *Journal of the Royal Statistical Society*, Series B, Vol. 26, 1964, pp. 211-252.

Box, G. E. P. and Jenkins, G. M., *Time Series Analysis Forecasting and Control*, second edition, Holden-Day, San Francisco, 1976.

Brockwell, P. J. and Davis, R. A., *Time Series: Theory and Methods*, Springer, New York, 1987.

Brown, M. W. and Miller, K. J., "A Theory for Fatigue Failure under Multiaxial Stress Strain Condition," *Institution of Mechanical Engineers,* Proceedings, Vol. 187, 1973, pp. 745-755.

Brown, M. W. and Miller, K. J., "Two Decades of Progress in the Assessment of Multiaxial Low-Cycle Fatigue Life," *Low-Cycle Fatigue and Life Prediction, ASTM STP 770*, C. Amzallag, B. N. Leis, and P. Raabe, eds., American Society for Testing and Materials, 1982, pp. 482-499.

Brown, M. W., and Miller, K. J., "Mode 1 Fatigue Crack Growth Under Biaxial Stress at Room and Elevated Temperature," *Multiaxial Fatigue*, *ASTM STP 853*, K. J. Miller and M. W. Brown, eds., American Society for Testing and Materials, Philadelphia, 1985, pp. 135-152.

Buxbaum, O. and Zaschel, J. M., "Beschreibung stochastischer Beanspruchungs-Zeit-Funktionen: Description of stochastic Loading Time Series," *Fraunhofer-Gesellschaft, Laboratorium für Betriebsfestigkeit*, Darmstadt, LBF FhG Report, No. FB-140, 1977.

Buxbaum, O., "Random Load Analysis as a Link Between Operational Stress Measurement and Fatigue Life Assessment," *Service Fatigue Loads Monitoring, Simulation, and Analysis, ASTM STP 671*, P. R. Abelkis and J. M. Potter, eds., American Society for Testing and Materials, 1979, pp. 5-20.

Buxbaum, O., Klätschke, H., and Oppermann, H., "Effect of Loading Sequence on the Fatigue Life of Notched Specimens Made from Steel and Aluminium Alloys," *Applied Mechanics Review*, Vol. 44, No. 1, Jan., 1991, pp. 27-35.

Čačko, J., Bílý, M. and Bukoveczky, J., *Random Processes: Measurement, Analysis and Simulation*, Elsevier, Amsterdam, 1988.

Cakmak, A. S. and Sherif, R. I., "Parametric Time Series Models for Earthquake Strong Ground Motions and their Relationship to Site Parameters," *Proceedings 8th World Conference Earthquake Engineering*, Vol. 2, 1984, pp. 581-588.

Chang, M. K., Kwiatkowski, J. W., Nau, R. F., Oliver, R. M., and Pister, K. S., *"*ARMA Models for Earthquake Ground Motions", *Earthquake Engineering and Structural Dynamics*, Vol. 10, 1982, pp. 651-662.

Chatfield, C., *The Analysis of Time Series*, Chapman and Hall, New York, 1980.

Coffin, L. F. and Tavernelli, J. F., "The Cyclic Straining and Fatigue of Metals," *Transactions of the Metallurgical Society of AIME*, Vol. 215, Oct., 1959, pp.794-807.

Conle, F. A. and Landgraf, R. W., "A Fatigue Analysis Program for Ground Vehicle Components," *Proceedings of the International Conferences on Digital Techniques in Fatigue*, SEECO '83, Society of Environmental Engineers, Mar., London, 1983, pp. 1-28.

Cooley, J. W. and Tukey, J. W., "An Algorithm for the Machine Calculation of Complex Fourier Series," *Mathematics of Computation*, Vol. 19, 1965, pp. 297-301.

Deodatis, G. and Shinozuka, M., "Auto-Regressive Model for Nonstationary Stochastic Processes," *Journal of Engineering Mechanics*, ASCE, Vol. 114, No. 11, Nov., 1988, pp. 1995-2012.

Dowling, N. E., "Fatigue Failure Predictions for Complicated Stress-Strain Histories," *Journal of Materials,* Vol. 7, No. 1, 1972, pp. 71-87.

Dowling, N. E., Brose, W. R., and Wilson, W. K., "Notched Member Fatigue Life Predictions by the Local Strain Approach," *Fatigue Under Complex Loading - Analysis and Experiments*, Vol. AE-6, Society of Automotive Engineers, Warrendale, PA, 1977, pp. 55-84.

Dowling, N. E. and Thangjitham, S., "Concise Description and Reconstruction of Spectrum Loading," *Proceedings 14th ICAF Symposium*, Ottawa, Canada, June 8-13, 1987, pp. 337-354.

Dowling, N. E. and Khosrovaneh, A. K., "Simplified Analysis of Helicopter Fatigue Loading Spectra," *Development of Fatigue Loading Spectra, ASTM STP 1006*, J. M. Potter and R. T. Watanabe, eds., American Society for Testing and Materials, Philadelphia, 1989, pp. 150-171.

Dowling, N. E., Thangjitham, S., Leser, C. and Fash, J. W., "Some Comments on Methods of Reducing and Reconstructing Irregular Fatigue Loading Histories," pp. 52-61, *The Rainflow Method in Fatigue*, Y. Murakami, ed., Butterworth-Heinemann, Oxford, 1992.

Dowling, N. E., *Mechanical Behavior of Materials*, Prentice Hall, Englewood Cliffs, 1993.

Durbin, H., "The Fitting of Time Series Models," *Reviews of the Institute of International Statistics*, Vol. 28, 1960, pp. 233-243.

Endo, T., Mitsunaga, K., Takahashi, K., Kobayashi, K., and Matsuishi, M., "Damage Evaluation of Metals for Random or Varying Loading," *Proceedings of the 1974 Sympo-*

sium on Mechanical Behavior of Materials, The Society of Material Science, Kyoto, Japan, Aug., 1974.

Finney, J. M. and Denton, A. D., "Cycle Counting and Reconstruction, with Application to the Aircraft Fatigue Data Analysis System," *IMechE*, Vol. C282, 1986, pp. 231-240.

Fash, J. W., Conle, F. A., and Minter, G. L., "Analysis of Irregular Loading Histories for SAE Biaxial Fatigue Program," *Multiaxial Fatigue: Analysis and Experiments*, Vol. AE-14, Society of Automotive Engineers, Warrendale, PA, 1989, pp. 33-59.

Fuchs, H. O. and Stephens, R. I., Metal Fatigue in Engineering, John Wiley & Sons, New York, 1980)

Fines, S., Houmb, O. G., Mo, K., and Overvik, T., "On the Estimation of Wind Spectra by Parametric Methods," *Coastal Engineering*, Vol. 5, 1981, pp. 97-109.

Frendahl, M. and Rychlik, I., "Rainflow Analysis: Markov Method, *International Journal of Fatigue*, Vol. 15, No. 4, 1993, pp. 265-272.

Garud, Y. S., "A New Approach to the Evaluation of Fatigue Under Multiaxial Loadings," *Journal of Engineering Materials and Technology*, Vol. 103, Apr., 1981, pp. 118-125.

Gassner, E., "Auswirkung betriebsähnlicher Belastungsfolgen auf die Festigkeit von Flugzeugbauteilen; Influence of Loadings Similar to Operational Loadings on the Strength of Aircraft Components," *Jahrbuch 1941 der Deutschen Luftfahrtforschung*, Vol. 1, 1941, pp. 472-483.

Gersch, W., Nielsen, N. N., and Akaike, H., "Maximum Likelihood Estimation of Structural Parameters from Random Vibration Data," *Journal of Sound and Vibration*, Vol. 31, No. 3, 1973, pp. 295-308.

Gersch, W. and Liu, R. S-Z., "Time Series Methods for the Synthesis of Random Vibration Systems," *Journal of Applied Mechanics*, Vol. 98, Mar., 1976, pp. 159-165.

Gersch, W. and Yonemoto, J., "Synthesis of Multivariate Random Vibration Systems: A Two-Stage Least Square AR-MA Model Approach," *Journal of Sound and Vibration*, Vol. 52, No. 4, 1977, pp. 553-565.

Gersch, W. and Kitagawa, G., "A Time Varying AR Coefficient Model for Modelling and Simulating Earthquake Ground Motion," *Earthquake Engineering and Structural Dynamics*, Vol. 13, 1985, pp. 243-254.

Gibbons, D. J., *Nonparametric Statistical Inference*, McGraw-Hill, New York, 1971.

Haibach, E., Fischer, R., Schütz, W. and Hück, M., "A Standard Random Load Sequence of Gaussian Type Recommended for General Application in Fatigue Testing; Its Mathematical Background and Digital Generation," *Fatigue Testing and Design*, Vol. 2, S.E.E. International Conference, London, 5 - 9 April, 1976, pp. 29.1-29.21.

Hald, A., *Statistical Theory with Engineering Applications*, John Wiley & Sons, New York, 1952.

Hashin, Z. and Rotem, A., "A Cumulative Damage Theory of Fatigue Failure," *Materials Science and Engineering*, Vol. 34, 1978, pp. 147-160.

Holm, S. and Hovem, J. M., "Estimation of Scalar Ocean Wave Spectra by the Maximum Entropy Method," *Journal of Oceanic Engineering*, IEEE, Vol. OE-4, No. 3, Jul., 1979, pp. 76-83.

Hoshiya, M., Nauyama, M. and Kurita, H., "Autoregressive Model of Spatially Propagating Earthquake Ground Motion," *Probabilistic Methods in Engineering*, P. D. Spanos, ed., ASCE, New York, 1988, pp. 257-260.

Houmb, O. G. and Overvik, T., "Some Applications of Maximum Entropy Spectral Estimation to Ocean Waves and Linear Systems Response in Waves," *Applied Ocean Resources*, Vol. 3, No. 4, 1981, pp. 154-162.

Hsu, D. A. and Hunter, J. S., "Time Series Analysis and Forecasting for Air Pollution Concentrations with Seasonal Variations," *Journal of Environmental Modeling and Simulation*, U.S. E.P.A., 1976, pp. 673-677.

Juneja, L. K., *Multiaxial Fatigue Damage Model for Random Amplitude Loading Histories*, M.S. Thesis, Virginia Polytechnic Institute and State University, 1992.

Kay, S. M., *Modern Spectral Estimation: Theory and Application*, Prentice Hall, Inc., Englewood Cliffs, 1988.

Khosrovaneh, A. K., *Fatigue Analysis and Reconstruction of Helicopter Load Spectra*, Ph.D. Dissertation, Virginia Polytechnic Institute and State University, 1989.

Klesnil, M., *Fatigue of Metallic Materials*, Elsevier, New York, 1992.

Kozin, F., "Autoregressive Moving Average Models of Earthquake Records," *Probabilistic Engineering Mechanics*, Vol. 3, No. 2, 1988, pp. 58-63.

Krüger, W., Scheutzow, M., Beste, A., and Petersen, J., "Markov- und Rainflow-Rekonstruktionen Stochastischer Beanspruchungszeitfunktionen; Markov and Rainflow Reconstructions of Stochastic Time Load Functions," *VDI-Report,* Series 18, No. 22, 1985.

Krüger, W. and Petersen, J., "Rekonstruktion von stochastischen Beanspruchungszeitverläufen aus extrapolierten Rainflow-Matrizen; Reconstruction of Random Loadings from the Distribution of Extrapolated Rain-Flow-Matrices," *VDI Bericht 552*, 9. DESA-Symposium, Berlin, Mai, 1985, pp. 319-331.

Krüger, W., Carmine, R., Dreßler, K. and Keul, M., "Optimale Datenreduktionsverfahren in der Betriebsfestigkeitsanalyse; Optimal Data Reduction Schemes in Fatigue Analysis," *VDI Fachtagung*, Berlin, Apr., 1992.

Kurath, P., Downing, S. D., and Galliart, D., "Chapter 2: Summary of Non-Hardened Shaft Round Robin Program", G. E. Leese and D. F. Socie, eds., *Multiaxial Fatigue: Analysis and Experiments*, Society of Automotive Engineers, Warrendale, PA, Vol. AE-14, 1989, pp. 13-31.

Landgraf, R. W., Morrow, J., and Endo, T., "Determination of the Cyclic Stress-Strain Curve," *Journal of Materials*, ASTM, Vol. 4, No. 1, Mar., 1969, pp. 176-188.

Leese, G. E., "Engineering Significance of Recent Multiaxial Research," *Low Cycle Fatigue*, *ASTM STP 942*, H. D. Solomon, G. R. Halford, L. R. Kais, and B. N. Leis, eds., American Society for Testing and Materials, Philadelphia, 1988, pp. 861-873.

Leser, C., Thangjitham, S., and Dowling, N. E., "Modeling of Random Vehicle Loading Histories for Fatigue Analysis," submitted to *International Journal of Vehicle Design*, 1993.

Li, Y. and Kareem, A., "Simulation of Multivariate Nonstationary Random Processes via FFT," *Journal of the Engineering Mechanics Division*, ASCE, Vol. 117, No. 5, May, 1990, pp. 1037-1057.

Lin, N. K. and Hartt, W. H., "Prediction of the Wide-Band Spectrum Fatigue for Offshore Structures," OMAE Conference, 1985.

Manson, S. S., "Fatigue: A Complex Subject - Some Simple Approximations," *Experimental Mechanics*, Vol. 5, No. 7, Jul., 1965, pp. 193-226.

Manson, S. S., Freche, J. C., and Ensign, C. R., "Application of a Double Linear Damage Rule to Cumulative Fatigue," NASA TN D-3839, 1967.

Marple, S. L., *Digital Spectral Analysis with Applications*, Prentice Hall Inc., Englewood Cliffs, 1987.

McLean, J. R. and Hoffmann, E. R.. "Analysis of Drivers' Control Movements," *Human Factors*, Vol. 13, No. 5, 1971, pp. 407-418.

Mignolet, M. P. and Spanos, P., "Recursive Simulation of Stationary Random Processes - Part 1," *Journal of Applied Mechanics*, ASME, Vol. 54, Sep., 1987, pp. 674-680.

Mignolet, M. P. and Spanos, P. D., "MA to ARMA Two-Stage Monte Carlo Simulation," *Probabilistic Methods in Civil Engineering*, Proceedings 5th ASCE Specialty Conference, P. D. Spanos, ed., May, 1988, pp. 265-268.

Mignolet, M. P. and Spanos, P. D., "Simulation of Homogeneous Two-Dimensional Random Fields: Part 1 - AR and ARMA models," *Journal of Applied Mechanics*, Vol. 59, Jun., 1992, pp. S260-S269.

Miller, I. and Freund, J. E., *Probability and Statistics for Engineers*, 2nd Edition, Prentice Hall, Englewood Cliffs, 1977.

Miller, K. J. and Zachariah, K. P., "Cumulative Damage Laws for Fatigue Initiation and Stage 1 Propagation," *Journal of Strain Analysis*, Vol. 12, 1977, pp. 262-270.

Miner, M. A., "Cumulative Damage in Fatigue," *Journal of Applied Mechanics*, Sep., 1945, pp. A-159-164.

Morrow, J., "Fatigue Properties of Metals," *Fatigue Design Handbook*, Society of Automotive Engineers, Warrendale, PA, Vol. AE 4, 1968, pp. 21-30.

MTS Systems Corporation, *Life Analysis Package Reference Manual*, Minneapolis, MN, MTS Systems Corporation, 1991.

Naganuma, T., Deodatis, G., and Shinozuka, M., "ARMA Model for Two-Dimensional Processes," *Journal of Engineering Mechanics*, ASCE, Vol. 113, No. 2, Feb., 1987, pp. 234-251.

Nau. R. F., Oliver, R. M., and Pister, K. S., "Simulating and Analyzing Artificial Nonstationary Earthquake Ground Motions," *Bulletin of the Seismological Society of America*, Vol. 72, Apr., 1982, pp. 615-636.

Palmgren, A., "Die Lebensdauer von Kugellagern; Service Life of Ball Bearings," Verein Deutscher Ingenieure, Vol. 68, 1924, pp. 339-341.

Palmgren, A., *Ball and Roller Engineering*, Translated by G. Palmgren and B. Ruley, SFK Industries, Inc., Philadelphia, 1945, pp. 82-83.

Pandit, S. M., *Data Dependent Systems: Modeling Analysis and Optimal Control via Time Series*, Ph.D. Thesis, University of Wisconsin - Madison, 1973.

Pandit, S. M. and Wu, S. M., *Time Series and System Analysis with Applications*, John Wiley and Sons, New York, 1983.

Pandit, S. M., *Modal and Spectrum Analysis: Data Dependent Systems in State Space*, John Wiley & Sons, New York, 1991.

Perret, B., "An Evaluation of a Method for Reconstituting Fatigue Test Loading Sequences from Rainflow Counting," *Proceedings of the 14th ICAF Symposium*, Ottawa, Canada, 1987, pp. 355-401.

Pi, Y. L. and Mickleborough, N. C., "Modal Identification of Vibrating Structures Using ARMA Model," *Journal of Engineering Mechanics*, ASCE, Vol. 115, No. 10, Oct., 1989, pp. 2232-2250.

Polhemus, N. W. and Cakmak, A. S., "Simulation of Earthquake Ground Motions using ARMA Models," *Earthquake Engineering and Structural Dynamics*, Vol. 9, 1981, pp. 343-354.

Priestley, M. B., "Evolutionary Spectra and Nonstationary Processes," *Journal of the Royal Statistical Society*, Series B, Vol. 27, 1965, pp. 204-237.

Priestley, M. B., *Spectral Analysis and Time Series*, Vol. 1 & 2, Academic Press, London, 1981.

Reed, D. A. and Scanlan, R. H., "Time Series Analysis of Cooling Tower Wind Loading," *Journal of the Engineering Mechanics Division*, ASCE, Vol. 109, No. 2, 1983, pp. 538-554.

Rice, S. O., "Mathematical Analysis of Random Noise," *Bell System Technical Journal*, Vol. 23, 1944, pp. 232-282.

Rychlik, I., "Simple Approximations of the Rain-Flow-Cycle Distribution for Discretized Random Loads," *Probabilistic Engineering Mechanics*, Vol. 4, No. 1, 1989, pp. 40-48.

Rychlik, I., "Rainflow Cycles in Gaussian Loads," *Fatigue Fracture Engineering Material Structure*, Vol. 15, No. 1, 1992, pp. 57-726.

Samaras, E., Shinozuka, M., and Tsurui, A., "ARMA Representation of Random Processes," *Journal of Engineering Mechanics*, ASCE, Vol. 111, No. 3, Mar., 1985, pp. 449-461.

Sarkani, S., "Feasibility of Auto-Regressive Simulation Model for Fatigue Studies," *Journal of Structural Engineering*, Vol. 116, No. 9, Sep., 1990, pp. 2481-2495.

Schütz, W., "Lebensdauer-Berechnung bei Beanspruchungen mit beliebigen Last-Zeit Funktionen," *VDI Bericht 268*, 1976, pp. 113-138.

Slutzky, E., "The Summation of Random Causes as the Source of Cyclic Processes," Econometrica, Vol. 5, 1937, pp. 105-146. Translated from the earlier paper of the same title in *Problems of Economic Conditions*, Conjuncture Institute, Moscow, 1927.

Smith, R. W., Hirschberg, M. H., and Manson, S. S., "Fatigue Behavior of Materials Under Strain Cycling in Low and Intermediate Life Range," *NASA*, Washington, D. C., NASA TN D-1574, Apr., 1963.

Socie, D., "Fatigue-life Prediction Using Local Stress-Strain Concepts," *Experimental Mechanics*, SESA, Vol. 17, no. 2, Feb., 1977, pp. 50-56.

Socie, D., Shifflet, G., and Berns, H., "A Field Recording System with Applications to Fatigue Analysis," *International Journal of Fatigue*, Vol. 1, No. 2, Apr., 1979, pp. 103-111.

Socie, D., "Multiaxial Fatigue Damage Assessment," *Low Cycle Fatigue and Elasto-Plastic Behavior of Materials*, K. -T. Rie, ed., Elsevier, London, 1987, pp. 465-486.

Spanos, P. D., "ARMA Algorithms for Ocean Wave Modeling," *Journal of Energy Resources Technology*, Transactions of the ASME, Vol. 105, Sep., 1983, pp. 300-309.

Spanos, P. D. and Schultz, K. P., "Two-Stage Order-of-Magnitude Matching for the von Karman Turbulence Spectrum," *Proceedings 4th International Conference on Structural Safety and Reliability*, ICOSSAR, Vol. 1, 1985, pp. 211-218.

Spanos, P. D. and Schultz, K. P., "Numerical Synthesis of Trivariate Velocity Realizations of Turbulence," *International Journal of Nonlinear Mechanics*, Vol. 21, No. 4, 1986, pp. 269-277.

Spanos, P. D. and Mignolet, M. P., "Recursive Simulation of Stationary Multivariate Random Processes - Part 2," *Journal of Applied Mechanics*, ASME, Vol. 54, Sep., 1987, pp. 681-687.

Spanos, P. D. and Mignolet, M. P., "ARMA Monte Carlo Simulation in Probabilistic Structural Analysis," *The Shock and Vibration Digest*, Vol. 21, No. 11, 1989, pp. 3-14.

Spanos, P. D. and Mignolet, M. P., "Simulation of Stationary Random Processes: Two Stage MA to ARMA Approach," *Journal of Engineering Mechanics*, ASCE, Vol. 116, No. 3, Mar., 1990, pp. 620-641.

Spanos, P. D. and Mignolet, M. P., "Simulation of Homogeneous Two-Dimensional Random Fields: Part 2 - MA and ARMA models," *Journal of Applied Mechanics*, Vol. 59, Jun., 1992, pp. S270-S277.

Tavares, L. V., "Extremes of Autocorrelated Load Model," *Journal of the Engineering Mechanics Division*, ASCE, Vol. 103, No. EM4, Aug., 1977, pp. 717-723.

ten Have, A. A., "European Approaches in Standard Spectrum Development," *Development of Fatigue Loading Spectra*, *ASTM STP 1006*, J. M. Potter and R. T. Watanabe, eds., American Society for Testing and Materials, 1989, pp. 17-35.

Thangjitham, S., Dowling, N. E., Leser, C., and Juneja, L. K., "Application of ARMA Processes in Modeling Random Fatigue Loading Histories, submitted to *International Journal of Fatigue*, 1993.

Theil, H., *Economic Forecasts and Policy*, North-Holland Publishing Company, Amsterdam, 1958.

Tiao, G. C. and Box, G. E. P., "Modeling Multiple Time Series with Applications," *Journal of the American Statistical Association*, Vol. 76, Dec., 1981, pp. 802-816.

Toki, K., Sato, T., and Kiyono, J., "Synthesizing Design Ground Motions from Microearthquake Records," *Proceedings of the Japanese Society of Civil Engineers*, Vol. 2, No. 2, Oct., 1985, pp. 423s-433s.

Turkstra, C. J., Tallin, A. G., Brahimi, M., and Kim, H. -J., "Applications of ARMA Models for Seismic Damage Prediction," *Probabilistic Methods in Civil Engineering*, Proceedings 5th ASCE Specialty Conference, P. D. Spanos, ed., 1988, pp. 277-280.

Wei, W. S., *Time Series Analysis*, Addison-Wesley, New York, 1990.

Wirsching, P. H. and Haugen, E. B., "Probabilistic Design for Random Fatigue Loads," *Journal of the Engineering Mechanics Division*, ASCE, Vol. 99, No. EM6, Dec., 1973, pp. 1165-1179.

Wirsching, P. H. and Shehata, A. M., "Fatigue Under Wide Band Random Stresses Using the Rain-Flow Method," *Journal of Engineering Materials and Technology*, Jul., 1977, pp. 205-211.

Wirsching, P. H. and Light, M. C., "Fatigue Under Wide Band Random Stresses", *Journal of the Structural Division*, ASCE, Vol. 106, No. St7, Jul., 1980, pp. 1593-1607.

Wöhler, A., "Bericht über die Versuche, welche auf der Königlich Niederschlesich-Märkischen Eisenbahn mit Apparaten zum Messen der Biegung und Verdrehung von Eisenbahnwagen-Achsen während der Fahrt, angestellt wurden.; Report about Tests, which have been Conducted on the Königlich Niederschlesich-Märkischen Railroads with Apparatuses for Measuring the Bending and Torsion of Railroad Car Axles During Operation.", *Zeitschrift für Bauwesen*, Vol. 8, 1858, pp. 641-652.

Wu, W.-F. and Huang, T.-H., "Prediction of Fatigue Damage and Fatigue life under Random Loading," *International Journal of Pressure Vessels and Piping*, Vol. 534, No. 2, 1993, pp. 273-298.

Yang, J.-N., "Simulation of Random Envelope Processes," *Journal of Sound and Vibration*, Vol. 21, 1972, pp. 73-85.

Yule, G. U., "On a Method Investigating Periodicities in Disturbed Series with Special Reference to Wölfer's Sunspot Numbers," *Philosophical Transactions of the Royal Society of London*, Series A, Vol. 226, 1927, pp. 267-298.

VITA

I was born on the 22nd of March 1963 in Bad Hersfeld, Germany, a very cold March that was, in the very early morning. This apparently was a good preparation for my *Grund-studium* (undergraduate studies) in Mechanical Engineering from 1982 until 1985 at Technische Universität Braunschweig, Germany, since during the Winter semester lectures started as early as 7:20 am. Upon receiving my *Vor-Diplom* (Bachelor) in 1985, besides studying for my *Hauptstudium* (graduate studies), I worked on getting to America. My efforts were rewarded in the Fall of 1986 with a sponsorship from International Student Exchange Program (ISEP) to study for one year at Virginia Polytechnic Institute and State University (VPI). Here I broadened my horizon, as well as burdened myself with extra homework, by pursuing a degree in Economics. I graduated with a Master of Science in Economics in May of 1988. In the meantime my wife Colleen had pursued me, and I transferred to the Department of Engineering Science and Mechanics (ESM) at VPI to complete my Engineering education. I received a Masters of Science in Engineering Mechanics in January of 1990. Having not had enough of Graduate School yet, I was admitted to the Ph.D. program in ESM. I defended my dissertation in November, 1993, and go on to become a *Versuchsingenieur für Betriebsfestigkeit* (Test-Engineer for Fatigue) in Ludwigsfelde, Germany.